https://www.mdc-berlin.de/de/veroeffentlichungstypen/clinical-journal-club

Als gemeinsame Einrichtung von MDC und Charité fördert das Experimental and Clinical Research Center die Zusammenarbeit zwischen Grundlagenwissenschaftlern und klinischen Forschern. Hier werden neue Ansätze für Diagnose, Prävention und Therapie von Herz-Kreislauf- und Stoffwechselerkrankungen, Krebs sowie neurologischen Erkrankungen entwickelt und zeitnah am Patienten eingesetzt. Sie sind eingeladen, um uns beizutreten. Bewerben Sie sich!

A 57-year-old woman presented to the emergency department with a 3-day history of shortness of breath and dizziness. The physical examination was notable for pallor. Laboratory studies showed a hemoglobin of 4.4 g per deciliter (reference range, 11.6 to 15.5), an elevated reticulocyte count, an elevated lactate dehydrogenase level, and a low haptoglobin level. The results of hemoglobin electrophoresis and glucose-6-phosphate dehydrogenase testing were normal, and methemoglobin and direct antiglobulin tests were negative. A peripheral blood smear (left, Giemsa staining) showed poikilocytosis, nucleated red cells (black arrows), and polychromatic cells (white arrows). The peripheral blood smear also showed bite cells (left, red arrows), blister cells (left, asterisks), and erythrocyte inclusions (middle, Giemsa staining). The erythrocyte inclusions were identified as Heinz bodies on the basis of positive staining with methyl violet (right). Which of the following is the most likely etiology of this patient's hemolytic anemia?

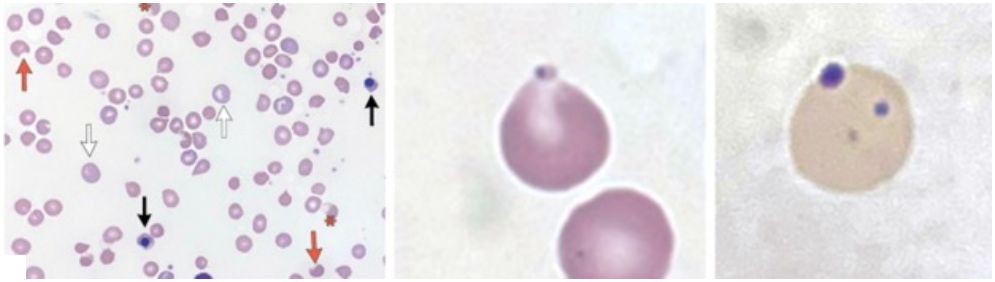

- ○ Immune-mediated
- ○ Infection
- ○ Intrinsic membrane defect
- ○ Oxidative Injury
- ○ Thrombotic microangiopathy

A diagnosis of drug-induced oxidative hemolysis was made. Blood transfusions were administered. After a prolonged toxicologic investigation that involved multiple readmissions over the course of 7 months, the patient eventually reported having taken 10 times the recommended daily dose of zopiclone (a nonbenzodiazepine hypnotic) every night to treat insomnia since 1 month before the presentation. Urine drug testing was positive for zopiclone.

Heinz-Körper (Syn. Heinz-Innenkörperchen, Heinz-Ehrlich-Körper, Heinz-Blaukörper)
sind mikroskopisch sichtbare Verklumpungen des roten Blutfarbstoffs (Hämoglobin) in den roten Blutkörperchen (Erythrozyten). Hierbei kommt es zu einer oxidativen Denaturierung dieses Eiweißes. Dieses veränderte Hämoglobin bildet Klumpen (Aggregate), die sich an der inneren Zellmembran der Erythrozyten anlagern.

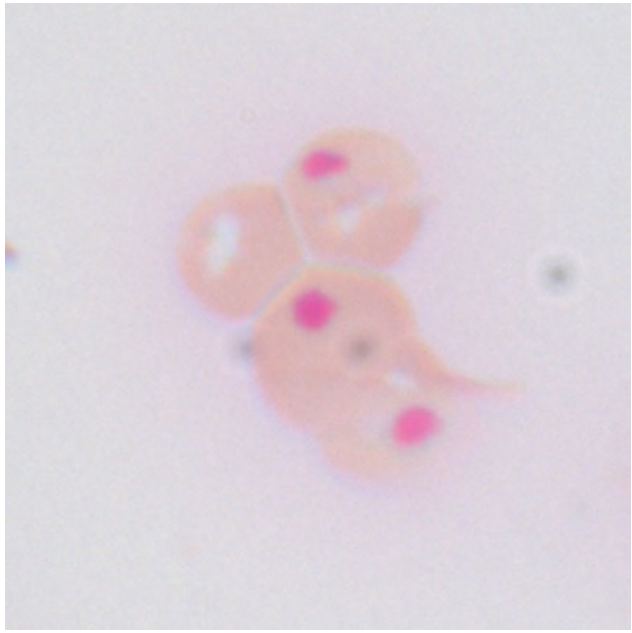

- Intoxikationen durch Phenylhydrazin, Chlorate, Amylnitrit, Nitrobenzol, Anilin
- Medikamenteneinnahme: Primaquin, Sulfonamide, Phenacetin
- Enzymatische Störungen: Glucose-6-Phosphat-Dehydrogenase-Mangel
- Hämoglobinopathien: Hämoglobin-Köln-Krankheit, Hämoglobin-M-Krankheit, Thalassämie

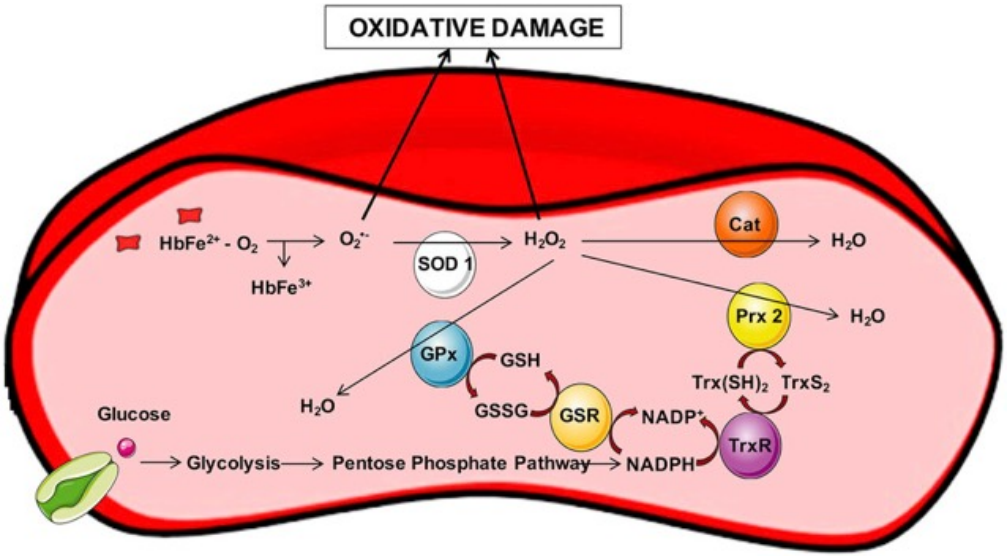

Superoxide production and breakdown in erythrocytes. Hemoglobin undergoes an auto-oxidation reaction leading to the formation of methemoglobin (Hb–Fe^{3+}). If methemoglobin is not converted back into Hb–Fe^{2+}, it is degraded leading to the formation of superoxide anion radical (O2•−). O2•− is dismutated into hydrogen peroxide by superoxide dismutase (SOD). Formation of O2•− and H2O2 and derived products may cause oxidative damage. Hydrogen peroxide can be reduced to water by catalase (Cat), peroxiredoxin 2 (Prx 2) thioredoxin (Trx(SH)2) or glutathione peroxidase (GPx). To carry out the reaction, Trx(SH)2 is oxidized into TrxS2, while GPx will oxidize reduced glutathione (GSH) into glutathione disulfide (GSSG). To reduce GSSG and TrxS2 the enzymes glutathionreductase (GSR) and thioredoxinreductase (TrxR) need NADPH as a hydrogen donor, which is delivered by the pentose phosphate pathway.

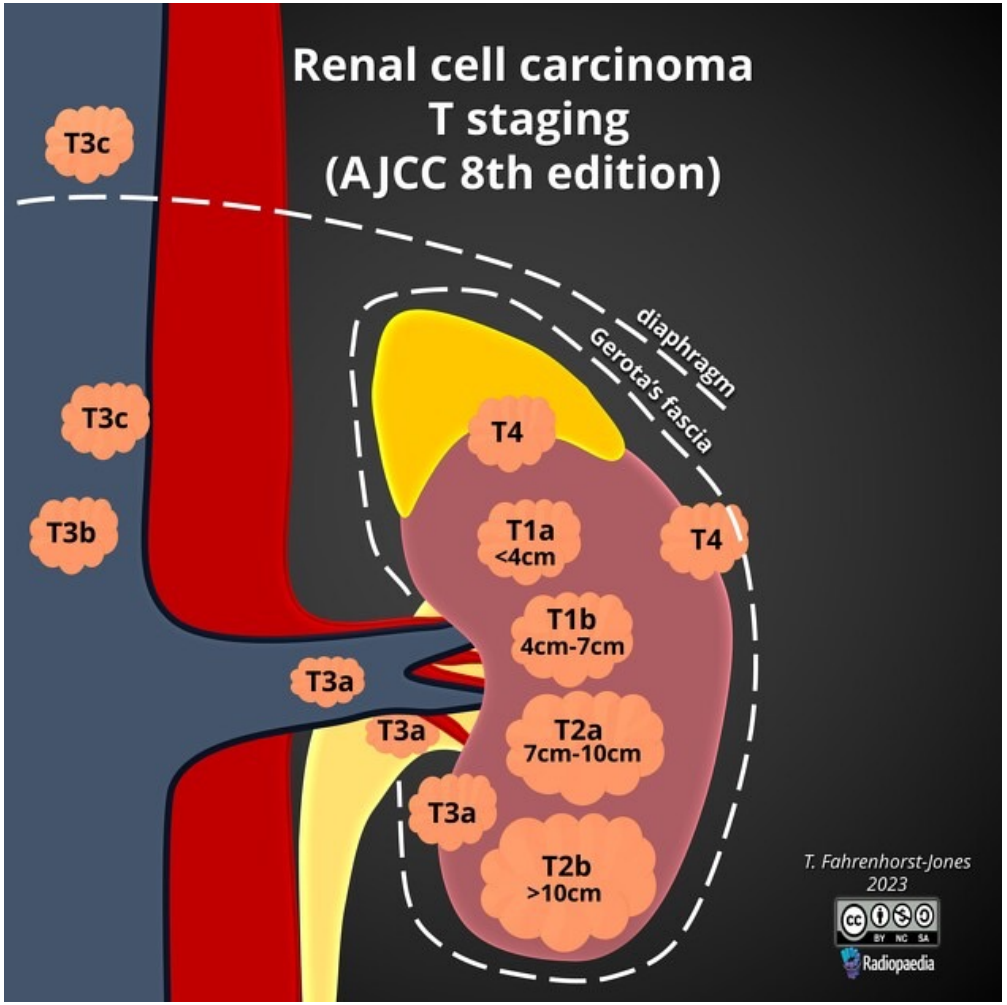
Renal cell carcinoma
T staging
(AJCC 8th edition)
T3c
T3c
T3b
T3a
T3a
T3a
T4
T1a
<4cm
T4
T1b
4cm-7cm
T2a
7cm-10cm
T2b
>10cm
diaphragm
Gerota's fascia
T. Fahrenhorst-Jones
2023
Radiopaedia

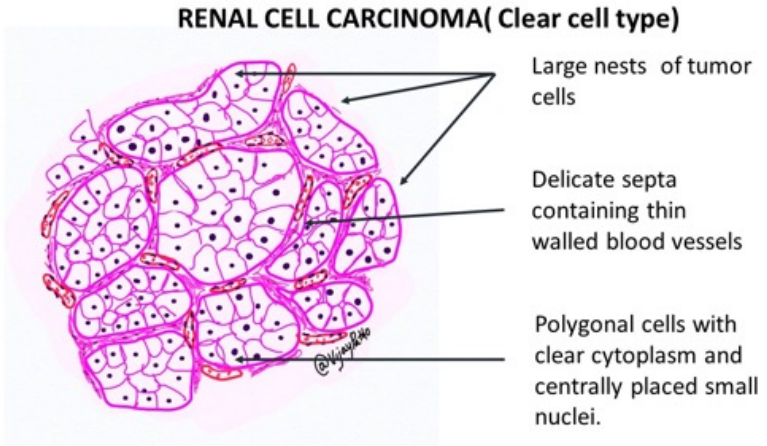
RENAL CELL CARCINOMA(Clear cell type)
Large nests of tumor cells
Delicate septa containing thin walled blood vessels
Polygonal cells with clear cytoplasm and centrally placed small nuclei.

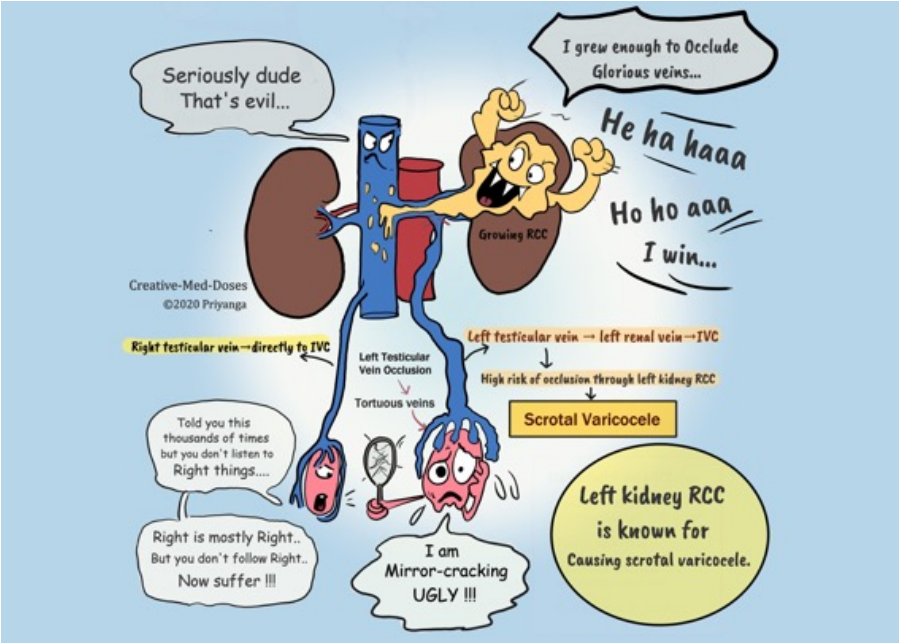
Seriously dude
That's evil...
I grew enough to Occlude
Glorious veins...
He ha haaa
Ho ho aaa
I win...
Growing RCC
Creative-Med-Doses
©2020 Priyanga
Right testicular vein→directly to IVC
Left Testicular
Vein Occlusion
Tortuous veins
Left testicular vein → left renal vein→IVC
High risk of occlusion through left kidney RCC
Scrotal Varicocele
Told you this
thousands of times
but you don't listen to
Right things....
Right is mostly Right..
But you don't follow Right..
Now suffer !!!
I am
Mirror-cracking
UGLY !!!
Left kidney RCC
is known for
Causing scrotal varicocele.

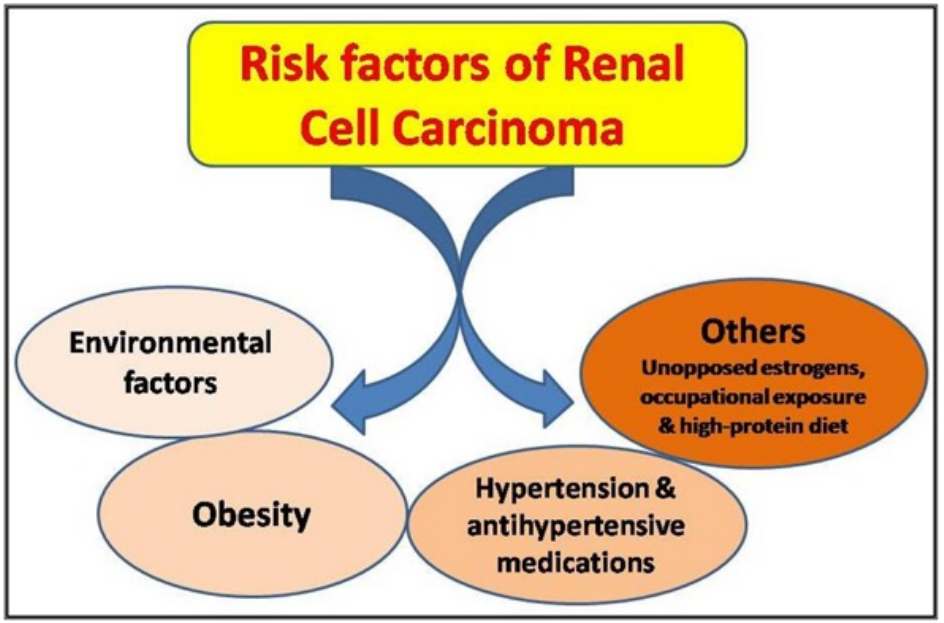
Risk factors of Renal Cell Carcinoma
Environmental factors
Others
Unopposed estrogens, occupational exposure & high-protein diet
Obesity
Hypertension & antihypertensive medications

Pembrolizumab

Pembrolizumab ist ein monoklonaler Antikörper und gehört zur Wirkstoffgruppe der PD-1-Inhibitoren. Das Medikament ist zugelassen zur Behandlung des fortgeschrittenen Melanoms, des nicht kleinzelligen Bronchialkarzinoms, des Hodgkin-Lymphoms, von Urothelkarzinomen und Tumoren im Kopf- und Hals-Bereich.

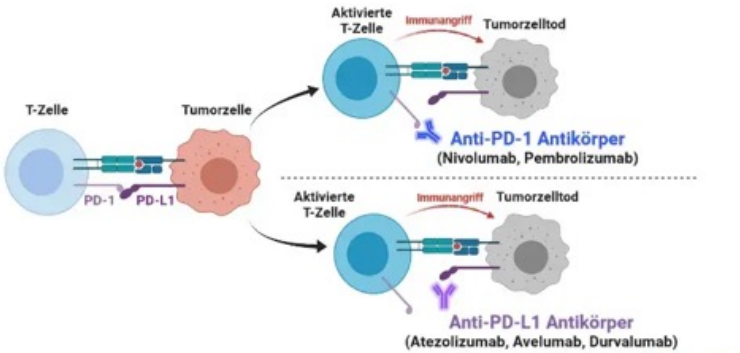

Der Checkpoint-Inhibitor Pembrolizumab ist zugelassen als:

- Monotherapie zur Behandlung des fortgeschrittenen (nicht resezierbaren oder metastasierten) Melanoms
- Monotherapie zur adjuvanten Behandlung des Melanoms im Tumorstadium III mit Lymphknotenbeteiligung nach vollständiger Resektion
- Monotherapie zur Erstlinienbehandlung des metastasierten nicht-kleinzelligen Lungenkarzinoms (NSCLC) mit PD-L1 exprimierenden Tumoren (TPS ≥ 50%) ohne EGFR- oder ALK-positive Tumormutationen
- Kombination mit Pemetrexed und Platin-Chemotherapie zur Erstlinienbehandlung des metastasierten nicht-plattenepithelialen NSCLC ohne EGFR- oder ALK-positiven Tumormutationen
- Kombination mit Carboplatin und entweder Paclitaxel oder nab-Paclitaxel zur Erstlinienbehandlung des metastasierten plattenepithelialen NSCLC
- Monotherapie zur Behandlung des lokal fortgeschrittenen oder metastasierten NSCLC mit PD-L1 exprimierenden Tumoren (TPS ≥ 1%) nach vorheriger Chemotherapie. Patienten mit EGFR- oder ALK-positiven Tumormutationen sollten vor der Therapie mit Pembrolizumab ebenfalls eine auf diese Mutationen zielgerichtete Therapie erhalten haben.
- Monotherapie zur Behandlung des rezidivierten oder refraktären klassischen Hodgkin-Lymphoms (HL) nach Versagen einer autologen Stammzelltransplantation und einer Behandlung mit Brentuximab Vedotin (BV), oder nach Versagen einer Behandlung mit BV, wenn eine auto-Stammzelltransplantation nicht in Frage kommt
- Monotherapie zur Behandlung des lokal fortgeschrittenen oder metastasierten Urothelkarzinoms nach vorheriger Platin-basierter Therapie
- Monotherapie zur Behandlung des lokal fortgeschrittenen oder metastasierten Urothelkarzinoms bei Patienten, die nicht für eine Cisplatin-basierte Therapie geeignet sind und deren Tumoren PD-L1 mit einem kombinierten positiven Score (CPS) ≥ 10 exprimieren
- Monotherapie zur Behandlung des rezidivierten oder metastasierten Plattenepithelkarzinoms der Kopf-Hals-Region (HNSCC) mit PD-L1 exprimierenden Tumoren (TPS ≥ 50%) und einem Fortschreiten der Krebserkrankung während oder nach vorheriger Platin-basierter Therapie
- Monotherapie oder in Kombination mit Platin- und 5-Fluorouracil(5-FU)-Chemotherapie zur Erstlinienbehandlung des metastasierten oder nicht resezierbaren rezidivierten HNSCC mit PD-L1-exprimierenden Tumoren (CPS≥1)
- Kombination mit Axitinib zur Erstlinienbehandlung des fortgeschrittenen Nierenzellkarzinoms (RCC)

Overall Survival with Adjuvant Pembrolizumab in Renal-Cell Carcinoma

Adjuvant pembrolizumab therapy after surgery for renal-cell carcinoma was approved on the basis of a significant improvement in disease-free survival in the KEYNOTE-564 trial. Whether the results regarding overall survival from the third prespecified interim analysis of the trial would also favor pembrolizumab was uncertain. In this phase 3, double-blind, placebo-controlled trial, we randomly assigned (in a 1:1 ratio) participants with clear-cell renal-cell carcinoma who had an increased risk of recurrence after surgery to receive pembrolizumab (at a dose of 200 mg) or placebo every 3 weeks for up to 17 cycles (approximately 1 year) or until recurrence, the occurrence of unacceptable toxic effects, or withdrawal of consent. A significant improvement in disease-free survival according to investigator assessment (the primary end point) was shown previously. Overall survival was the key secondary end point. Safety was a secondary end point.

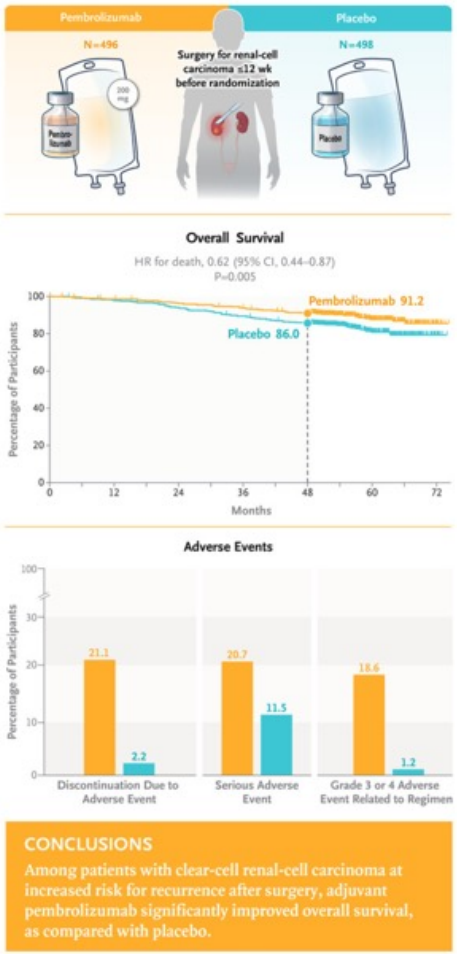

Participants

Eligible participants were adults with confirmed clear-cell renal-cell carcinoma who had undergone surgery within 12 weeks before randomization. Surgery could include partial or radical nephrectomy and synchronous or metachronous (within 1 year after nephrectomy) metastasectomy of any solid, isolated, soft-tissue, nonosseous, nonbrain metastatic lesions that could be resected completely with negative surgical margins. The risk of disease recurrence was classified according to protocol-defined criteria as intermediate to high (tumor stage T2 with nuclear grade 4 or sarcomatoid features, or tumor stage T3; no regional lymph node or distant metastasis present), high (tumor stage T4 with no regional lymph node or distant metastasis, or any tumor stage with the presence of regional lymph-node involvement), or stage M1 NED (no evidence of disease).

End Points and Assessments

Disease-free survival according to the investigator's assessment (defined as the time from randomization to the first documented recurrence of renal-cell carcinoma or death from any cause, whichever occurred first) was the primary end point. Overall survival (defined as the time from randomization to death from any cause) was the key secondary end point.

Characteristic	Pembrolizumab (N=496)	Placebo (N=498)
Age		
Median (range) — yr	60 (27–81)	60 (25–84)
≥65 yr — no. (%)	158 (31.9)	172 (34.5)
Male sex — no. (%)	347 (70.0)	359 (72.1)
Race or ethnic group — no. (%)†		
American Indian or Alaska Native	10 (2.0)	2 (0.4)
Asian	63 (12.7)	75 (15.1)
Black	7 (1.4)	5 (1.0)
Multiple	8 (1.6)	5 (1.0)
White	372 (75.0)	376 (75.5)
Missing data	36 (7.3)	35 (7.0)
ECOG performance-status score of 1 — no. (%)‡	75 (15.1)	72 (14.5)
PD-L1 combined positive score — no. (%)§		
<1	124 (25.0)	113 (22.7)
≥1	365 (73.6)	383 (76.9)
Missing data	7 (1.4)	2 (0.4)
Geographic location — no. (%)		
North America	133 (26.8)	125 (25.1)
European Union	188 (37.9)	187 (37.6)
Rest of world	175 (35.3)	186 (37.3)
Geographic region — no. (%)		
United States	114 (23.0)	117 (23.5)
Other	382 (77.0)	381 (76.5)
Radical nephrectomy — no. (%)	459 (92.5)	459 (92.2)
Disease risk category — no. (%)¶		
M0 intermediate-to-high risk	422 (85.1)	433 (86.9)
M0 high risk	40 (8.1)	37 (7.4)
M0 other	5 (1.0)	0
M1 NED	29 (5.8)	28 (5.6)
Sarcomatoid features — no. (%)		
Present	52 (10.5)	59 (11.8)
Absent	414 (83.5)	415 (83.3)
Unknown	30 (6.0)	24 (4.8)

Subsequent Anticancer Therapy for Renal-Cell Carcinoma among Participants Who Received Subsequent Therapy (Intention-to-Treat Population).

Subsequent Anticancer Therapy	Pembrolizumab (N=132)	Placebo (N=172)
	number/total number (percent)	
Drug therapy	105/132 (79.5)	145/172 (84.3)
Anti–PD-1 or anti–PD-L1 therapy†	43/105 (41.0)	101/145 (69.7)
VEGF- or VEGF receptor–targeted therapy‡	97/105 (92.4)	123/145 (84.8)
Other§	32/105 (30.5)	60/145 (41.4)
Radiation therapy	32/132 (24.2)	34/172 (19.8)
Surgery	36/132 (27.3)	50/172 (29.1)

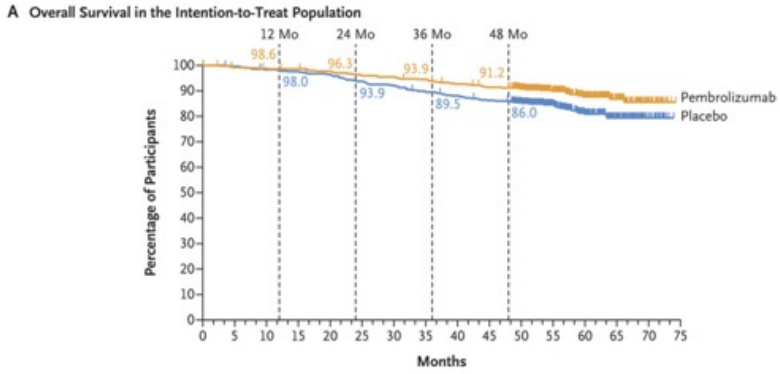

B **Subgroup Analysis for Overall Survival**

Subgroup	Pembrolizumab	Placebo	Hazard Ratio for Death (95% CI)
	no. of deaths/no. of participants		
Overall	55/496	86/498	0.62 (0.44–0.87)
Age			
<65 yr	25/338	46/326	0.51 (0.31–0.83)
≥65 yr	30/158	40/172	0.77 (0.48–1.23)
Sex			
Female	20/149	18/139	1.08 (0.57–2.04)
Male	35/347	68/359	0.50 (0.33–0.75)
Race			
White	46/372	67/376	0.67 (0.46–0.98)
Other	6/88	13/87	0.45 (0.17–1.20)
ECOG performance-status score			
0	38/421	67/426	0.55 (0.37–0.82)
1	17/75	19/72	0.84 (0.44–1.63)
PD-L1 combined positive score			
<1	12/124	16/113	0.65 (0.31–1.38)
≥1	42/365	69/383	0.62 (0.42–0.91)
Geographic region			
United States	11/114	16/117	0.68 (0.32–1.47)
Other	44/382	70/381	0.61 (0.42–0.88)
Metastatic staging			
M0	51/467	79/470	0.63 (0.44–0.90)
M1 NED	4/29	7/28	0.51 (0.15–1.75)
Disease risk category			
M0 intermediate-to-high risk	41/422	69/433	0.59 (0.40–0.87)
M0 high risk	9/40	10/37	0.78 (0.32–1.93)
M1 NED	4/29	7/28	0.51 (0.15–1.75)
Sarcomatoid features			
Present	8/52	12/59	0.69 (0.28–1.70)
Absent	41/414	70/415	0.57 (0.39–0.84)

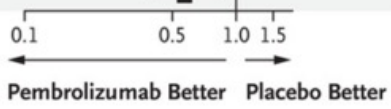

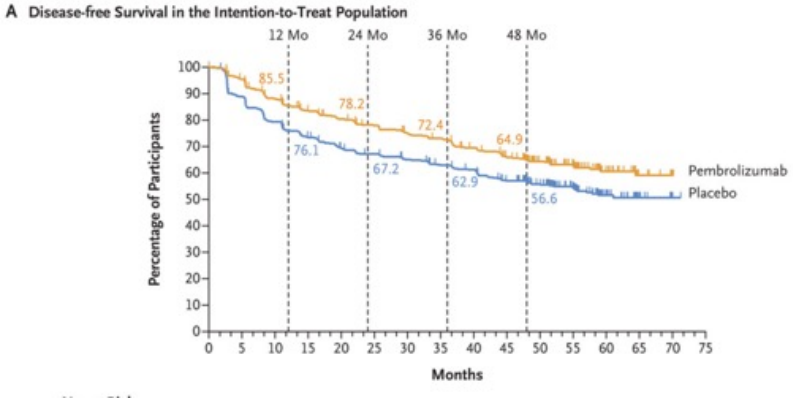

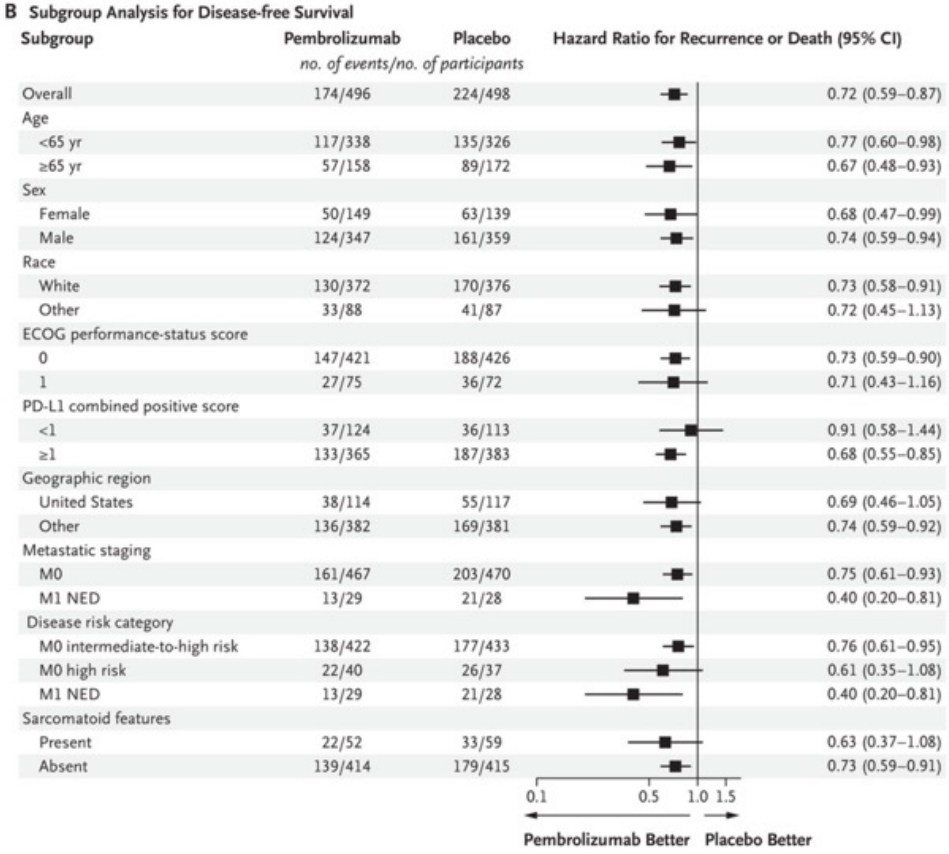

Subsequent Anticancer Therapy for Renal-Cell Carcinoma among Participants Who Received Subsequent Therapy (Intention-to-Treat Population).

Subsequent Anticancer Therapy	Pembrolizumab (N=132)	Placebo (N=172)
	number/total number (percent)	
Drug therapy	105/132 (79.5)	145/172 (84.3)
Anti–PD-1 or anti–PD-L1 therapy†	43/105 (41.0)	101/145 (69.7)
VEGF- or VEGF receptor–targeted therapy‡	97/105 (92.4)	123/145 (84.8)
Other§	32/105 (30.5)	60/145 (41.4)
Radiation therapy	32/132 (24.2)	34/172 (19.8)
Surgery	36/132 (27.3)	50/172 (29.1)


KEYNOTE-564
Trial
Improvements in
Disease-free
Survival
Pembro-
lizumab


PRIMARY END POINT
Disease-free Survival
Percentage of Participants
Months
85.5
78.2
72.4
64.9
76.1
67.2
62.9
56.6
Pembrolizumab
Placebo

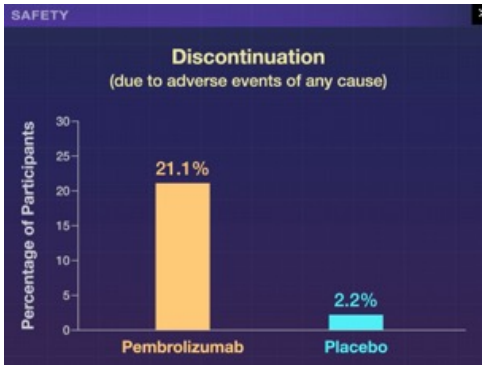
SAFETY
Discontinuation
(due to adverse events of any cause)
Percentage of Participants
21.1%
2.2%
Pembrolizumab
Placebo


KEYNOTE-564
Trial
Results for
Overall
Survival
from an interim
analysis
Pembro-
lizumab


SECONDARY END POINT
Overall Survival
Percentage of Participants
Months
98.6
96.3
93.9
91.2
98.0
93.9
89.5
86.0
Pembrolizumab
Placebo
During a median follow-up
of ~57 months
Overall survival was
significantly improved
Hazard ratio for death, 0.62
(95% CI, 0.44–0.87); P=0.005

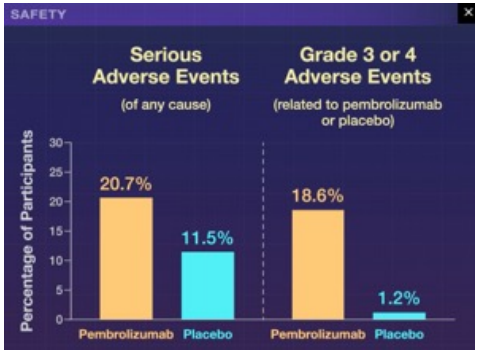
SAFETY
Serious
Adverse Events
(of any cause)
Grade 3 or 4
Adverse Events
(related to pembrolizumab
or placebo)
Percentage of Participants
20.7%
11.5%
18.6%
1.2%
Pembrolizumab
Placebo
Pembrolizumab
Placebo

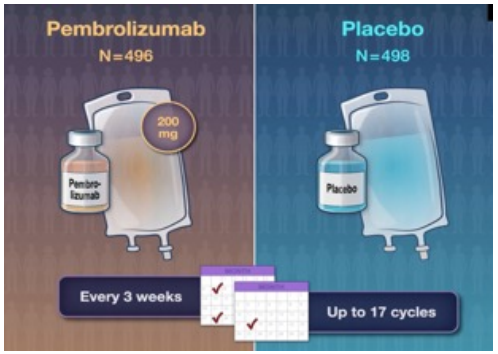
Pembrolizumab
N=496
Placebo
N=498
200
mg
Pembro-
lizumab
Placebo
Every 3 weeks
Up to 17 cycles

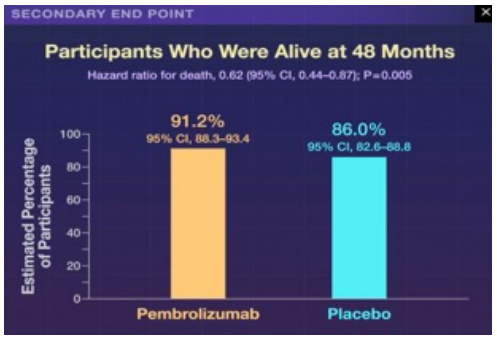
SECONDARY END POINT
Participants Who Were Alive at 48 Months
Hazard ratio for death, 0.62 (95% CI, 0.44–0.87); P=0.005
Estimated Percentage
of Participants
91.2%
95% CI, 88.3–93.4
86.0%
95% CI, 82.6–88.8
Pembrolizumab
Placebo


Pembro-
lizumab
Significantly
prolonged
overall survival
As compared with placebo

Evidence Based Use of Beta-Blockers in 2017

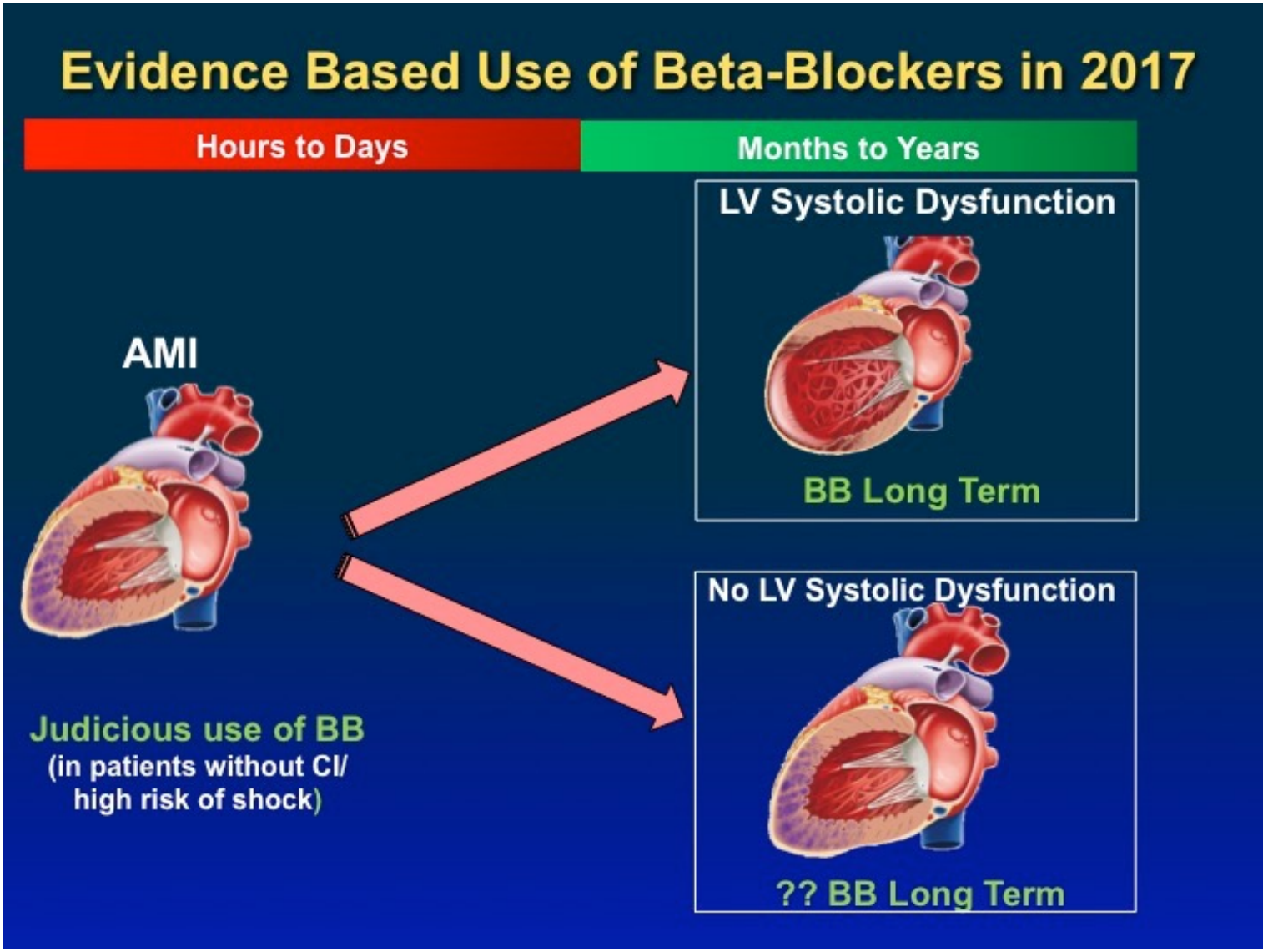

Beta-Blockers after Myocardial Infarction and Preserved Ejection Fraction

Most trials that have shown a benefit of beta-blocker treatment after myocardial infarction included patients with large myocardial infarctions and were conducted in an era before modern biomarker-based diagnosis of myocardial infarction and treatment with percutaneous coronary intervention, antithrombotic agents, high-intensity statins, and renin–angiotensin–aldosterone system antagonists. In a parallel-group, open-label trial performed at 45 centers in Sweden, Estonia, and New Zealand, we randomly assigned patients with an acute myocardial infarction who had undergone coronary angiography and had a left ventricular ejection fraction of at least 50% to receive either long-term treatment with a beta-blocker (metoprolol or bisoprolol) or no beta-blocker treatment. The primary end point was a composite of death from any cause or new myocardial infarction.

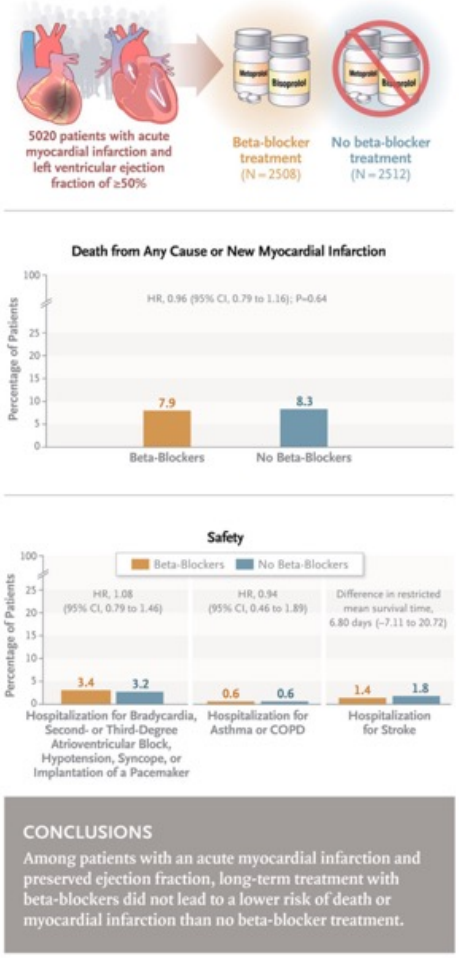

CONCLUSIONS

Among patients with an acute myocardial infarction and preserved ejection fraction, long-term treatment with beta-blockers did not lead to a lower risk of death or myocardial infarction than no beta-blocker treatment.

Patients

Adult patients who provided written informed consent 1 to 7 days after myocardial infarction and who had undergone coronary angiography and echocardiography with a preserved left ventricular ejection fraction (≥50%) were eligible. Patients were also required to have obstructive coronary artery disease as documented by coronary angiography (i.e., stenosis of ≥50%, a fractional flow reserve of ≤0.80, or an instantaneous wave-free ratio of ≤0.89 in any segment) at any time point before randomization. Major exclusion criteria were an indication for or contraindication to beta-blocker treatment. To ensure completeness of follow-up, nonresidents of the three trial countries could not undergo randomization. For blood-pressure control, drugs other than beta-blockers were recommended according to guidelines. If a patient was already receiving treatment with a beta-blocker when enrolled and randomly assigned to the no–beta-blocker group, a tapering of the beta-blocker had to be carried out during a period of 2 to 4 weeks.

Clinical End Points

The primary end point was a composite of death from any cause or new myocardial infarction. Secondary end points were death from any cause, death from cardiovascular causes, myocardial infarction, hospitalization for atrial fibrillation (as a primary diagnosis), and hospitalization for heart failure (as a primary diagnosis). Safety end points were hospitalization for bradycardia, second- or third-degree atrioventricular block, hypotension, syncope, or implantation of a pacemaker; hospitalization for asthma or chronic obstructive pulmonary disease (as a primary diagnosis); and hospitalization for stroke. Angina pectoris (according to Canadian Cardiovascular Society class) and dyspnea (according to New York Heart Association class) after 6 to 10 weeks and after 11 to 13 months were also end points.

Characteristics of the Patients.

Characteristic	Beta-Blockers (N=2508)	No Beta-Blockers (N=2512)
Median age (IQR) — yr	65 (57–73)	65 (57–73)
Female sex — no. (%)	563 (22.4)	568 (22.6)
Country — no. (%)		
Sweden	2392 (95.4)	2396 (95.4)
Estonia	16 (0.6)	16 (0.6)
New Zealand	100 (4.0)	100 (4.0)
Risk factors — no./total no. (%)		
Current smoking	478/2466 (19.4)	530/2483 (21.3)
Hypertension	1155/2507 (46.1)	1163/2509 (46.4)
Diabetes mellitus	346/2506 (13.8)	354/2509 (14.1)
Previous cardiovascular disease — no./total no. (%)		
Previous myocardial infarction	165/2503 (6.6)	192/2507 (7.7)
Previous PCI	147/2504 (5.9)	175/2505 (7.0)
Previous CABG	33/2504 (1.3)	36/2507 (1.4)
Previous stroke	52/2506 (2.1)	67/2507 (2.7)
Previous heart failure	13/2486 (0.5)	22/2481 (0.9)
Characteristic at presentation		
Chest pain as main symptom — no./total no. (%)	2421/2507 (96.6)	2417/2512 (96.2)
CPR before hospital arrival — no./total no. (%)	10/2483 (0.4)	11/2485 (0.4)
Pulmonary rales — no./total no. (%)	29/2445 (1.2)	42/2462 (1.7)
Median heart rate (IQR) — beats/min†	74 (65–85)	73 (64–84)
Median systolic blood pressure (IQR) — mm Hg‡	150 (135–170)	151 (136–170)
Atrial fibrillation — no./total no. (%)	21/2502 (0.8)	23/2504 (0.9)
ST-segment elevation myocardial infarction — no./total no. (%)	877/2507 (35.0)	892/2512 (35.5)
Current oral beta-blocker treatment — no./total no. (%)	269/2468 (10.9)	302/2472 (12.2)
Median no. of days from hospital admission to randomization (IQR)	2 (1–3)	2 (1–3)
In-hospital course — no./total no. (%)		
Coronary angiography		
No stenosis	26/2484 (1.0)	25/2491 (1.0)
One-vessel disease	1378/2484 (55.5)	1378/2491 (55.3)
Two-vessel disease	676/2484 (27.2)	668/2491 (26.8)
Left main or three-vessel disease	404/2484 (16.3)	420/2491 (16.9)
PCI	2387/2491 (95.8)	2376/2496 (95.2)
CABG	92/2491 (3.7)	103/2496 (4.1)
Medication at discharge — no./total no. (%)		
Aspirin	2450/2507 (97.7)	2440/2512 (97.1)
P2Y12 receptor blocker	2411/2507 (96.2)	2398/2512 (95.5)
Beta-blocker	2399/2505 (95.8)	247/2512 (9.8)
ACE inhibitor or ARB	1985/2507 (79.2)	2040/2512 (81.2)
Statin	2481/2507 (99.0)	2461/2510 (98.0)
Diuretic agent	211/2507 (8.4)	191/2512 (7.6)
Calcium-channel blocker	416/2508 (16.6)	496/2511 (19.8)

Primary and Secondary End Points.

End Point	Beta-Blockers (N=2508)	No Beta-Blockers (N=2512)	Hazard Ratio (95% CI)†	P Value
	number (percent)			
Primary end point				
Death from any cause or myocardial infarction	199 (7.9)	208 (8.3)	0.96 (0.79 to 1.16)	0.64
Secondary end points				
Death from any cause	97 (3.9)	103 (4.1)	0.94 (0.71 to 1.24)	
Death from cardiovascular causes	38 (1.5)	33 (1.3)	1.15 (0.72 to 1.84)	
Myocardial infarction	112 (4.5)	117 (4.7)	0.96 (0.74 to 1.24)	
Hospitalization for atrial fibrillation	27 (1.1)	34 (1.4)	0.79 (0.48 to 1.31)	
Hospitalization for heart failure	20 (0.8)	22 (0.9)	0.91 (0.50 to 1.66)	
Safety end points				
Hospitalization for bradycardia, second- or third-degree atrioventricular block, hypotension, syncope, or implantation of a pacemaker	86 (3.4)	80 (3.2)	1.08 (0.79 to 1.46)	
Hospitalization for asthma or COPD	15 (0.6)	16 (0.6)	0.94 (0.46 to 1.89)	
Hospitalization for stroke	36 (1.4)	46 (1.8)	6.80 (–7.11 to 20.72)†	

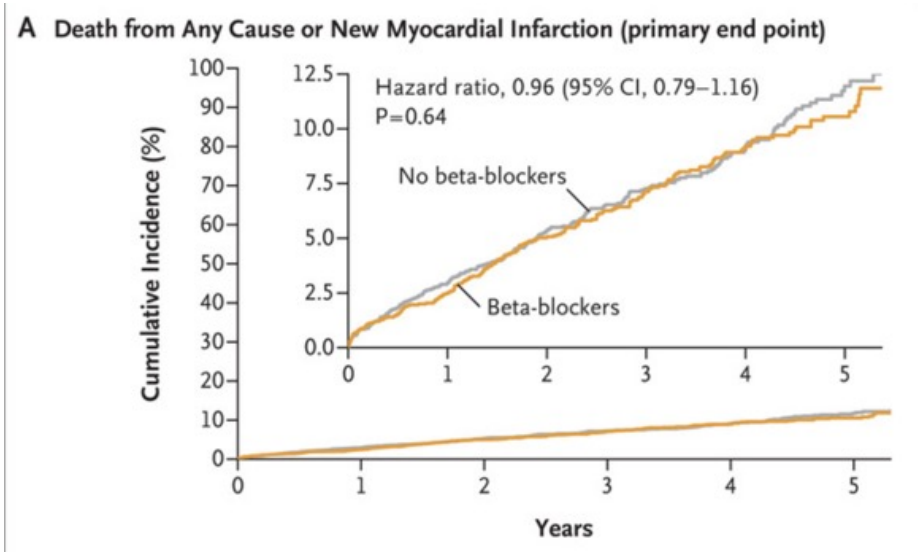

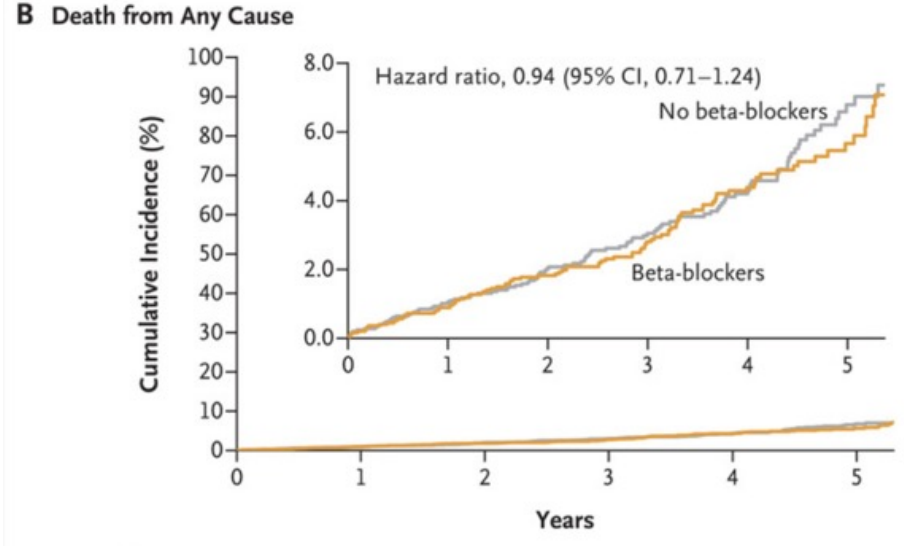

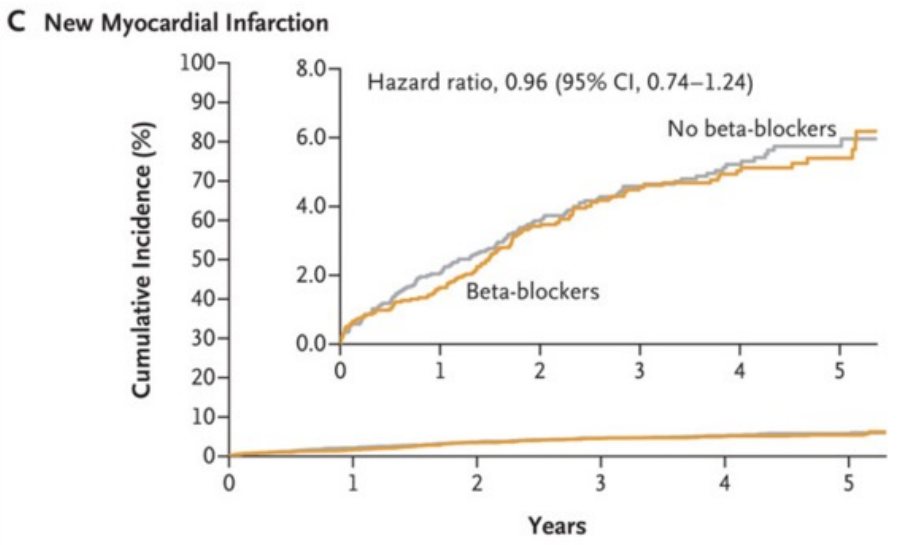

Death from Any Cause and New Myocardial Infarction.

The primary end point was a composite of death from any cause or new myocardial infarction. Secondary end points included the individual components of the primary end point. In all panels, the inset shows the same data on an enlarged y axis. CI denotes confidence interval.

Primary and Secondary End Points.

End Point	Beta-Blockers (N=2508)	No Beta-Blockers (N=2512)	Hazard Ratio (95% CI)†	P Value
	number (percent)			
Primary end point				
Death from any cause or myocardial infarction	199 (7.9)	208 (8.3)	0.96 (0.79 to 1.16)	0.64
Secondary end points				
Death from any cause	97 (3.9)	103 (4.1)	0.94 (0.71 to 1.24)	
Death from cardiovascular causes	38 (1.5)	33 (1.3)	1.15 (0.72 to 1.84)	
Myocardial infarction	112 (4.5)	117 (4.7)	0.96 (0.74 to 1.24)	
Hospitalization for atrial fibrillation	27 (1.1)	34 (1.4)	0.79 (0.48 to 1.31)	
Hospitalization for heart failure	20 (0.8)	22 (0.9)	0.91 (0.50 to 1.66)	
Safety end points				
Hospitalization for bradycardia, second- or third-degree atrioventricular block, hypotension, syncope, or implantation of a pacemaker	86 (3.4)	80 (3.2)	1.08 (0.79 to 1.46)	
Hospitalization for asthma or COPD	15 (0.6)	16 (0.6)	0.94 (0.46 to 1.89)	
Hospitalization for stroke	36 (1.4)	46 (1.8)	6.80 (–7.11 to 20.72)†	

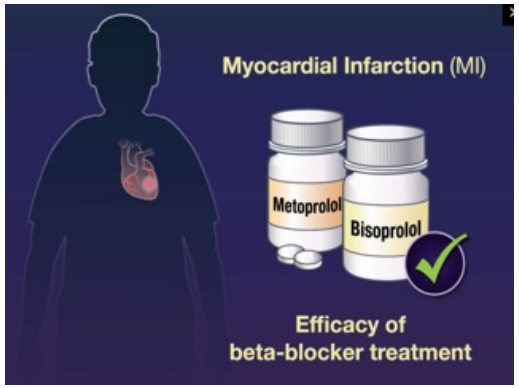

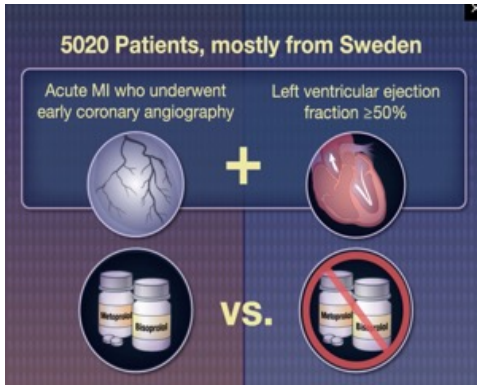

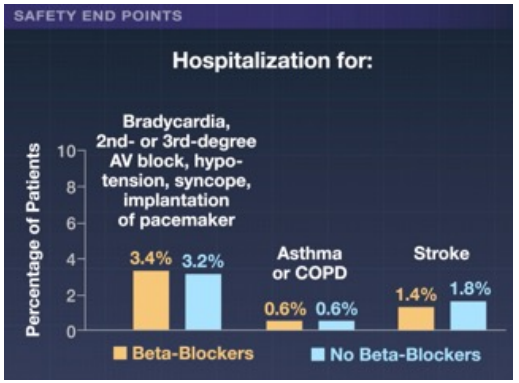

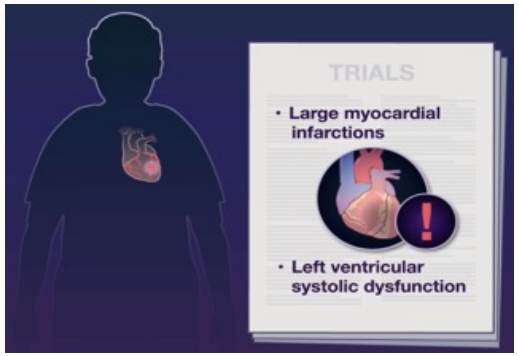

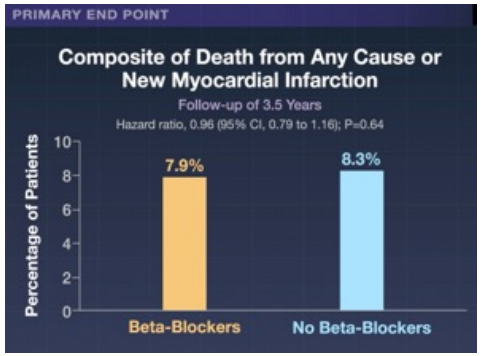

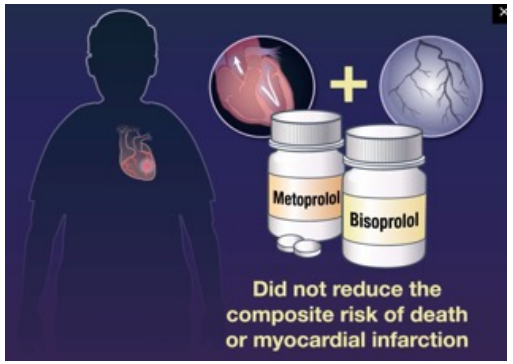

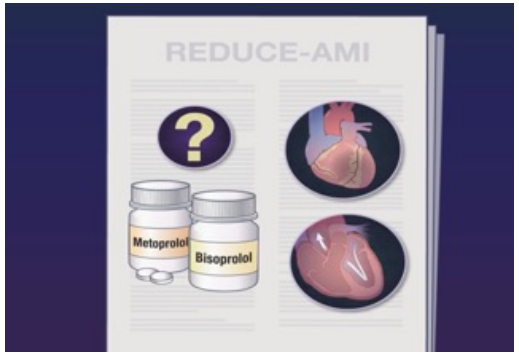

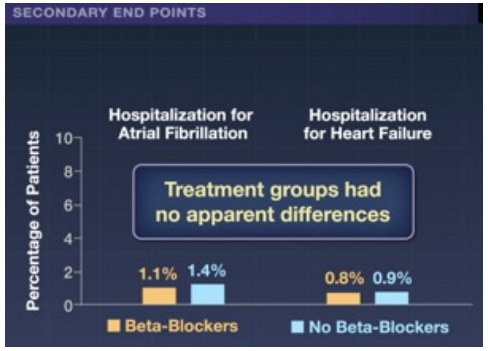

LIMITATIONS AND REMAINING QUESTIONS

- The trial was open-label, because blinding was not judged to be feasible.
- Only safety end points that were associated with hospitalization were assessed.
- Despite strategies to mitigate crossovers, 14% of the patients who had been assigned to the no–beta-blocker group were taking beta-blockers after 1 year of follow-up.

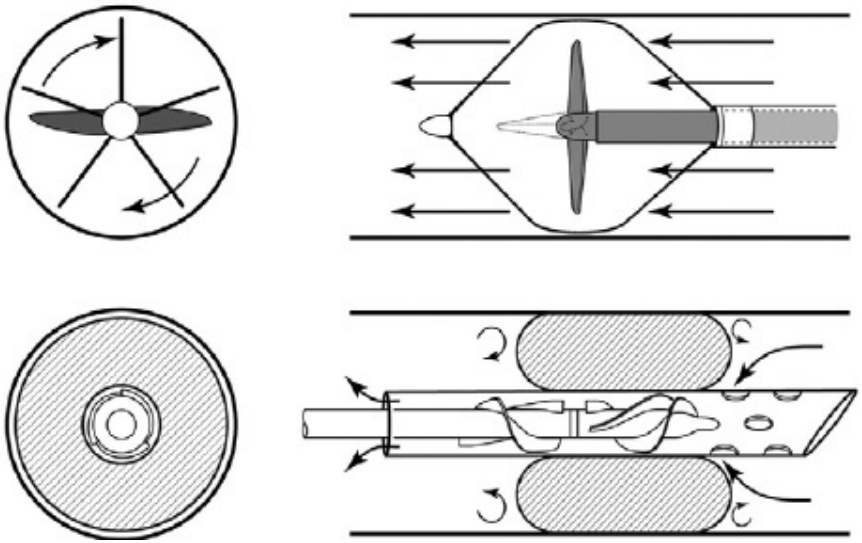

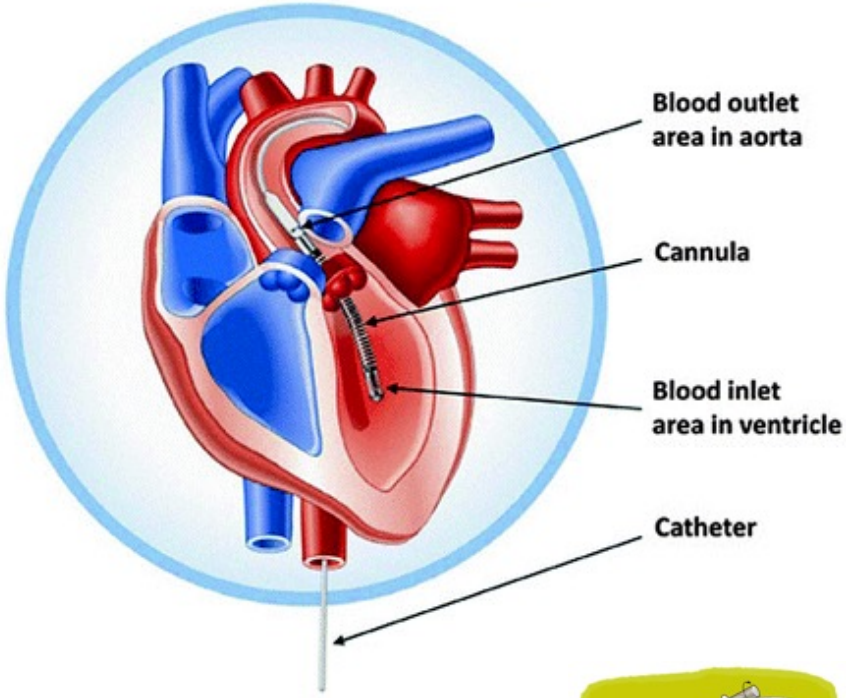
Impella 2.5 & 5.0: Peripheral Implantation
Blood outlet area in aorta
Cannula
Blood inlet area in ventricle
Catheter

Archimides

Percutaneous Transvalvular Microaxial Flow Pump Support in Cardiology

Abstract

The Impella device (Impella, Abiomed, Danvers, MA) is a percutaneous transvalvular microaxial flow pump that is currently used for (1) cardiogenic shock, (2) left ventricular unloading (combination of venoarterial extracorporeal membrane oxygenation and Impella concept), (3) high-risk percutaneous coronary interventions, (4) ablation of ventricular tachycardia, and (5) treatment of right ventricular failure. Impella-assisted forward blood flow increased mean arterial pressure and cardiac output, peripheral tissue perfusion, and coronary blood flow in observational studies and some randomized trials. However, because of the need for large-bore femoral access (14 F for the commonly used Impella CP device) and anticoagulation, the incidences of bleeding and ischemic complications are as much as 44% and 18%, respectively. Hemolysis is reported in as many as 32% of patients and stroke in as many as 13%. Despite the rapidly growing use of the Impella device, there are still insufficient data on its effect on outcome and complications on the basis of large, adequately powered randomized controlled trials. The only 2 small and also underpowered randomized controlled trials in cardiogenic shock comparing Impella versus intra-aortic balloon pump did not show improved mortality. Several larger randomized controlled trials are currently recruiting patients or are in preparation in cardiogenic shock (DanGer Shock [Danish-German Cardiogenic Shock Trial

As reviewed in *Circulation*

Microaxial Flow Pump or Standard Care in Infarct-Related Cardiogenic Shock

The effects of temporary mechanical circulatory support with a microaxial flow pump on mortality among patients with ST-segment elevation myocardial infarction (STEMI) complicated by cardiogenic shock remains unclear. In an international, multicenter, randomized trial, we assigned patients with STEMI and cardiogenic shock to receive a microaxial flow pump (Impella CP) plus standard care or standard care alone. The primary end point was death from any cause at 180 days. A composite safety end point was severe bleeding, limb ischemia, hemolysis, device failure, or worsening aortic regurgitation.

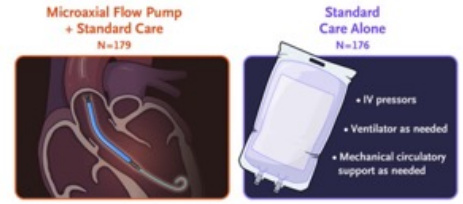

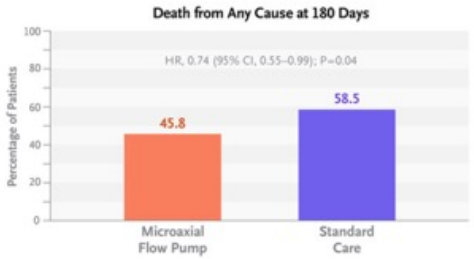

CONCLUSIONS

Among patients with STEMI-associated cardiogenic shock, mortality was lower with the use of a microaxial flow pump in addition to standard care than with standard care alone.

Patients

Patients 18 years of age or older with STEMI and cardiogenic shock were eligible for enrollment. Cardiogenic shock was defined as hypotension (systolic blood pressure below 100 mm Hg or an ongoing need for vasopressor support), end-organ hypoperfusion with an arterial lactate level of 2.5 mmol per liter or greater, and a left ventricular ejection fraction of less than 45%. Patients who had been resuscitated from out-of-hospital cardiac arrest and remained comatose on arrival to the cardiac catheterization laboratory and patients with overt right ventricular failure were excluded.

Trial End Points

The primary end point was death from any cause at 180 days. The first secondary end point was escalation of treatment to additional mechanical circulatory support (short- or long-term), heart transplantation, or death from any cause, whichever came first (composite cardiac end point). The second secondary end point was days alive and out of the hospital, which was calculated as the number of days from discharge to death or data censoring at 180 days minus the number of days of readmission in the case of hospitalization after discharge. Prespecified exploratory end points were the results of the primary and secondary end-point analyses in the as-treated population and a composite end point of unplanned readmission for a cardiovascular cause or death after discharge.

Demographic and Clinical Characteristics of the Patients at Baseline and Timing of Randomization.

Characteristic	Microaxial Flow Pump plus Standard Care (N=179)	Standard Care Alone (N=176)
Median age (IQR) — yr	67 (58–76)	69 (61–76)
Male sex — no. (%)	142 (79.3)	139 (79.0)
Medical history — no. (%)		
Hypertension	89 (49.7)	94 (53.4)
Diabetes	33 (18.4)	47 (26.7)
Myocardial infarction	29 (16.2)	28 (15.9)
Heart failure	16 (8.9)	17 (9.7)
Chronic kidney disease	17 (9.5)	18 (10.2)
Median systolic blood pressure (IQR) — mm Hg	84 (72–91)	82 (72–91)
Median of the mean arterial blood pressure (IQR) — mm Hg	63 (55–72)	64 (55–73)
Median heart rate (IQR) — beats/min	94 (77–110)	95 (76–111)
Median arterial lactate level (IQR) — mmol/liter	4.6 (3.4–7.1)	4.5 (3.2–6.9)
Median left ventricular ejection fraction (IQR) — %	25 (20–31)	25 (15–30)
Resuscitation before randomization — no. (%)	39 (21.8)	33 (18.8)
Intubation before randomization — no. (%)	35 (19.6)	28 (15.9)
Transfer from outside hospital — no. (%)	51 (28.5)	48 (27.3)
Anterior myocardial infarction — no. (%)	126 (70.4)	129 (73.3)
SCAI–CSWG stage at admission — no. (%)†		
C	100 (55.9)	97 (55.1)
D	51 (28.5)	50 (28.4)
E	28 (15.6)	29 (16.5)
No. of diseased vessels on coronary angiography — no. (%)		
0	1 (0.6)	0
1	52 (29.1)	47 (26.7)
2	70 (39.1)	64 (36.4)
3	56 (31.3)	65 (36.9)
Timing of randomization		
Median time from symptom onset to randomization (IQR) — hr	4.8 (2.4–12.8)	3.8 (2.2–9.4)
Randomization performed before revascularization — no. (%)	99 (55.3)	102 (58.0)
Randomization performed in the catheterization laboratory but after revascularization — no. (%)	48 (26.8)	48 (27.3)
Randomization performed ≤12 hr after departure from the catheterization laboratory — no. (%)	32 (17.9)	26 (14.8)

In-Hospital Management of Cardiogenic Shock.

Management	Microaxial Flow Pump plus Standard Care (N=179)	Standard Care Alone (N=176)
Revascularization		
PCI — no. (%)	171 (95.5)	172 (97.7)
Non–culprit vessel PCI — no./no. of patients with multivessel disease (%)	59/127 (46.5)	55/129 (42.6)
Immediate CABG — no. (%)	1 (0.6)	4 (2.3)
Median time from admission to balloon inflation (IQR) — min	58 (36–114)	45 (31–81)
Mechanical circulatory support		
Placement of Impella CP device — no. (%)†	170 (95.0)	3 (1.7)
Randomization occurred before PCI and microaxial flow pump placed before PCI — no./total no. (%)	84/99 (84.8)	3/3 (100)
Median time from randomization to placement of microaxial flow pump (IQR) — min	14 (8–29)	15 (8–31)
Median duration of microaxial flow pump support (IQR) — hr	59 (30–87)	60 (31–92)
Mechanical hemolysis — no./total no. (%)	21/170 (12.4)	1/3 (33.3)
Device malfunction — no./total no. (%)‡	2/170 (1.2)	1/3 (33.3)
Successful weaning from microaxial flow pump — no./total no. (%)	138/170 (81.2)	1/3 (33.3)
Escalation to additional mechanical circulatory support		
Placement of Impella 5.0 device — no. (%)	7 (3.9)	5 (2.8)
Placement of Impella CP for venting during venoarterial ECMO therapy — no. (%)	0	4 (2.3)
Placement of Impella 2.5 device — no. (%)	0	1 (0.6)
Placement of Impella RP device — no. (%)	0	0
Venoarterial ECMO — no. (%)	21 (11.7)	33 (18.8)
Median time from randomization to placement of venoarterial ECMO (IQR) — hr	14 (4–54)	2 (1–5)
Placement of permanent LVAD — no. (%)	10 (5.6)	4 (2.3)
Any escalation to additional mechanical circulatory support — no. (%)	28 (15.6)§	37 (21.0)¶
Intensive care management		
Mechanical ventilation — no. (%)	133 (74.3)	116 (65.9)
Median duration of mechanical ventilation (IQR) — days	5 (2–10)	3 (1–10)
Medication use — no. (%)		
Any vasopressor	159 (88.8)	146 (83.0)
Norepinephrine	156 (87.2)	142 (80.7)
Dopamine	51 (28.5)	41 (23.3)
Epinephrine	67 (37.4)	66 (37.5)
Any inotrope	124 (69.3)	109 (61.9)
Dobutamine	62 (34.6)	59 (33.5)
Milrinone	63 (35.2)	58 (33.0)
Levosimendan	40 (22.3)	39 (22.2)
Staged in-hospital revascularization procedures		
PCI — no. (%)	7 (3.9)	10 (5.7)
CABG — no. (%)	0	3 (1.7)
Median duration of ICU admission (IQR) — days	6 (2–15)	3 (0–10)
Still in ICU at day 30 — no. (%)	22 (12.3)	11 (6.2)
Median duration of hospitalization (IQR) — days	12 (4–27)	7 (1–19)
Still in hospital at day 30 — no. (%)	41 (22.9)	19 (10.8)

End Points and Adverse Events in the Intention-to-Treat Population.

Event	Microaxial Flow Pump plus Standard Care (N=179)	Standard Care Alone (N=176)	Effect Size (95% CI)†
Primary end point: death from any cause at 180 days — no. (%)	82 (45.8)	103 (58.5)	0.74 (0.55 to 0.99)‡
Secondary end point			
Composite cardiac end point — no. (%)§	94 (52.5)	112 (63.6)	0.72 (0.55 to 0.95)
No. of days alive and out of the hospital (range)¶	82 (0 to 177)	73 (0 to 179)	8 (–8 to 25)
Adverse events			
Composite safety end point — no. (%)‖	43 (24.0)	11 (6.2)	4.74 (2.36 to 9.55)
Moderate or severe bleeding — no. (%)**	39 (21.8)	21 (11.9)	2.06 (1.15 to 3.66)
Limb ischemia — no. (%)	10 (5.6)	2 (1.1)	5.15 (1.11 to 23.84)
Renal-replacement therapy — no. (%)	75 (41.9)	47 (26.7)	1.98 (1.27 to 3.09)
Stroke — no. (%)	7 (3.9)	4 (2.3)	1.75 (0.50 to 6.01)
Cardioversion after ventricular tachycardia or fibrillation — no. (%)	59 (33.0)	52 (29.5)	1.17 (0.75 to 1.83)
Sepsis with positive blood culture†† — no. (%)	21 (11.7)	8 (4.5)	2.79 (1.20 to 6.48)

Time to Death from Any Cause at 180 Days and Time to Treatment Escalation, Heart Transplantation, or Death from Any Cause.

Shown are time-to-event curves for death from any cause at 180 days (Panel A) and for a composite cardiac end-point event (escalation of treatment to additional mechanical circulatory support [short-term or long-term]), heart transplantation, or death from any cause, whichever came first) in the intention-to-treat population. The hazard ratios are from the unadjusted analysis, and the shaded areas indicate 95% confidence intervals. The 95% confidence intervals in Panel B have not been adjusted for multiplicity, and the width of the confidence intervals should not be used to estimate treatment effects. The abbreviation mAFP denotes microaxial flow pump.

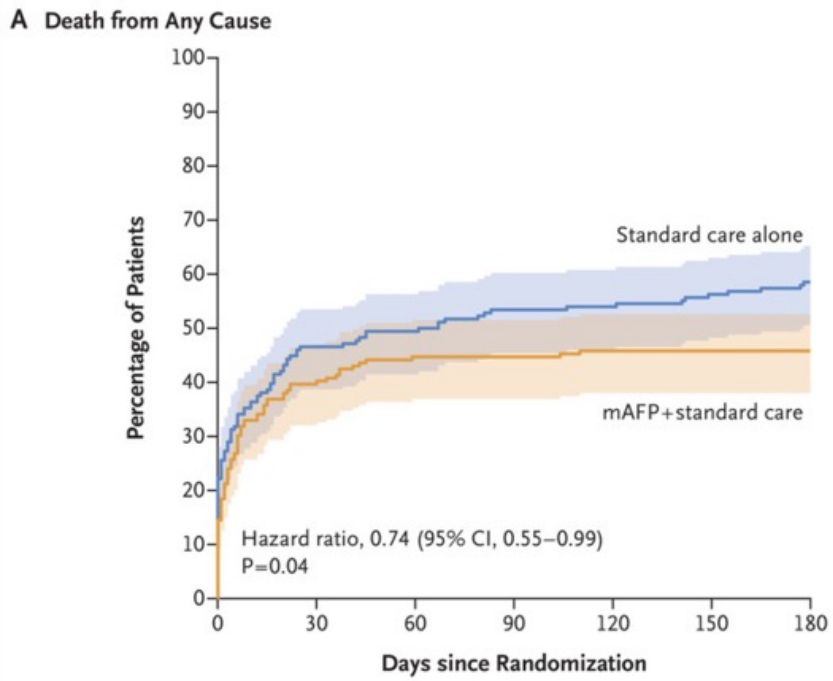

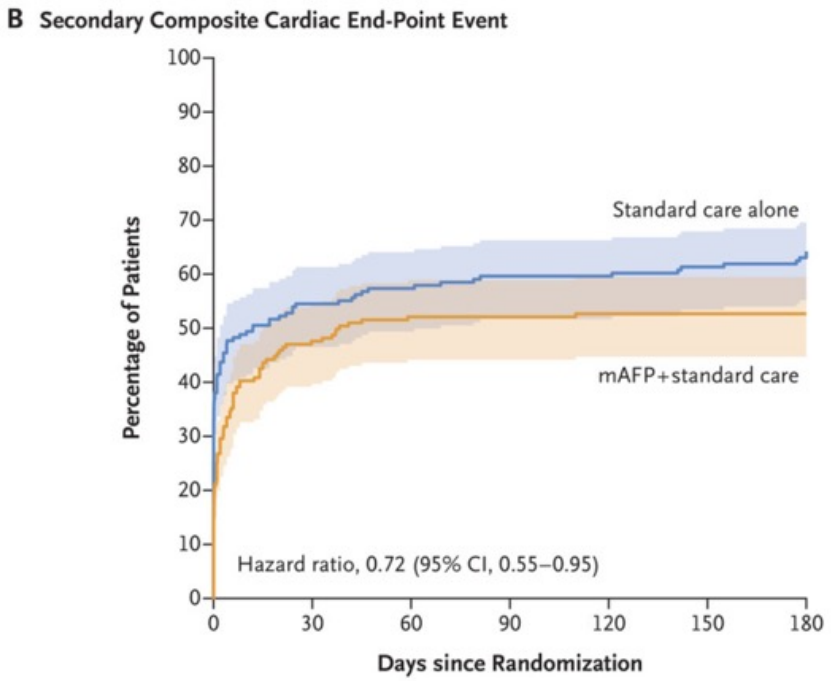

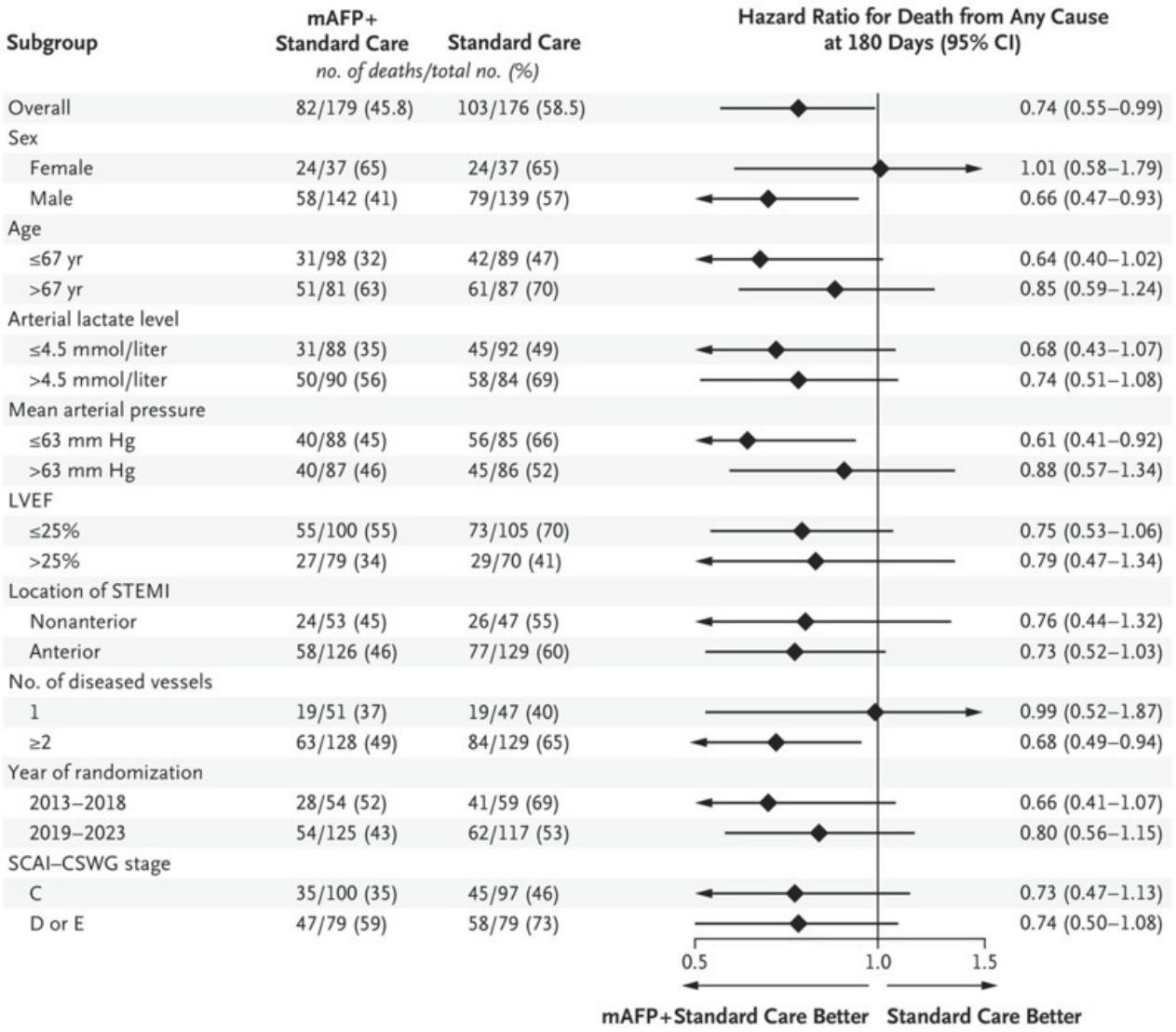
Subgroup
mAFP+ Standard Care
Standard Care
no. of deaths/total no. (%)
Hazard Ratio for Death from Any Cause at 180 Days (95% CI)
Overall 82/179 (45.8) 103/176 (58.5) 0.74 (0.55–0.99)
Sex
Female 24/37 (65) 24/37 (65) 1.01 (0.58–1.79)
Male 58/142 (41) 79/139 (57) 0.66 (0.47–0.93)
Age
≤67 yr 31/98 (32) 42/89 (47) 0.64 (0.40–1.02)
>67 yr 51/81 (63) 61/87 (70) 0.85 (0.59–1.24)
Arterial lactate level
≤4.5 mmol/liter 31/88 (35) 45/92 (49) 0.68 (0.43–1.07)
>4.5 mmol/liter 50/90 (56) 58/84 (69) 0.74 (0.51–1.08)
Mean arterial pressure
≤63 mm Hg 40/88 (45) 56/85 (66) 0.61 (0.41–0.92)
>63 mm Hg 40/87 (46) 45/86 (52) 0.88 (0.57–1.34)
LVEF
≤25% 55/100 (55) 73/105 (70) 0.75 (0.53–1.06)
>25% 27/79 (34) 29/70 (41) 0.79 (0.47–1.34)
Location of STEMI
Nonanterior 24/53 (45) 26/47 (55) 0.76 (0.44–1.32)
Anterior 58/126 (46) 77/129 (60) 0.73 (0.52–1.03)
No. of diseased vessels
1 19/51 (37) 19/47 (40) 0.99 (0.52–1.87)
≥2 63/128 (49) 84/129 (65) 0.68 (0.49–0.94)
Year of randomization
2013–2018 28/54 (52) 41/59 (69) 0.66 (0.41–1.07)
2019–2023 54/125 (43) 62/117 (53) 0.80 (0.56–1.15)
SCAI–CSWG stage
C 35/100 (35) 45/97 (46) 0.73 (0.47–1.13)
D or E 47/79 (59) 58/79 (73) 0.74 (0.50–1.08)
0.5
1.0
1.5
mAFP+Standard Care Better
Standard Care Better

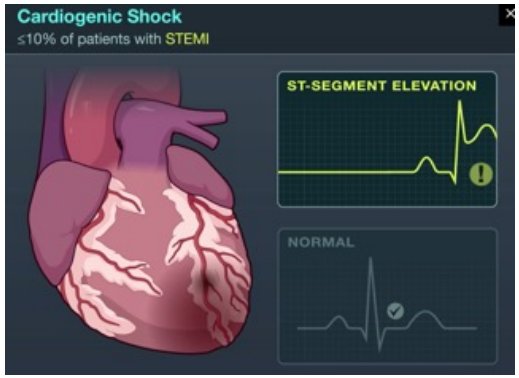

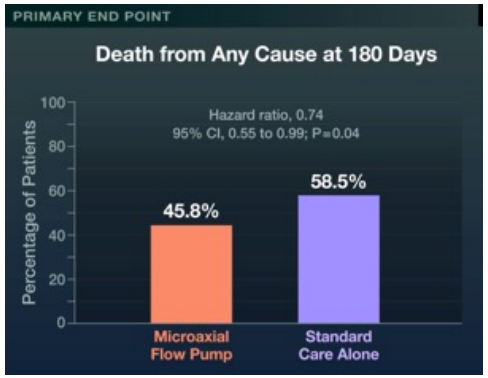

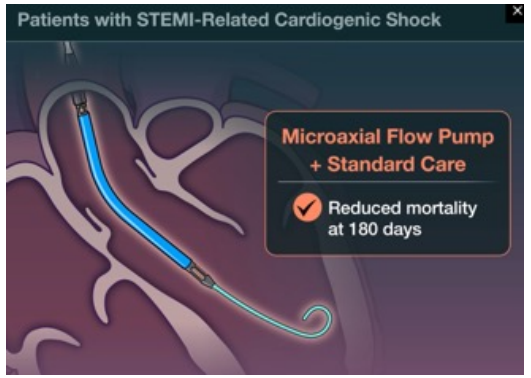

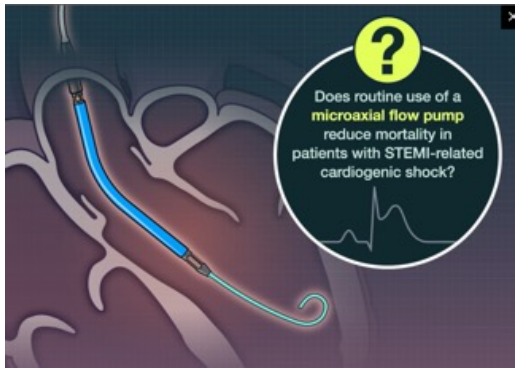

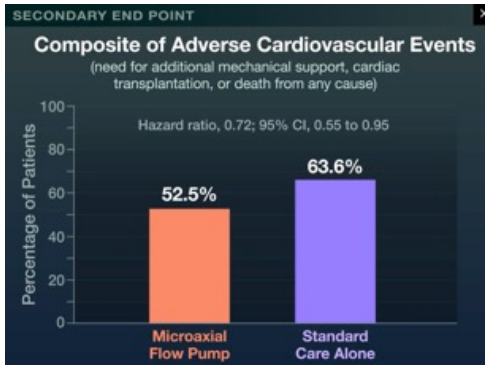

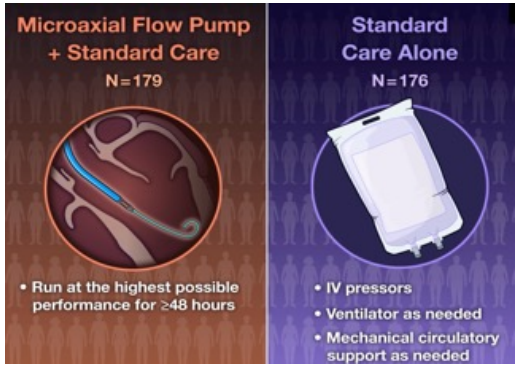

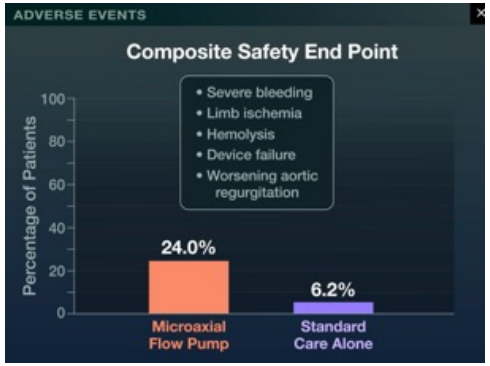

LIMITATIONS AND REMAINING QUESTIONS

- The findings cannot be extrapolated to patients with cardiogenic shock who remain comatose after cardiac arrest and those with non–STEMI-associated cardiogenic shock.
- The trial was conducted at 15 centers in Denmark, Germany, and the United Kingdom; results may differ in other health care systems.
- Data on race and ethnic group were not collected.

HFPEF bei Typ-2 adipösen Diabetiker*innen

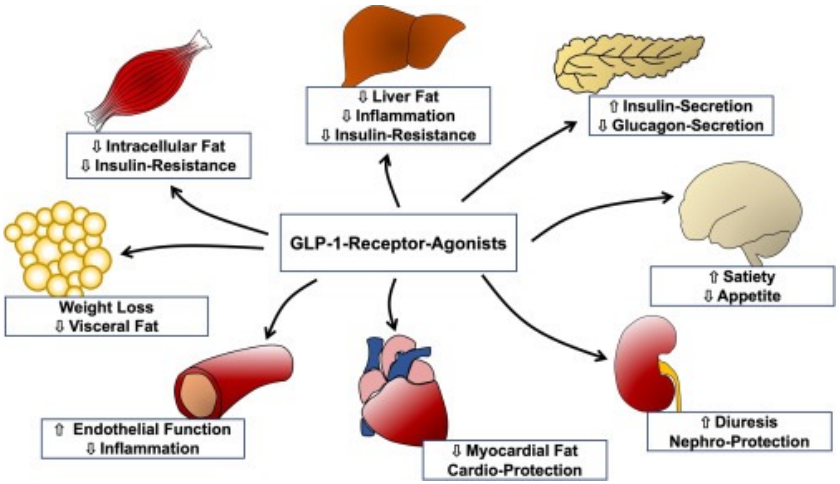

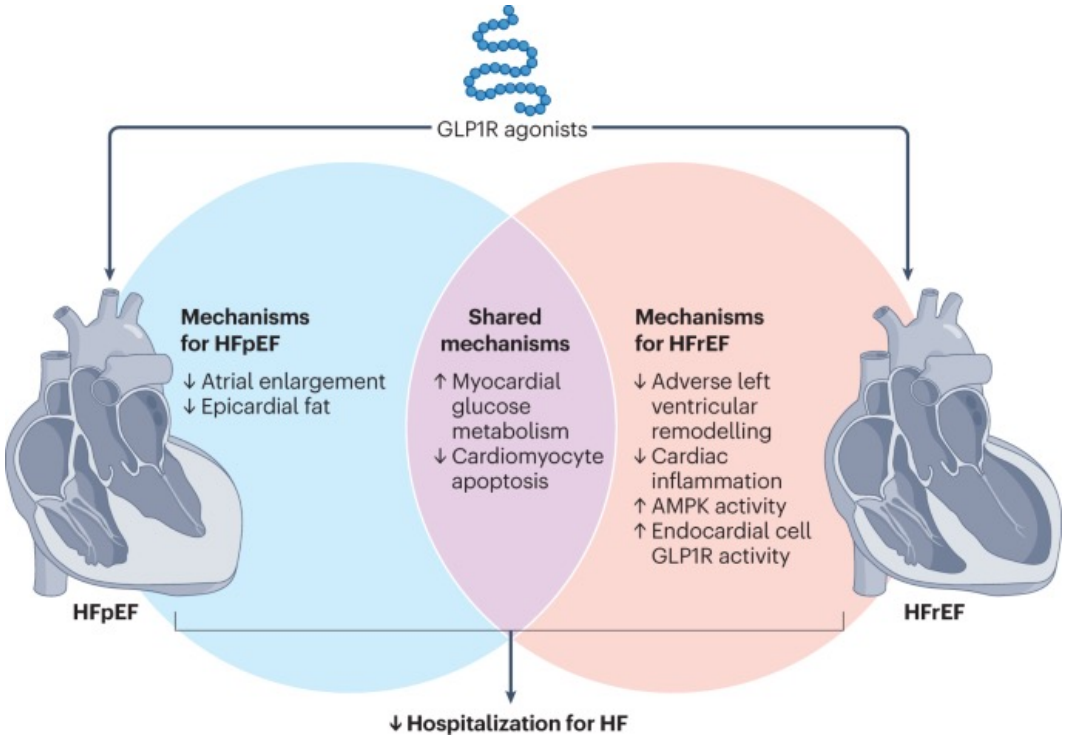

Semaglutide in Patients with Obesity-Related Heart Failure and Type 2 Diabetes

Obesity and type 2 diabetes are prevalent in patients with heart failure with preserved ejection fraction and are characterized by a high symptom burden. No approved therapies specifically target obesity-related heart failure with preserved ejection fraction in persons with type 2 diabetes. We randomly assigned patients who had heart failure with preserved ejection fraction, a body-mass index (the weight in kilograms divided by the square of the height in meters) of 30 or more, and type 2 diabetes to receive once-weekly semaglutide (2.4 mg) or placebo for 52 weeks. The primary end points were the change from baseline in the Kansas City Cardiomyopathy Questionnaire clinical summary score (KCCQ-CSS; scores range from 0 to 100, with higher scores indicating fewer symptoms and physical limitations) and the change in body weight. Confirmatory secondary end points included the change in 6-minute walk distance; a hierarchical composite end point that included death, heart failure events, and differences in the change in the KCCQ-CSS and 6-minute walk distance; and the change in the C-reactive protein (CRP) level.

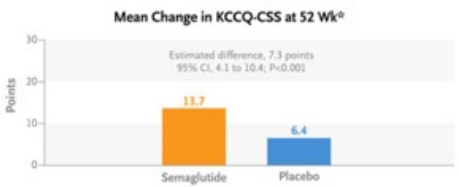

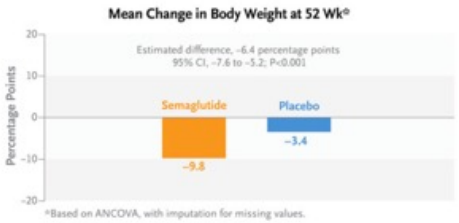

CONCLUSIONS

In patients with type 2 diabetes and heart failure with preserved ejection fraction, once-weekly semaglutide led to fewer heart failure–related symptoms and physical limitations and greater weight loss than placebo at 1 year.

Trial Participants

Persons 18 years of age or older were eligible if they had documented heart failure, a left ventricular ejection fraction of at least 45%, a body-mass index (BMI, the weight in kilograms divided by the square of the height in meters) of at least 30, and at least one of the following findings: elevated left ventricular filling pressures; elevated natriuretic peptide levels plus echocardiographic abnormalities; or hospitalization for heart failure within 12 months before screening plus echocardiographic abnormalities or ongoing treatment with diuretics. Participants were required to have received a diagnosis of type 2 diabetes at least 90 days before screening and to have a glycated hemoglobin level of no more than 10%. Key exclusion criteria were a change in body weight of more than 5 kg within 90 days before screening, a history of type 1 diabetes, use of a GLP-1 receptor agonist within 90 days before screening, and uncontrolled diabetic retinopathy.

End Points

The dual primary end points were the change in the Kansas City Cardiomyopathy Questionnaire clinical summary score (KCCQ-CSS) and the percentage change in body weight from baseline to week 52. The KCCQ is a 23-item, participant-administered instrument that quantifies heart failure–related symptoms, physical function, quality of life, and social function. Scores range from 0 to 100, with higher scores reflecting better health status; the KCCQ-CSS includes the symptom and physical function domains.

The confirmatory secondary end points were the change in the 6-minute walk distance from baseline to week 52, a hierarchical composite end point (described below), and the change in the log-transformed C-reactive protein (CRP) level from screening (week −2) to week 52. The hierarchical composite end point included death from any cause from baseline to week 57.

Demographic and Clinical Characteristics of the Participants at Baseline.

Characteristic	Semaglutide (N=310)	Placebo (N=306)
Female sex — no. (%)	128 (41.3)	145 (47.4)
Median age — yr	69.0 (62.0–74.0)	70.0 (63.0–75.0)
Race — no. (%)†		
Asian	45 (14.5)	31 (10.1)
Black	13 (4.2)	5 (1.6)
White	251 (81.0)	268 (87.6)
Other	1 (0.3)	2 (0.7)
Median BMI (IQR)	36.9 (33.6–41.5)	36.9 (33.5–41.1)
Median NT-proBNP level (IQR) — pg/ml	477.8 (251.2–969.2)	502.3 (240.2–1114.6)
Median CRP level (IQR) — mg/liter	3.7 (1.8–8.4)	3.3 (1.6–8.4)
Median duration of diabetes (IQR) — yr	8.0 (3.6–14.3)	8.0 (4.1–15.2)
Median glycated hemoglobin level (IQR) — %	6.7 (6.2–7.4)	6.9 (6.2–7.7)
Median LVEF (IQR) — %	57.0 (50.0–61.0)	55.0 (50.0–60.0)
Median KCCQ-CSS (IQR) — points‡	60.4 (44.8–72.9)	58.3 (41.1–70.8)
Median 6-minute walk distance (IQR) — m	280.0 (205.1–357.6)	280.0 (200.0–345.0)
Hospitalization for heart failure within 1 year — no. (%)	49 (15.8)	63 (20.6)
Coexisting conditions at screening — no. (%)		
Atrial fibrillation	117 (37.7)	126 (41.2)
Hypertension	255 (82.3)	271 (88.6)
Coronary artery disease	79 (25.5)	69 (22.5)
Obstructive sleep apnea	25 (8.1)	28 (9.2)
NYHA functional class — no. (%)		
II	223 (71.9)	212 (69.3)
III or IV	87 (28.1)	94 (30.7)
Concomitant medication — no. (%)		
Diuretic	246 (79.4)	252 (82.4)
Loop diuretic	186 (60.0)	187 (61.1)
Thiazide	42 (13.5)	43 (14.1)
MRA	105 (33.9)	95 (31.0)
ACEI, ARB, or ARNI	249 (80.3)	253 (82.7)
Beta-blocker	257 (82.9)	253 (82.7)
SGLT2 inhibitor	107 (34.5)	95 (31.0)

Efficacy End Points

End Point	Semaglutide (N=310)	Placebo (N=306)	Estimated Difference or Ratio (95% CI)	P Value
Dual primary end points				
Change in KCCQ-CSS from baseline to week 52 — points	13.7	6.4	7.3 (4.1 to 10.4)†	<0.001
Percentage change in body weight from baseline to week 52	−9.8	−3.4	−6.4 (−7.6 to −5.2)†	<0.001
Confirmatory secondary end points				
Change from baseline to week 52 in 6-minute walk distance — m	12.7	−1.6	14.3 (3.7 to 24.9)†	0.008
Hierarchical composite end point — crude percentage of wins‡	58.7	36.8	1.58 (1.29 to 1.94)§	<0.001
Change from baseline to week 52 in CRP level — %¶	−42.0	−12.8	0.67 (0.55 to 0.80)‖**	<0.001
Supportive secondary end points				
Change from baseline to week 52 in systolic blood pressure — mm Hg	−4.2	−1.7	−2.5 (−5.3 to 0.3)†	—
Change from baseline to week 52 in waist circumference — cm	−9.0	−2.6	−6.4 (−7.7 to −5.0)†	—
Change from baseline to week 52 in KCCQ-OSS — points††	13.5	6.2	7.3 (4.2 to 10.4)†	—
Change from baseline to week 52 in glycated hemoglobin level — %	−0.7	0.1	−0.8 (−1.0 to −0.6)†	—
Percentage reduction in body weight at week 52 — % of participants				
≥10% reduction	51.4	10.4	7.3 (4.7 to 11.4)§	—
≥15% reduction	22.4	4.0	5.4 (2.8 to 10.2)§	—
≥20% reduction	7.3	1.8	3.2 (1.3 to 8.2)§	—
Increase in KCCQ-CSS at week 52 — % of participants				
≥5-point increase	73.0	54.8	2.3 (1.6 to 3.3)§	—
≥10-point increase	58.0	42.6	2.1 (1.4 to 2.9)§	—
Attainment of anchor-based threshold for change in KCCQ-CSS — % of participants‡‡	42.7	30.5	2.0 (1.4 to 2.9)§	—
Attainment of anchor-based threshold for change in 6-minute walk distance — % of participants§§	52.7	39.2	1.7 (1.2 to 2.3)§	—
Exploratory end points assessed in the overall population				
Change from baseline to week 52 in NT-proBNP level — %	−23.2	−4.6	0.8 (0.7 to 0.9)‖¶¶	—
Adjudicated heart failure event (hospitalization or urgent visit for heart failure), time-to-event analysis — no. of events (% of participants)	7 (2.3)	18 (5.9)	0.40 (0.15 to 0.92)‖‖	—
≥15-point increase in KCCQ-CSS at week 52 — % of participants	44.5	32.7	1.9 (1.3 to 2.8)§	—

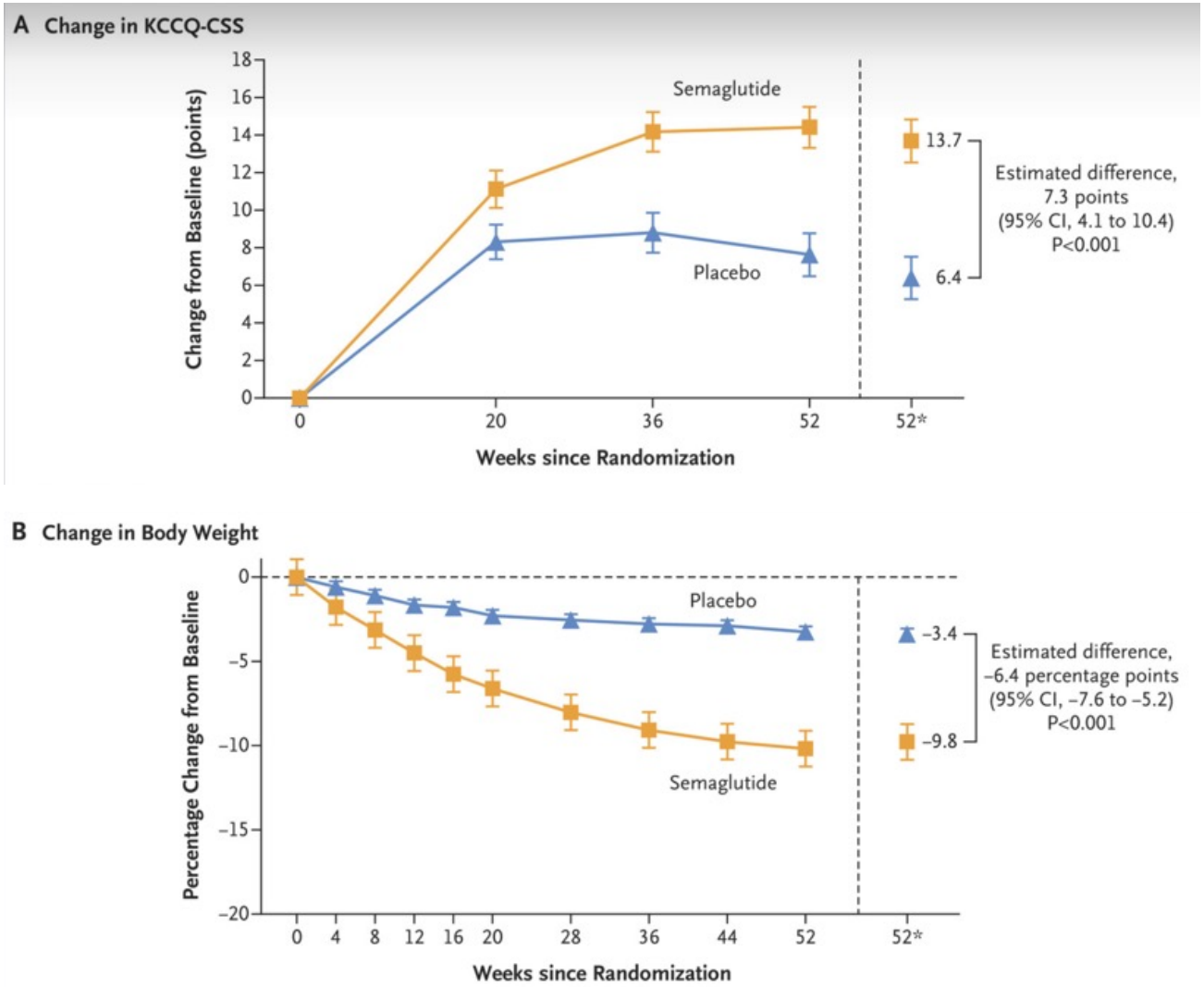

Change from Baseline to Week 52 in the Dual Primary End Points.

Analyses are based on the treatment policy estimand, reflect the full analysis population, and are from the in-trial period. Shown are the observed (i.e., as-measured) mean changes from baseline in the Kansas City Cardiomyopathy Questionnaire clinical summary score (KCCQ-CSS; scores range from 0 to 100, with higher scores indicating fewer symptoms and physical limitations) and percentage changes in body weight. I bars indicate the standard error, and the numbers below the graphs are the numbers of participants contributing to the mean (with variations in participants attending certain trial visits). The data at week 52* are the estimated mean changes from baseline to week 52 based on analysis of covariance (ANCOVA) and an imputation approach for missing data.

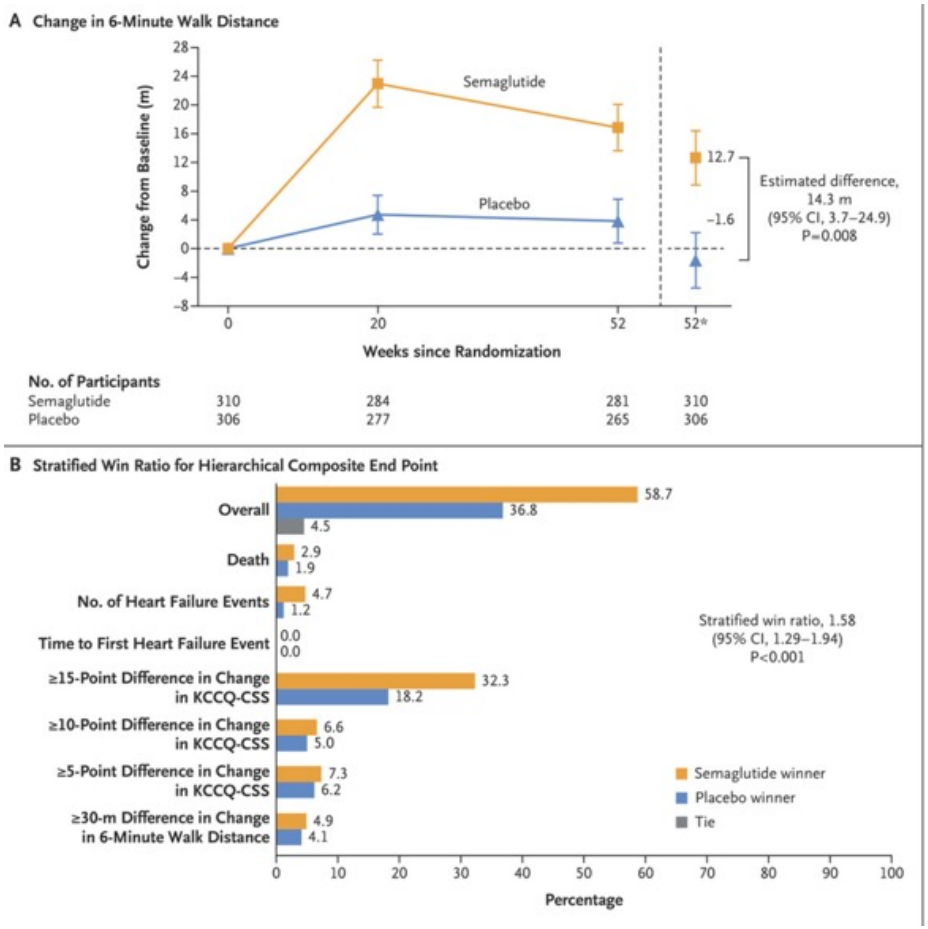

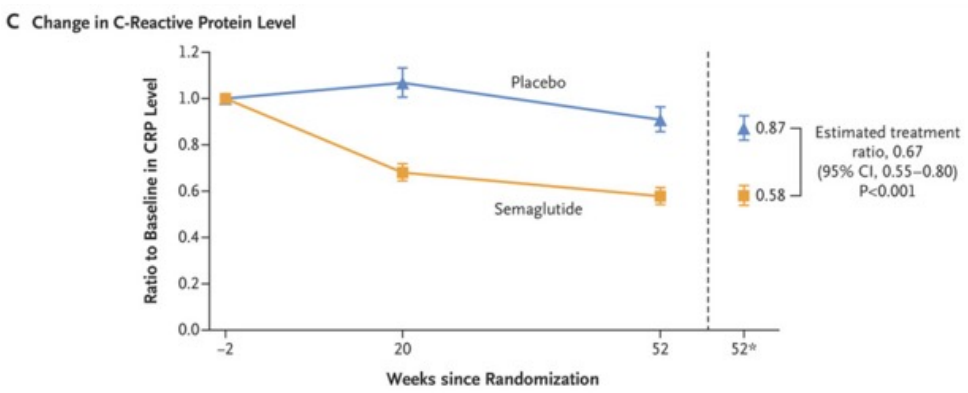

Change from Baseline to Week 52 in Confirmatory Secondary End Points. Analyses are based on the treatment policy estimand, reflect the full analysis population, and are from the in-trial period. Panel A shows the observed (i.e., as-measured) mean changes from baseline in the 6-minute walk distance; I bars indicate the standard error. Panel B shows the stratified win ratio for the hierarchical composite end point, which included death from any cause from baseline to week 57; the number and timing of heart failure events (defined as adjudicated events of hospitalization for heart failure or urgent visits in which intravenous therapy was administered, baseline to week 57); differences of at least 15, at least 10, and at least 5 points in the change in the KCCQ-CSS from baseline to week 52; and a difference of a least 30 m in the change in the 6-minute walk distance from baseline to week 52. Panel C shows the observed mean changes in the C-reactive protein (CRP) levels calculated on a logarithmic scale and back-transformed to a linear scale

Reportable Adverse Events during the Treatment Period.

Beats placebo

Adverse Event	Semaglutide (N=310)			Placebo (N=306)			P Value†
	no. of participants (%)	*no. of events*	*events/100 person-yr*	*no. of participants (%)*	*no. of events*	*events/100 person-yr*	
Serious adverse event	55 (17.7)	101	33.1	88 (28.8)	168	55.0	0.002
Serious adverse event leading to discontinuation of semaglutide or placebo	6 (1.9)	6	2.0	11 (3.6)	14	4.6	—
Gastrointestinal disorder	1 (0.3)	1	0.3	0	0	0	—
Adverse event leading to discontinuation of semaglutide or placebo	33 (10.6)	45	14.7	25 (8.2)	34	11.1	—
Gastrointestinal disorder	20 (6.5)	27	8.8	9 (2.9)	10	3.3	—
Fatal event	4 (1.3)	4	1.3	10 (3.3)	15	4.9	—
Most frequent serious adverse events‡							—
Cardiac disorder§	19 (6.1)	23	7.5	40 (13.1)	58	19.0	0.004
Cardiac arrhythmia	12 (3.9)	13	4.3	10 (3.3)	12	3.9	—
Coronary artery disorder	5 (1.6)	5	1.6	9 (2.9)	10	3.3	—
Heart failure	4 (1.3)	4	1.3	27 (8.8)	35	11.5	—
Vascular disorder	5 (1.6)	5	1.6	6 (2.0)	6	2.0	0.77
Infection or infestation	12 (3.9)	17	5.6	27 (8.8)	38	12.4	0.01
Gastrointestinal disorder	5 (1.6)	5	1.6	5 (1.6)	5	1.6	1.00
Nervous system disorder	6 (1.9)	7	2.3	6 (2.0)	7	2.3	1.00
Renal or urinary disorder	2 (0.6)	2	0.7	8 (2.6)	8	2.6	0.06
Respiratory, thoracic, or mediastinal event	6 (1.9)	6	2.0	6 (2.0)	7	2.3	1.00
Musculoskeletal or connective-tissue event	5 (1.6)	6	2.0	8 (2.6)	8	2.6	0.42
Injury, poisoning, or procedural event	7 (2.3)	11	3.6	2 (0.7)	2	0.7	0.18
Metabolism or nutrition disorder	3 (1.0)	3	1.0	4 (1.3)	4	1.3	0.72
General disorder or administration-site reaction	1 (0.3)	1	0.3	3 (1.0)	3	1.0	0.37
Benign, malignant, or unspecified neoplasm	8 (2.6)	8	2.6	7 (2.3)	7	2.3	1.00
Adjudicated events¶							—
Death from any cause	6 (1.9)	6	1.8	10 (3.3)	10	3.0	—
Death from cardiovascular causes	1 (0.3)	1	0.3	4 (1.3)	4	1.2	—
Heart failure event	7 (2.3)	8	2.4	18 (5.9)	23	7.0	—
Death from undetermined cause	1 (0.3)	1	0.3	0	0	0	—

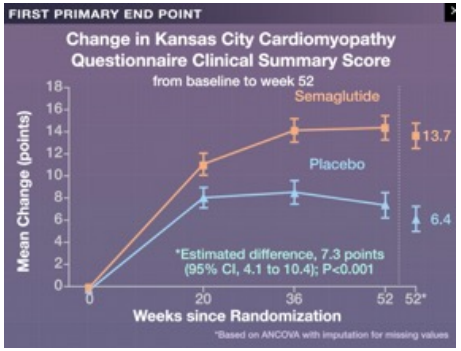

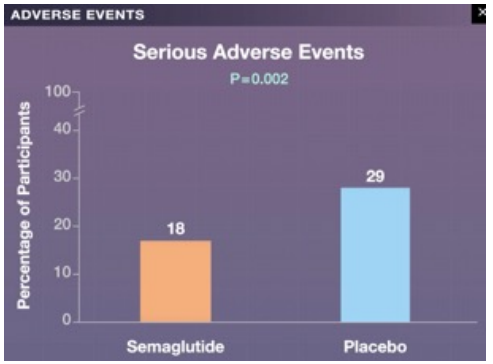

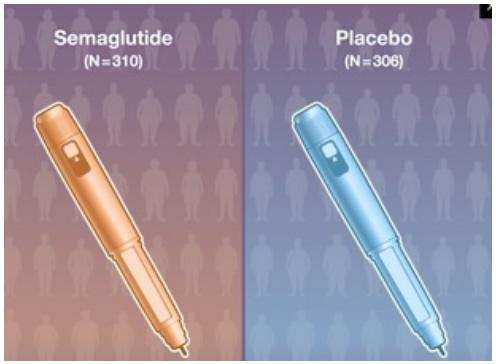

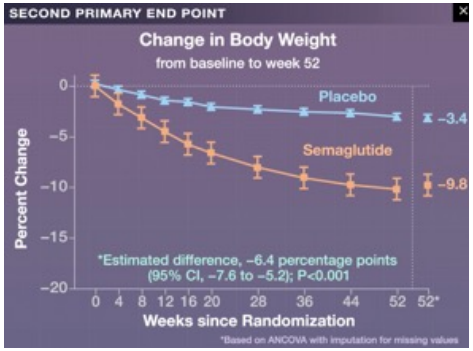

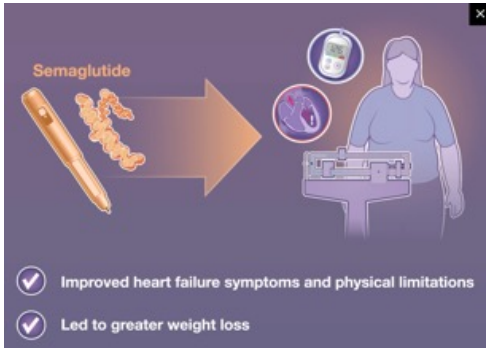

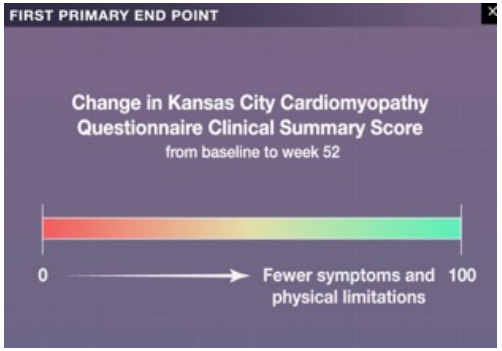

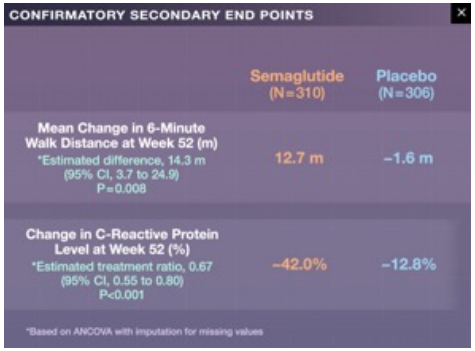

LIMITATIONS AND REMAINING QUESTIONS

- Non-White participants were underrepresented in the trial, thus limiting generalizability.
- The trial was not designed to evaluate clinical events such as hospitalizations and urgent visits for heart failure.
- The trajectory of the effects of semaglutide suggested persistent improvements over time as compared with placebo, but the durability of these effects beyond 1 year is unknown.

Das Retinoblastom-Protein, kurz pRB, ist ein Tumorsuppressor, der eine entscheidende Rolle in der Regulation des Zellzyklus spielt. Es kontrolliert den Übergang von der G1-Phase zur S-Phase des Zellzyklus.
Der Name des Retinoblastom-Proteins geht auf seine Rolle bei der Entstehung des Retinoblastoms zurück. In diesem Zusammenhang wurde es als erstes Tumorsuppressorprotein entdeckt. Sein Vorkommen ist jedoch keinesfalls auf Zellen der Retina beschränkt. Das Retinoblastom-Protein entfaltet seine Wirkung durch Bindung (und somit Inaktivierung) des Transkriptionsfaktors E2F. E2F würde normalerweise die S-Phase des Zellzyklus durch Expression entsprechender Gene einleiten. Das Retinoblastom-Protein ist dephosphoryliert aktiv und inaktiviert in dieser Form E2F so lange, bis es phosphoryliert wird. Dies geschieht durch den CDK2/Cyclin E-Komplex oder den CDK4/Cyclin D- sowie CDK6/Cyclin D-Komplex, die ein Fortschreiten des Zellzykluses bewirken. Das Retinoblastom-Protein kontrolliert also den Übergang von der G1-Phase in die S-Phase des Zellzyklus.

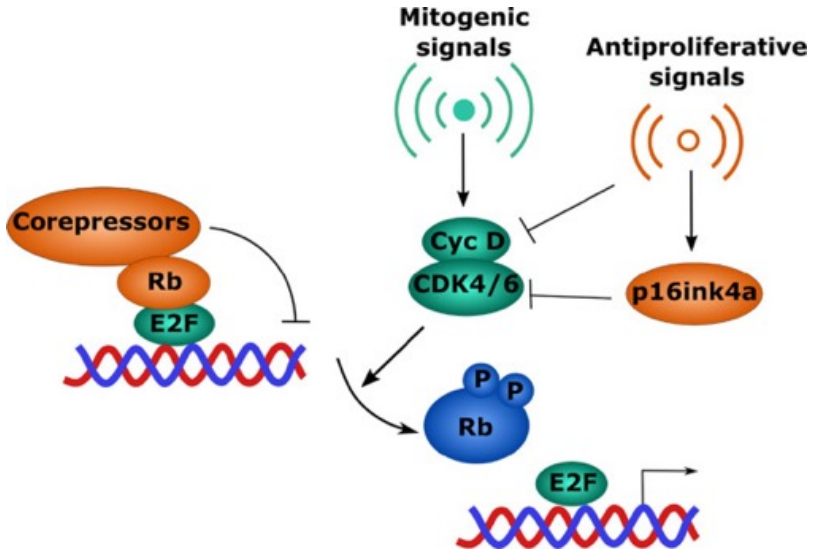

The *RB1* Story: Characterization and Cloning of the First Tumor Suppressor Gene. Genes (Basel) 2019

REVIEW ARTICLE

Retinoblastoma Origins and Destinations

Retinoblastoma is a childhood retinal cancer that occurs in approximately 6 of 100,000 live births, with 250 to 300 new cases per year in the United States and approximately 8000 worldwide. Although retinoblastoma is routinely cured when detected early, more advanced and genomically altered retinoblastomas present substantial clinical challenges and risk for recurrence, metastasis, and death. We have long known that most retinoblastomas are initiated by biallelic inactivation of the retinoblastoma gene (*RB1*), but until recently the basis and clinical relevance of the retina-specific tropism have been unclear. Studies performed in the past decade have identified the retinoblastoma cell of origin, the basis of its sensitivity to *RB1* loss, the steps preceding tumor emergence, and postemergence genomic and epigenetic changes associated with treatment resistance and metastasis. Our growing understanding of the genesis of retinoblastoma may enable the development of improved therapies for recurrent and metastatic tumors, and deeper understanding may enable the prevention of retinoblastoma in children with a genetic predisposition.

Human Retina-specific Effects of a Ubiquitous Cell-Cycle Regulator

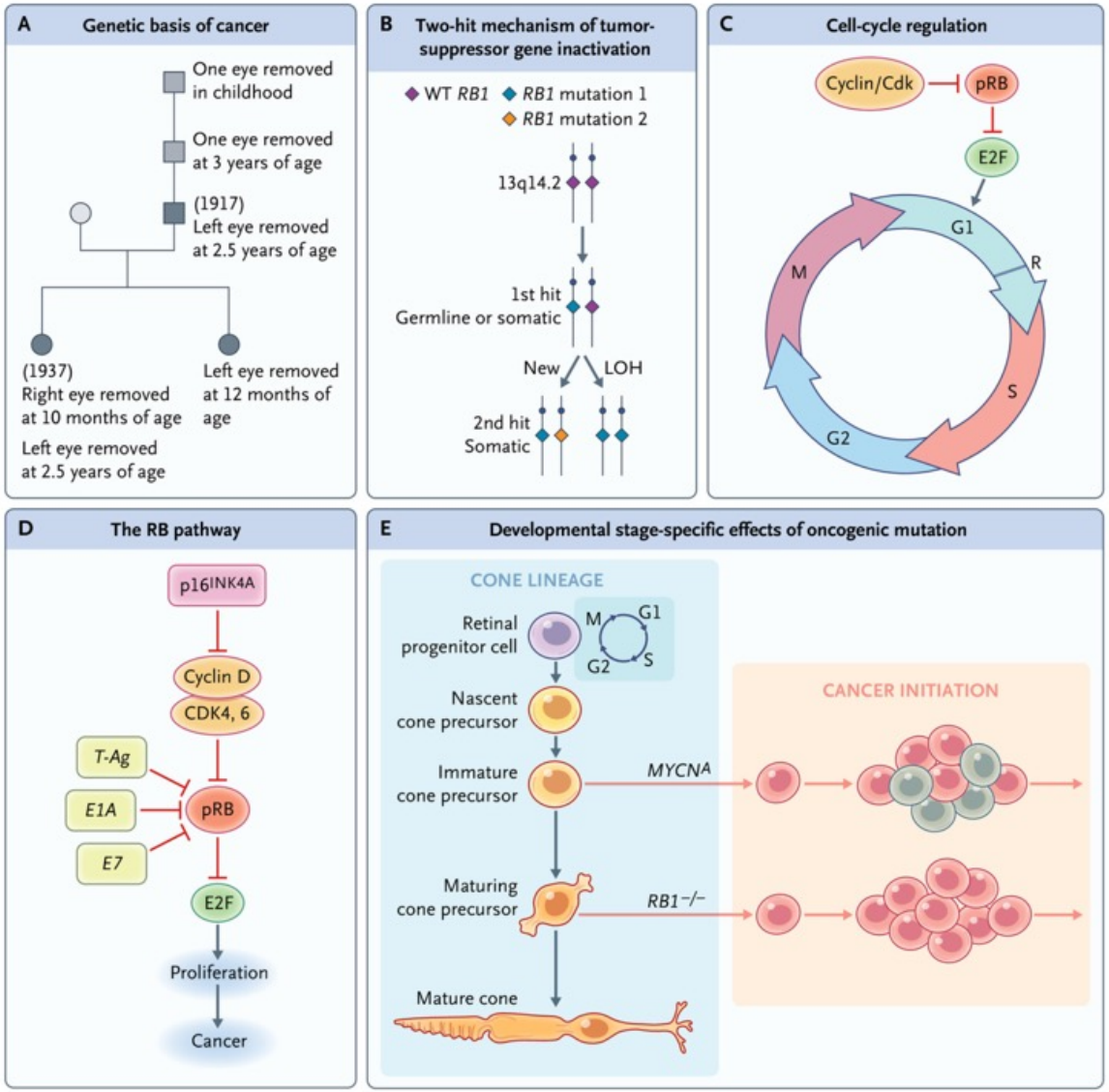

Contributions of Retinoblastoma Research to Our Understanding of Human Tumorigenesis.
Panel A shows the pedigree of a family with genetic transmission of retinoblastoma predisposition, which showed that cancer can be a genetic disease. Panel B shows the two-hit mechanism of tumor-suppressor gene inactivation, which was inferred from the timing of retinoblastoma appearance and biallelic *RB1* inactivation in retinoblastoma tumors. The two *RB1* alleles are mutated somatically in nonheritable cases and through a germline first hit plus a somatic second hit in heritable cases. The second hit may be independent of the first or reproduce the first through loss of heterozygosity (LOH). Panel C shows pRB-mediated cell-cycle regulation, wherein pRB inhibits E2F-activated transcription of genes required for G1-to-S phase progression, and phosphorylation of pRB by cyclin-dependent kinase (CDK) releases E2F and enables cell-cycle entry. Panel D shows the RB pathway, which is disrupted in human cancers through pRB loss, deregulated cyclin D:CDK4 or cyclin D:CDK6 activity, $p16^{INK4A}$ loss, or expression of DNA tumor virus oncoproteins such as human papilloma virus E7. Panel E shows the cooperation of oncogenic mutations and cell-of-origin circuitry that is specific to the developmental stage of the cone precursors, illustrated by the sensitivity of the immature cone precursor to *MYCN* amplification ($MYCN^A$) and the sensitivity of the maturing cone precursor to biallelic *RB1* loss.

N-Myc, kurz für N-Myc-Protoonkogen-Protein, ist ein Transkriptionsfaktor der MYC-Familie. Er reguliert die Transkription verschiedener Gene in Tumorzellen, insbesondere in Tumoren des Nervensystems.

An Intrinsically Cancer-Predisposed Retinoblastoma Origin

We and others identified retinoblastoma features that suggested that the tumors originate in long- and medium-wavelength cone precursors, and we discovered features of these cone precursors that contribute to their sensitivity to pRB loss. After maturation, these long- and medium-wavelength cone precursors form the cone photoreceptors responsible for red and green color vision (short-wavelength cones are responsible for blue color vision, and rods for night vision). Long- and medium-wavelength cones are present across the entire retina, concentrated in the central macular region and especially in the fovea, which is used for high-acuity vision.

Multistep Tumorigenesis in *RB1*$^{-/-}$ and *MYCN*^{A}*RB1*$^{+/+}$ Contexts

Despite the rapid responses of cone precursors to pRB loss and MYCN overexpression, their initial proliferation probably does not lead to retinoblastoma directly. Indeed, *RB1*$^{-/-}$ retinoblastomas are usually detected from a few weeks before birth until 8 years of age, which is inconsistent with uniform proliferation. A clue to the variable onset comes from the finding that 15 to 20% of retinoblastomas have histologic features of retinoma — a benign lesion that rarely progresses to retinoblastoma when observed in patients — in the region where the tumor emerges from the retina.

Genomic and Epigenomic Progression toward More Malignant Behavior

After the emergence of retinoblastoma foci, secondary genomic and epigenomic changes are thought to mediate progression to more invasive and therapy-resistant states. Indeed, most *RB1*$^{-/-}$ retinoblastomas that warrant surgical removal have somatic chromosome copy-number alterations and single nucleotide variants. However, the changes are usually present in only a subset of the tumor cells, which suggests that individual changes usually occur in a single cell after tumors emerge and become more prevalent within the tumor through their ability to accelerate tumor cell proliferation. *MYCN*^{A}*RB1*$^{+/+}$ retinoblastomas have fewer copy-number alterations, which is consistent with their requiring less genomic evolution than *RB1*$^{-/-}$ retinoblastomas before clinical presentation.

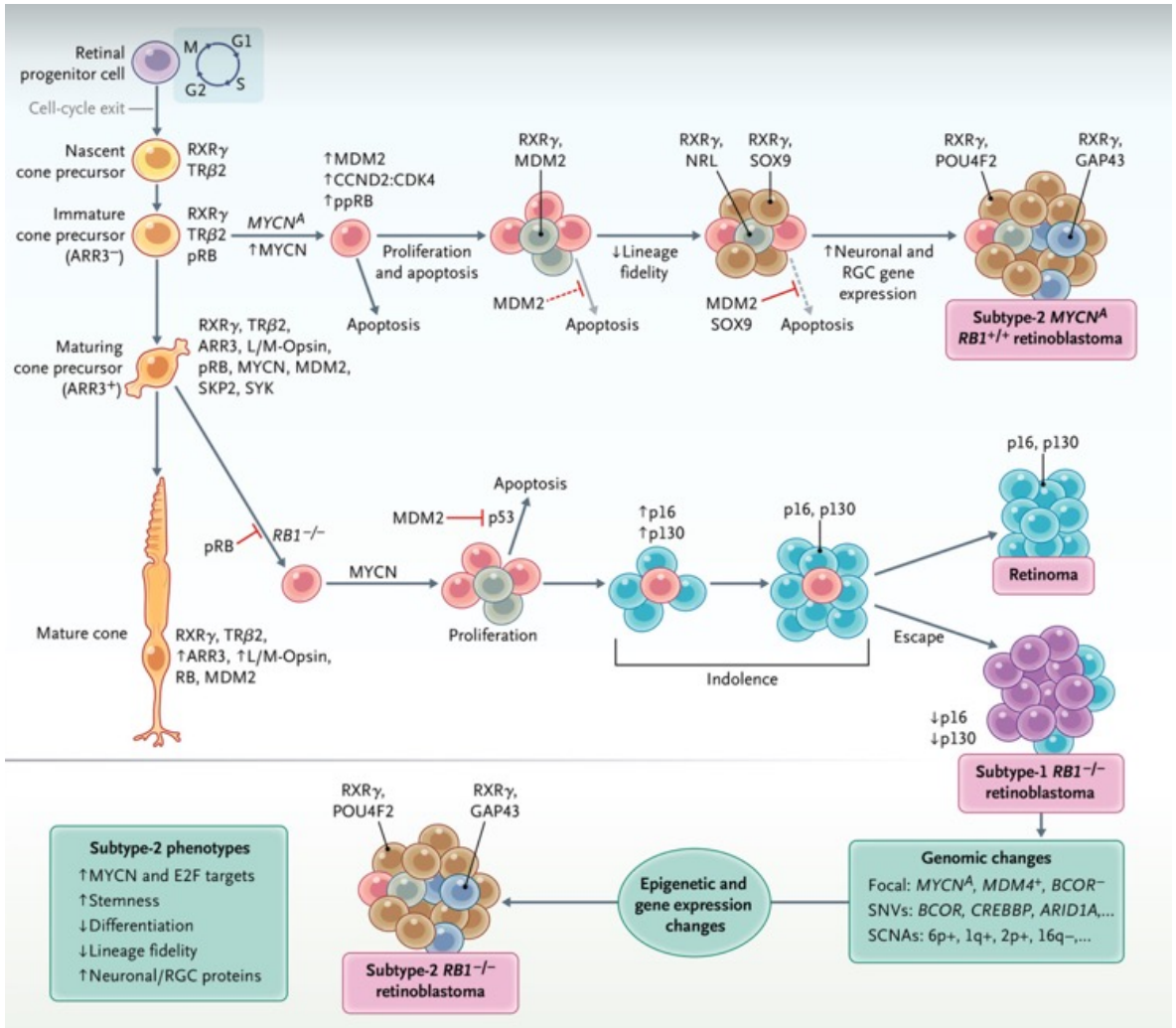

Cone-Precursor Origins of *RB1*$^{-/-}$ and *MYCN*^{A}*RB1*$^{+/+}$ Retinoblastoma.

Shown are the pathways through which normal cone photoreceptor development may be diverted to retinoblastoma genesis in response to biallelic *RB1* inactivation (*RB1*$^{-/-}$) or *MYCN*^{A}. The path on the left-hand side shows proliferating retinal progenitor cells that exit the cell cycle to form nascent, immature, and maturing cone precursors and mature cone photoreceptors. Maturing cone precursors are distinguished by up-regulated phototransduction proteins (retinal cone arrestin-3 [ARR3], long- and medium-wavelength [L/M]–opsin) and proliferation-related proteins (pRB, MYCN, MDM2, SKP2, SYK) and early morphologic changes. Whereas *MYCN*^{A} and biallelic *RB1* loss most likely occur in retinal progenitor cells, MYCN overexpression and pRB depletion first elicited aberrant proliferation in immature and maturing cone precursors, respectively.

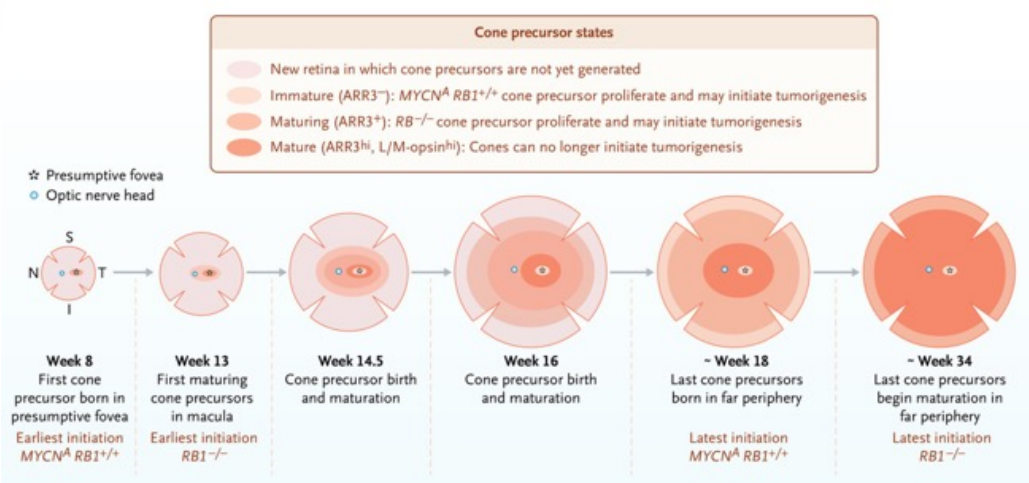

Proposed Spatiotemporal Pattern of Cone-Precursor Birth, Maturation, and Retinoblastoma Initiation.
Shown is the spatiotemporal pattern of cone-precursor differentiation states at different embryonic postconception retinal ages, viewed as a flat-mounted left retina. Orientation is shown at week 8 (S, superior; T, temporal; I, inferior; N, nasal). The first and most central cone precursors in the presumptive fovea (asterisk) are inferred to be present at approximately week 8 and first express maturation marker ARR3 at approximately week 13.This is followed by a central-to-peripheral wave of cone-precursor birth and maturation, with the last, most peripheral cone precursors born by week 18 and expected to initiate maturation by approximately week 34 (given initial L/M opsin expression in peripheral retina between weeks 34 and 37 and slightly earlier ARR3 than L/M opsin expression as in central retina). In vitro studies in which overexpressed MYCN induces immature cone-precursor proliferation and pRB loss induces maturing cone-precursor proliferation predict the timing of the initial $MYCN^{A}RB1^{+/+}$ and $RB1^{-/-}$ cone-precursor proliferation, signifying the initiation of each type of retinoblastoma, at each retinal position. Cone-precursor birth and maturation ages are estimated according to available data, assume that maturation occurs in a largely symmetric pattern, and were not experimentally verified.

Therapeutic Targets Identified in Human Retinoblastoma Genesis Studies.

Candidate Target (Agent Class) and Tumorigenesis Stage*	References
Targets evaluated with preclinical agents	
MDM2 (MDM2 antagonists)	
Initiation and propagation	Target identified: Xu, 2009[17]; Xu, 2014[25] Agents tested: Elison, 2006[60]; Laurie, 2006[61]
MYCN (Aurora kinase inhibitors)	
Initiation, propagation, and progression to subtype 2	Target identified: Xu, 2009[17]; Rushlow, 2012[11]; Xu, 2014[25]; Liu, 2021[19]; Singh, 2022[23]; Blixt, 2022[24] Agents tested: Gong, 2019[62]; Oser, 2019[63]; Yang, 2022[64]
SKP2 (NEDD8 activating enzyme [NAE] inhibitor)	
Initiation and propagation	Target identified: Wang, 2010[29]; Xu, 2014[25]; Xu, 2017[33]; Li, 2019[32] Agents tested: Aubry, 2020[65]
SYK (SYK inhibitors)	
Initiation and propagation	Target identified and agents tested: Zhang, 2012[31]; Liu, 2020[22]; Shayler, 2022[30]
E2F1 (E2F inhibitor)	
MYN^{A}*RB1*$^{+/+}$ and subtype 2	Target identified: Liu, 2021[19] Target identified and agents tested: Zhang, 2023[66]
Potential targets based on shRNA-mediated knockdown in cone precursors	
TRβ2	
Initiation and propagation	Target identified: Xu, 2009[17]; Xu, 2014[25]
RXRγ	
Initiation and propagation	Target identified: Xu, 2009[17]; Xu, 2014[25]

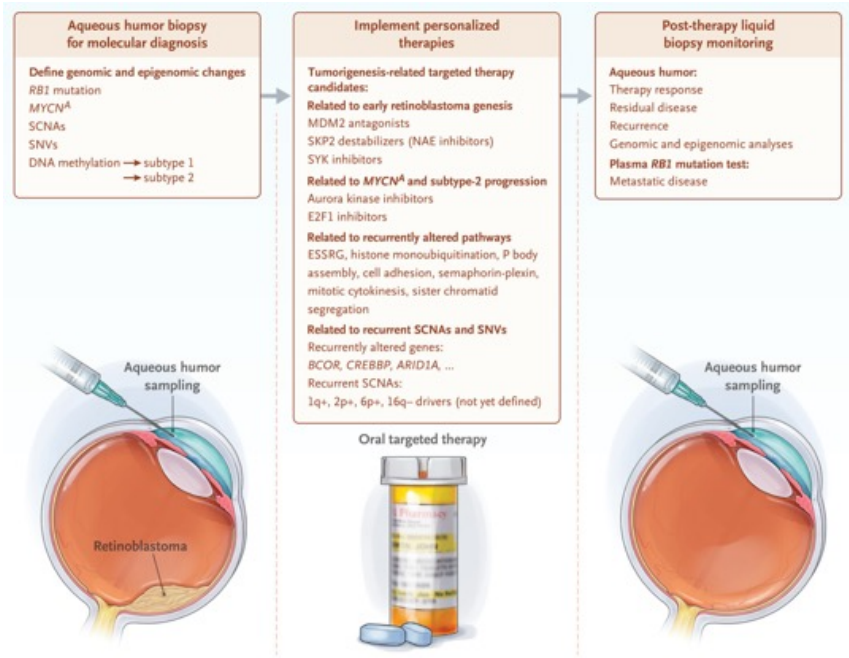

Future Approaches: Genomically and Epigenomically–Informed Retinoblastoma Diagnosis, Therapy, and Monitoring.

Current investigational studies suggest that future clinical practice may include liquid biopsy of aqueous humor at diagnosis to assess genomic and epigenomic properties and identify precision therapies. Investigational studies show the detection of *RB1* mutations, *MYCN*^{A}, secondary SCNAs and SNVs, and DNA methylation-based discrimination of subtype-1 tumors as compared with subtype-2 tumors

Aortic Coarctation

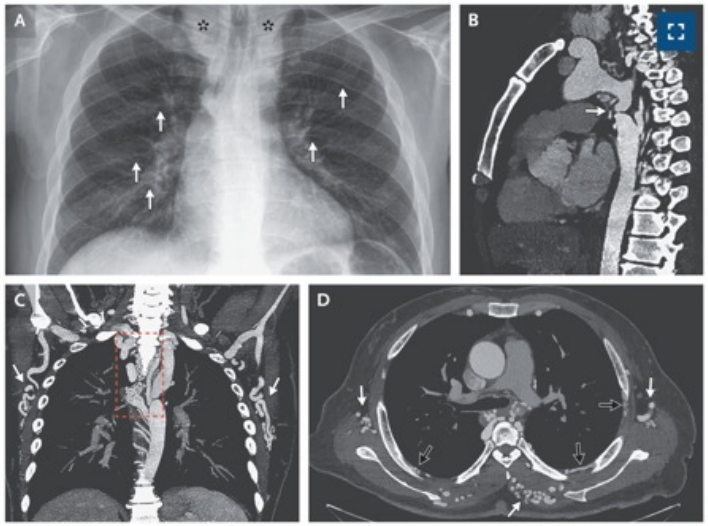

A 35-year-old man was referred to his primary care physician for evaluation of previously unknown hypertension that had been identified during a medical screening for his rugby team. The patient was asymptomatic. The blood pressure was 146/89 mm Hg in the left arm, 146/99 mm Hg in the right arm, 104/83 mm Hg in the left leg, and 109/90 mm Hg in the right leg. On physical examination, a radial–femoral delay was present. A chest radiograph showed notching of posterior ribs 3 through 8 (Panel A, arrows) and widened paratracheal stripes (Panel A, asterisks). Computed tomographic (CT) angiography of the chest revealed coarctation of the descending aorta, with the isthmus measuring 3 mm in diameter (reference range for the patient's age and size, 18 to 25) (Panel B, arrow). CT angiography also showed extensive collateral arterial circulation in the soft tissues (Panels C and D, white arrows), along the trachea (which accounted for the paratracheal stripes seen on chest radiography) (Panel C, dashed box), and in the intercostal spaces (which accounted for the notching of the ribs seen on chest radiography) (Panel D, black arrows). A transthoracic echocardiogram showed left ventricular hypertrophy and a pressure gradient of 25 mm Hg across the coarctation. No other cardiac abnormalities were identified. Percutaneous stenting of the aortic coarctation was performed without complications. At a follow-up visit 1 month after the procedure, the patient's blood pressure had improved. At a 3-month follow-up visit, repeat imaging showed a marked decrease in collateral arterial circulation.

Hemotympanum with a Basilar Skull Fracture

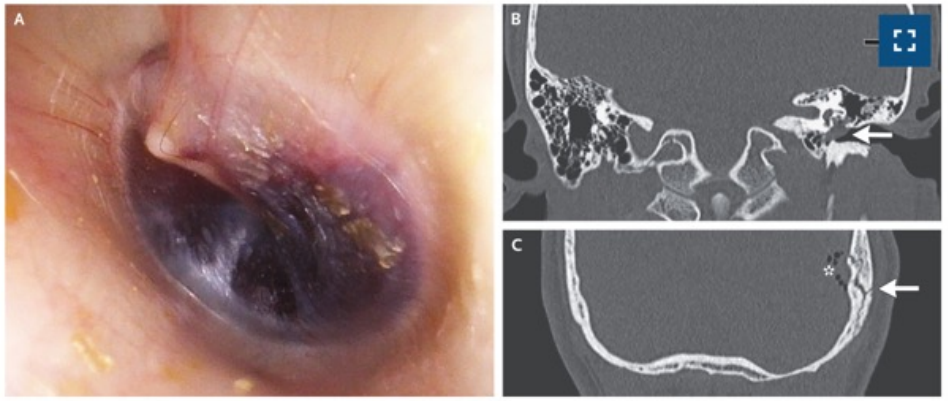

A 15-year-old boy presented to the emergency department with a 1-hour history of hearing loss and pain in the left ear after he had tripped and fallen on the street, striking his head on the pavement. He reported a headache but no ear drainage, tinnitus, vertigo, nasal discharge, or vomiting. The physical examination was notable for mild swelling behind the left ear, with no bruising. An otoscopic examination of the left ear showed blood behind the tympanic membrane (Panel A). Rinne and Weber testing, as well as pure-tone audiometry, indicated the presence of mild conductive hearing loss in the left ear. The remainder of the neurologic examination was normal. Computed tomography of the head revealed fluid in the middle ear (Panel B, white arrow) and a longitudinal left temporal bone fracture (Panel B, black arrow), as well as separation of the occipitotemporal suture (Panel C, arrow) and pneumocephalus (Panel C, asterisk). A final diagnosis of a basilar skull fracture resulting in hemotympanum was made. The patient was admitted for observation, serial neurologic examinations, and repeat imaging. At a follow-up visit 2 weeks after hospital discharge, his ear pain and hemotympanum had abated and his hearing had returned to normal.

Mitochondrial DNA

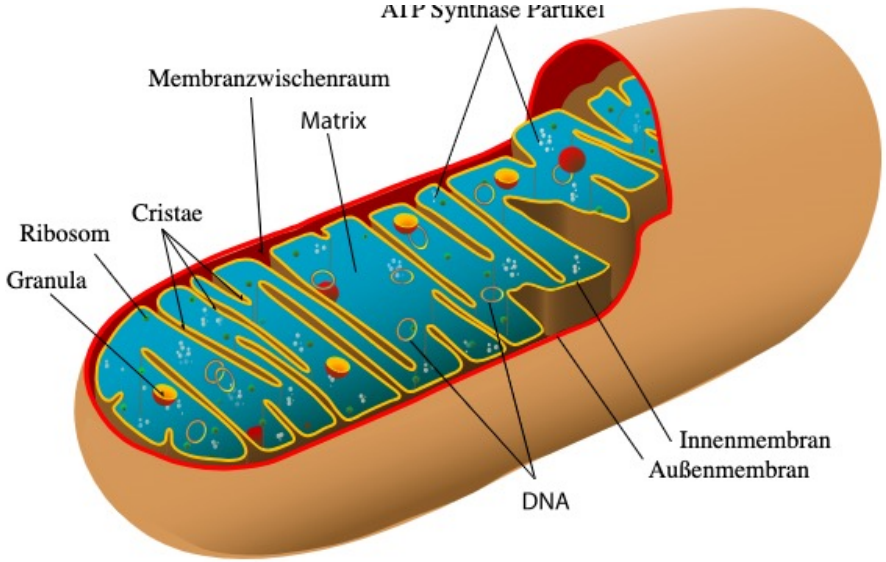

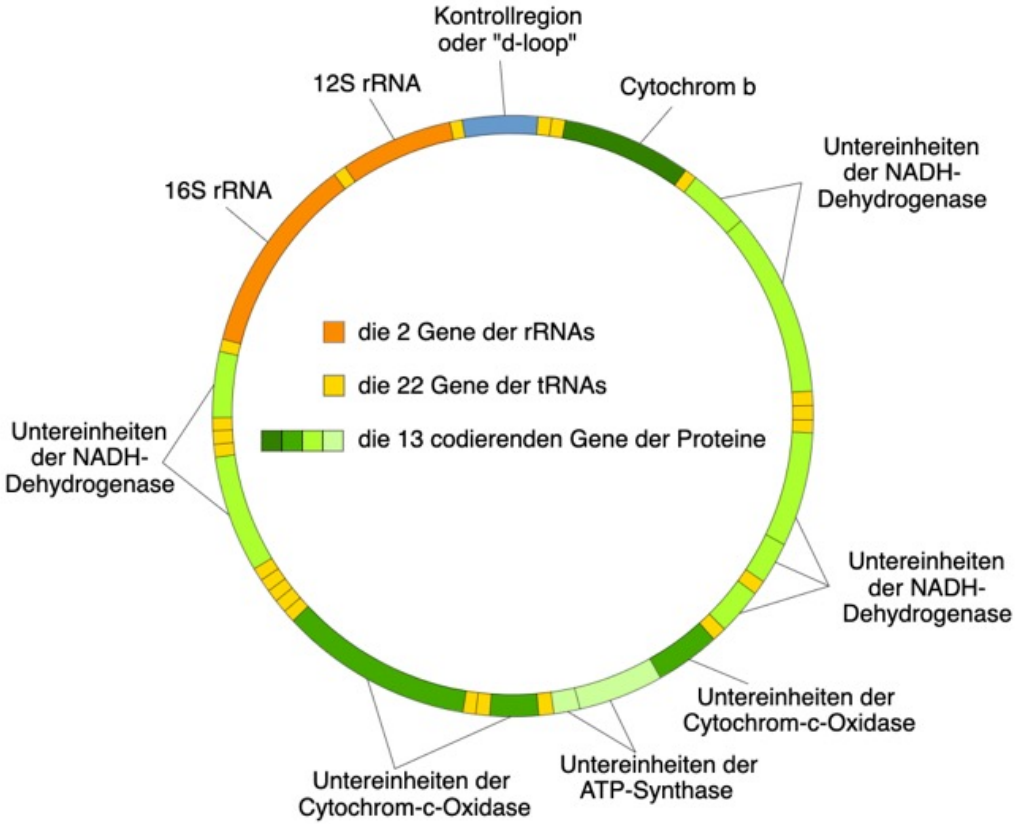

The MELAS mutation m.3243A>G alters the expression of mitochondrial tRNA fragments

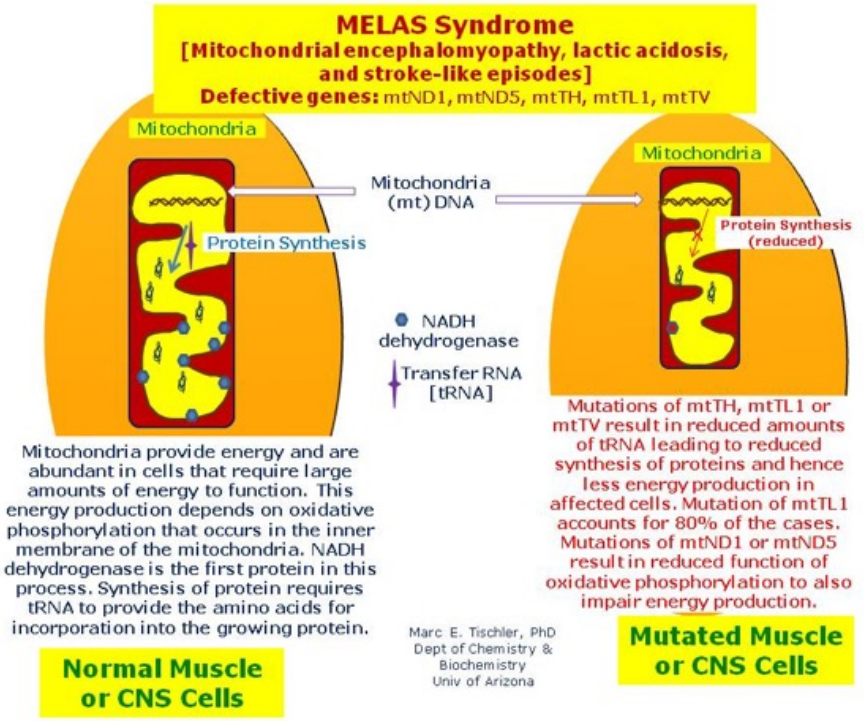

The MELAS mutation m.3243A>G alters the expression of mitochondrial tRNA fragments

Mutation (**m.3243A**-to-**G**) verursachten Phänotypen variabel sind und von schwerem **MELAS** über Diabetes bis hin zu Taubheit oder sogar Symptomlosigkeit reichen.

A 58-Year-Old Woman with Confusion, Aphasia, and Abnormal Head Imaging

A 58-year-old woman was transferred to this hospital because of progressively worsening confusion and evolving changes on magnetic resonance imaging (MRI) of the head.

The patient had been in her usual state of health until 16 months before the current presentation, when confusion and expressive and auditory aphasia developed. She was evaluated at another hospital. The findings of computed tomographic (CT) angiography of the head and neck were reportedly normal. MRI of the head reportedly showed signal hyperintensities in the left temporal lobe on T2-weighted fluid-attenuated inversion recovery (FLAIR) images. Evaluation of the cerebrospinal fluid (CSF) showed elevated levels of glucose and protein with a normal cell count; nucleic acid testing for herpes simplex virus DNA was negative. Blood and CSF paraneoplastic autoantibody and autoimmune encephalopathy panels were unrevealing. The results of serum protein electrophoresis were normal. Screening tests for syphilis and antinuclear antibodies were negative. An electroencephalogram (EEG) showed generalized slowing, with no epileptiform discharges. A diagnosis of autoimmune encephalitis was considered, and treatment included intravenous glucocorticoids for 5 days, followed by treatment with daily oral prednisone. Expressive aphasia resolved and confusion abated, but auditory aphasia persisted.

CT of the chest, abdomen, and pelvis revealed a mass measuring 5 cm in diameter in the pelvis that was composed of fat, soft tissue, and calcifications. Laparotomy was performed, and pathological examination of the resected specimen revealed findings consistent with a mature cystic teratoma. The patient was discharged home after a 3-week hospitalization, with a plan to taper the dose of oral prednisone after discharge.

One week after the patient's discharge from the other hospital, after the dose of prednisone had been decreased, malaise developed and confusion recurred. The patient was readmitted to the other hospital. MRI of the head reportedly showed a decrease in the left temporal lobe hyperintensities relative to the previous imaging study. The dose of prednisone was increased, confusion again abated, and the patient was discharged home. The dose of glucocorticoids was gradually tapered.

A diagnosis of autoimmune encephalitis was again considered. Treatment with intravenous glucocorticoids was reinitiated, which resulted in some reduction in confusion. The patient was discharged home with instructions to continue oral prednisone therapy, with a plan to again gradually taper the dose. Three months before the current presentation, confusion recurred. The patient was again admitted to the other hospital, and imaging studies were repeated. MRI of the head reportedly showed progression of the hyperintensities in the left temporal lobe and new signal hyperintensities in the right temporal and left occipital lobes. Treatment with intravenous glucocorticoids, trimethoprim–sulfamethoxazole, intravenous immunoglobulin, and rituximab was initiated. The patient was discharged to a skilled nursing facility, with a plan for weekly rituximab infusions for 5 weeks and a 6-week tapering course of daily oral prednisone therapy. Confusion resolved and did not recur.

Three weeks before the current presentation, MRI of the head, which was performed to evaluate the response to immunosuppressive medications, reportedly showed hyperintensity in both temporal lobes, with extension to the anterior aspects of the parietal lobes, on T2-weighted FLAIR images. Enhancement involving the subinsular regions was present, along with restricted diffusion in the insular cortexes. Positron-emission tomography (PET)–CT of the skull base to the midthighs reportedly showed no abnormalities. Two weeks before the current presentation, the patient was evaluated by her neurologist in the clinic, who recommended admission to the hospital for additional treatment owing to the progressively worsening findings on head imaging. One week before the current presentation, she was admitted to the other hospital. Treatment included daily intravenous immunoglobulin for 5 days and mycophenolate mofetil. On the third hospital day, she fell and struck her forehead while walking to the bathroom. On the sixth hospital day, she was transferred to this hospital to potentially undergo a brain biopsy.

On arrival at this hospital, the patient reported pain on her forehead where she had struck her head during her fall. Other medical history included type 2 diabetes mellitus, hypertension, sensorineural hearing loss (which had been diagnosed when she was 45 years of age), and depression. The results of a routine screening colonoscopy that had been performed 4 years before the current presentation had been normal. In additional to metformin, mycophenolate mofetil and trimethoprim–sulfamethoxazole, medications included ascorbic acid, cholecalciferol, glipizide, magnesium oxide, metoprolol, omeprazole, sertraline, and thiamine.

Treatment with metformin had been stopped at the other hospital because the blood level of lactate had been 12.4 mmol per liter (112 mg per deciliter; reference range, 0.5 to 2.0 mmol per liter [4.5 to 18 mg per deciliter]) on presentation. There were no known drug allergies. She had worked in health care until the onset of neurologic symptoms 16 months earlier. Before being discharged to the skilled nursing facility, she had lived alone. She was a lifelong nonsmoker and did not drink alcohol or use illicit drugs. Her mother had had diabetes and had died from heart disease at 59 years of age; she had used hearing aids. Her father had died from heart disease at 78 years of age. Both her brothers had diabetes, along with hearing loss in both ears.

On examination, the temporal temperature was 36.6°C, the blood pressure 154/90 mm Hg, the pulse 76 beats per minute, the respiratory rate 18 breaths per minute, and the oxygen saturation 98% while the patient was breathing ambient air. The height was 157.5 cm, the weight 34 kg, and the body-mass index (BMI; the weight in kilograms divided by the square of the height in meters) 13.7. Ecchymoses and a healing laceration were present on the right side of the forehead. The patient had receptive aphasia, which severely limited her ability to understand oral speech, but she could comprehend written or typed questions. She was alert and interactive and oriented to person, place, and time. Her speech was fluent, with no paraphasic errors. She was able to follow simple and complex commands without difficulty. Concentration and attention were intact. No abnormalities involving the cranial nerves were noted, with the exception of anisocoria; the left pupil measured 5 mm in diameter, and the right pupil measured 3 mm in diameter. Both pupils were reactive to light. The muscle bulk was decreased, but muscle tone and strength were normal. Tests of sensation, deep-tendon reflexes, and cerebellar function showed normal results.

The blood levels of electrolytes, glucose, alanine aminotransferase, aspartate aminotransferase, and total bilirubin were normal, as were the results of kidney-function tests. The blood level of lactate was 2.6 mmol per liter. The complete blood count with differential count was normal, except for the level of hemoglobin (11.3 g per deciliter; reference range, 12.0 to 16.0).

Diagnostic tests were performed.

Differential Diagnosis

Dr. Jenny J. Linnoila: This 58-year-old woman initially presented with confusion and expressive and auditory aphasia and was found to have signal hyperintensities in the left temporal lobe on MRI of the head, elevated levels of glucose and protein in the CSF, diffuse slowing on EEG, and a teratoma on pelvic CT. A presumed diagnosis of autoimmune encephalitis was made, for which she received glucocorticoids and underwent removal of the teratoma.

Autoimmune Encephalitis

To establish a diagnosis of possible autoimmune encephalitis, a patient must meet the following conditions: subacute working memory deficits, altered mental status, or psychiatric symptoms; new focal central nervous system (CNS) findings, new unexplained seizures, CSF pleocytosis, or abnormalities on MRI of the head that are suggestive of encephalitis (e.g., hyperintensities in one or both temporal lobes or in multifocal areas on T2-weighted FLAIR imaging); and other causes must be ruled out.

Infection

Several infections involving the CNS are characteristically associated with hyperintensities on T2-weighted FLAIR images from MRI of the head. Herpes simplex encephalitis commonly involves the temporal lobes, but it is frequently fulminant. West Nile virus infection most often involves deeper structures, such as the basal ganglia and thalamus, but these regions were not affected in this patient.

Multifocal Strokes

Strokes could explain the patient's neurologic symptoms and hyperintensities on MRI of the head. However, multiple strokes would have needed to occur in different vascular territories to account for her MRI findings.

Cancer

Autoimmune encephalitis–related inflammation, particularly of the limbic system, can lead to hyperintensities in the medial temporal lobes on T2-weighted FLAIR imaging. Low-grade infiltrating gliomas can also involve this area of the brain and are an important consideration in this patient, since they can be nonenhancing early in the course of disease.

Demyelinating and Inflammatory Disorder

The patient's lesions on MRI of the head were not in locations that would be typical for demyelinating disease and were mostly nonenhancing, which would be unexpected. Progressive multifocal leukoencephalopathy is a demyelinating disease that involves lesions that are typically nonenhancing; however, it is caused by the reactivation of JC virus in immunosuppressed hosts, and this patient was not known to be immunosuppressed.

Toxic Exposure or Metabolic Disorder

Persons with toxic exposures or metabolic disorders can have presentations that are similar to that of this patient. However, a toxic cause is unlikely in this patient, owing to the fact that she had repeated episodes, a progressive course, and no known exposures. In addition, the asymmetry of this patient's lesions on MRI of the head and the lack of involvement of deeper structures, such as the basal ganglia, argues against toxic and metabolic causes.

Genetic Disorder

Several aspects of this patient's presentation suggest the possibility of a maternally inherited genetic disorder, specifically a mitochondrial disorder. The patient's mother had died relatively early, at 59 years of age. Diabetes and hearing loss were present in the patient, her mother, and her brothers. The patient's BMI was low, and she had decreased muscle bulk, which is suggestive of a chronic disease. She had anisocoria, which, along with hearing loss, could implicate the involvement of multiple cranial nerves and could be consistent with a mitochondrial disorder. The patient's blood lactate level at the other hospital was markedly elevated, at 12.4 mmol per liter. Elevated lactate levels are not uncommon after the occurrence of convulsive seizures, but there was no mention of tonic–clonic activity in this patient. The lactate level remained mildly elevated, at 2.6 mmol per liter, on transfer to this hospital, which may indicate the presence of a mitochondrial disorder.

Maternally Inherited Diabetes and Deafness

Given the patient's striking family history, I searched for a known maternally inherited genetic disorder that could lead to hearing impairment and diabetes. I learned that maternally inherited diabetes and deafness (MIDD) arises from a pathogenic variant in mitochondrial DNA.

Dr. Jenny J. Linnoila's Diagnosis

Mitochondrial disease due to the m.3243A→G pathogenic variant in *MT-TL1*.

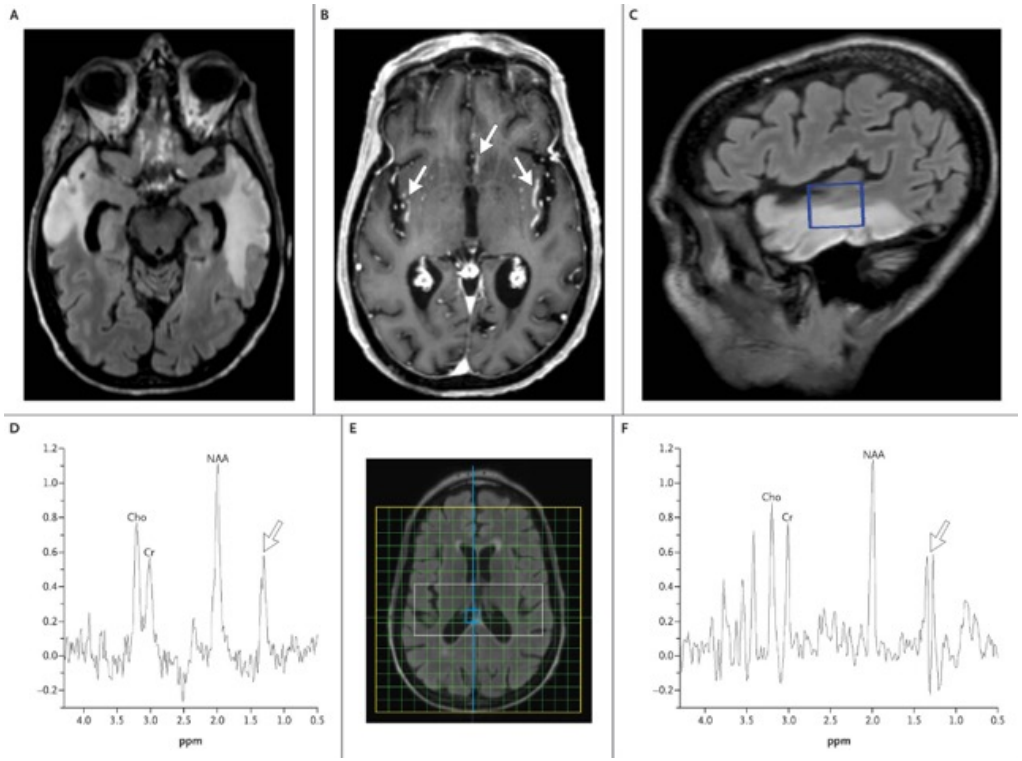

MRI of the Head and Magnetic Resonance Spectroscopy on Admission. An axial T2-weighted fluid-attenuated inversion recovery image (Panel A) shows the presence of hyperintense signal abnormalities in both temporal lobes. An axial T1-weighted contrast-enhanced image (Panel B) shows the presence of abnormal subcortical enhancement in the insulae and in the left posterior gyrus rectus (arrows). Magnetic resonance spectroscopy targeting the signal hyperintensities in the left temporal lobe (voxel indicated by the blue box in Panel C) was performed with the use of a single voxel technique with a long echo time (270 msec) (Panel D). This technique shows the presence of a positive doublet at 1.3 ppm, which is compatible with a lactate peak (Panel D, arrow). Magnetic resonance spectroscopy targeting the central brain parenchyma and lateral ventricles was performed with the use of a multivoxel technique with a short echo time (30 msec) (Panel F); the spectroscopy grid (green grid), volume of interest (white box), and a small target voxel (blue box) are shown in Panel E. This technique also shows a marked elevation in the lactate level, with a positive doublet at 1.3 ppm (Panel F, arrow), in the chosen voxel in the anterior splenium and adjacent right ventricular atrium. Cho denotes choline, Cr creatine, and NAA N-acetylaspartate.

Overall, clinical trials have proposed the use of oral and IV arginine in the therapy of MELAS. IV arginine seems to be effective in improving symptoms during acute attacks of MELAS, while oral arginine supplementation increases endothelial function, preventing further stroke-like episodes.

Pathological Discussion

An open biopsy of the right quadriceps was performed. Hematoxylin and eosin staining of frozen sections of the muscle specimen showed mild variation in the size and shape of the myofibers, with sporadic mildly atrophic fibers, and no evidence of necrosis, regenerating fibers, or distinct inflammatory infiltrates (Figure 2A). Scattered myocytes showed focally irregular, coarse cytoplasm in the subsarcolemmal area (Figure 2B). On Gomori trichrome staining, these fibers were found to contain irregular material that stained red and had a cracking appearance, features that were consistent with ragged-red fibers (Figure 2C). An enzyme histochemical analysis for NADH–tetrazolium reductase activity revealed the presence of occasional so-called ragged-blue fibers (not shown). A combined assay for the detection of cytochrome *c* oxidase (COX) and succinate dehydrogenase activity showed the presence of scattered blue COX-deficient fibers; increased enzymatic activity, reflecting increased numbers of mitochondria, was present in the subsarcolemmal compartment of some fibers (Figure 2D).

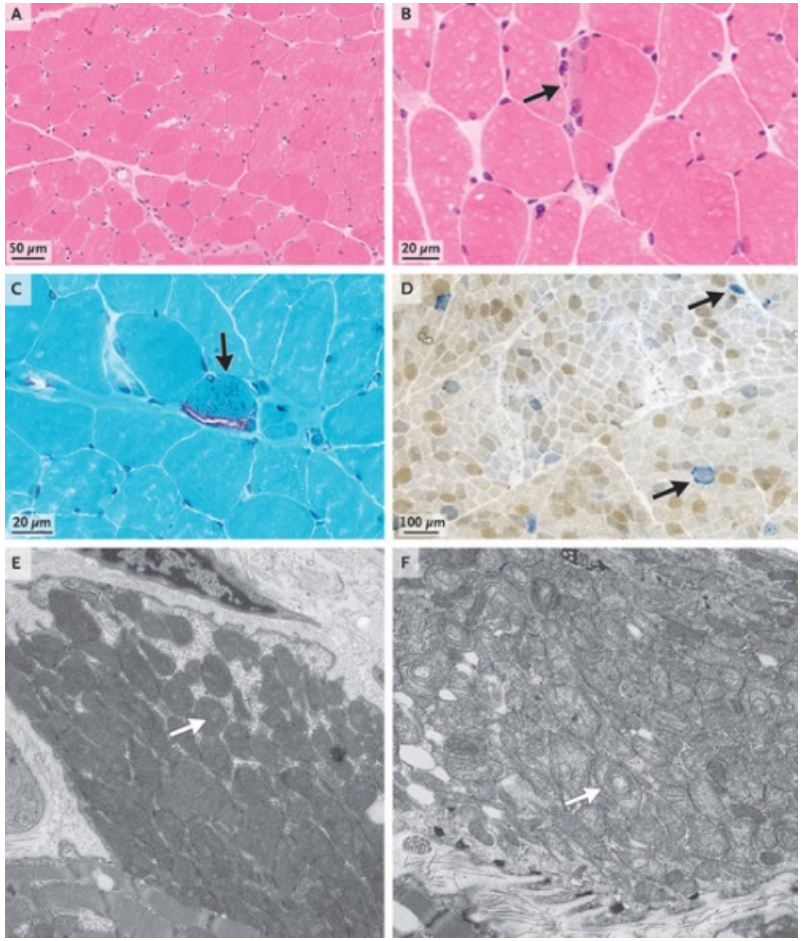

Discussion of Management

The patient was discharged from this hospital to an acute inpatient rehabilitation facility and subsequently to a skilled nursing facility. The medications that the patient was receiving at the time of discharge included supplements and cofactors for mitochondrial biochemical pathways, as well as oral arginine supplementation for secondary stroke prevention — a common management strategy that is supported by expert consensus. Arginine is hypothesized to prevent or ameliorate strokelike episodes that are associated with the m.3243A→G pathogenic variant in patients with MELAS by serving as a substrate for the generation of nitric oxide, a signaling molecule that is known to induce vasodilation by binding to guanylyl cyclase. Some researchers have postulated that patients with MELAS might have a local deficiency of nitric oxide that results in cerebral vasomotor dysfunction; however, the use of arginine in patients with MELAS is not approved by the Food and Drug Administration and remains a subject of ongoing study.

Repeat MRI of the head was performed approximately 1 year after discharge. The lesions that had been seen on T2-weighted FLAIR imaging were stable, no abnormal signal was seen on diffusion-weighted imaging, and there was complete resolution of contrast enhancement. At a virtual follow-up visit in the mitochondrial disorders clinic at this hospital, a neurologic examination that included an assessment of mental status showed no change from the previous examination.

At a subsequent follow-up visit approximately 2 years after discharge, anorexia and weight loss were noted, and the patient and care team staff reported that the patient had been having anorexia and diarrhea associated with oral arginine therapy. Treatment with arginine was stopped. Staff members also reported persistent elevations in the glycated hemoglobin level and in point-of-care blood glucose levels, despite the receipt of multiple medications. The patient's cognition remained stable but poor. During the subsequent year, anorexia and weight loss progressed. The patient was hospitalized after having a seizure at her residential facility. She was transitioned to hospice care and died shortly thereafter.

Final Diagnosis

MIDD (maternally inherited diabetes and deafness) and MELAS (mitochondrial encephalopathy, lactic acidosis, and strokelike episodes) associated with the m.3243A→G pathogenic variant.

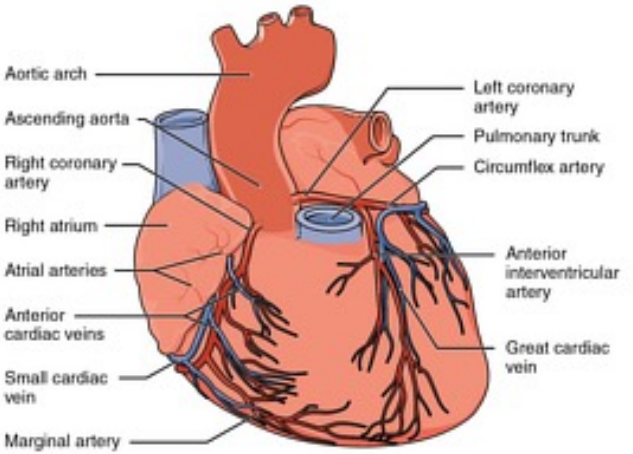

Anterior view

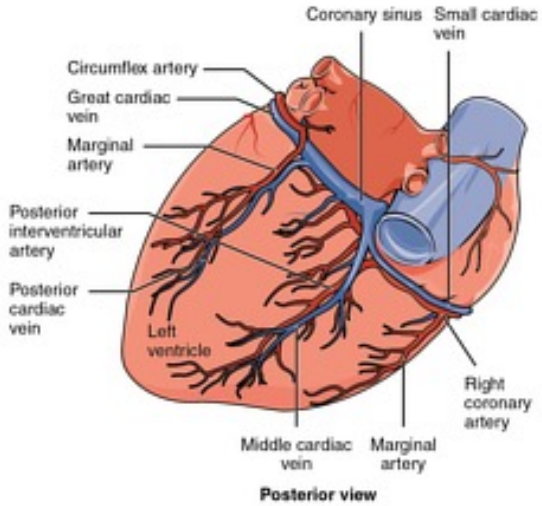

Posterior view

Venous development

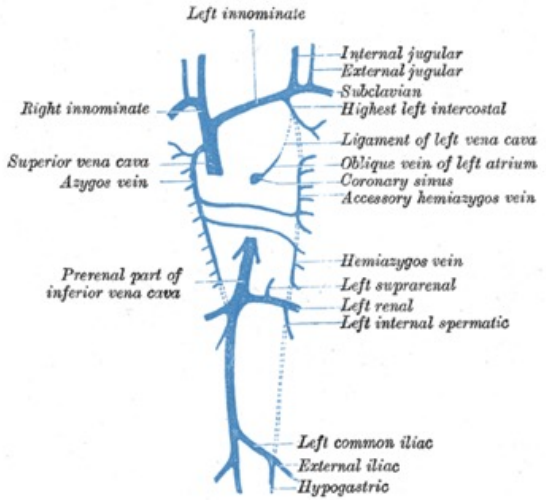

Koronarsinus-Reducer bei refraktärer Angina Pectoris

*Refraktäre Angina Pectoris (AP) definiert sich durch lang andauernde Symptome (3 Monate und länger), die durch eine bestehende reversible Ischämie bei obstruktiver koronarer Herzkrankheit (KHK) hervorgerufen werden und nicht mittels einer medikamentösen Therapie mit Zweit- und Drittlinien-Medikamenten, Bypassoperationen oder Stentimplantation unter Kontrolle gebracht werden können. Der Koronarsinus-Reducer (Coronary sinus reducing stent, CSRS) soll eine fokale Verengung im Lumen des Koronarsinus erzeugen. Das AIHTA bewertete im Zuge eines Updates erneut den Koronarsinus-Reducer (Neovasc ReducerTM System). Die vorhandene Evidenz weist zwar darauf hin, dass der CSRS – bei Patient*innen mit refraktärer AP, für die keine andere Behandlungsmöglichkeit verfügbar ist – potenziell wirksamer ist als die entsprechende Scheinprozedur, allerdings werden die teilweise positiven Ergebnisse durch die fehlende innere Validität der Studien unterminiert. Um den CSRS in der klinischen Routine zu etablieren, werden umfangreichere RCTs benötigt.*

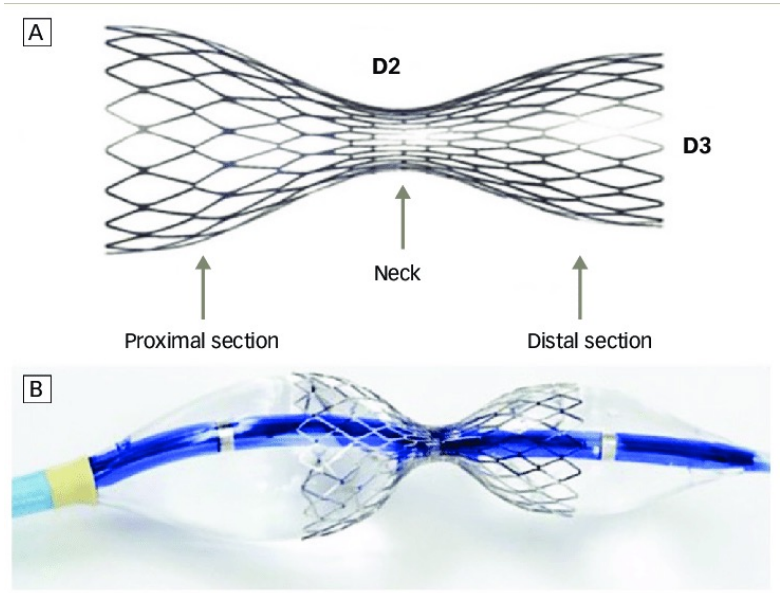

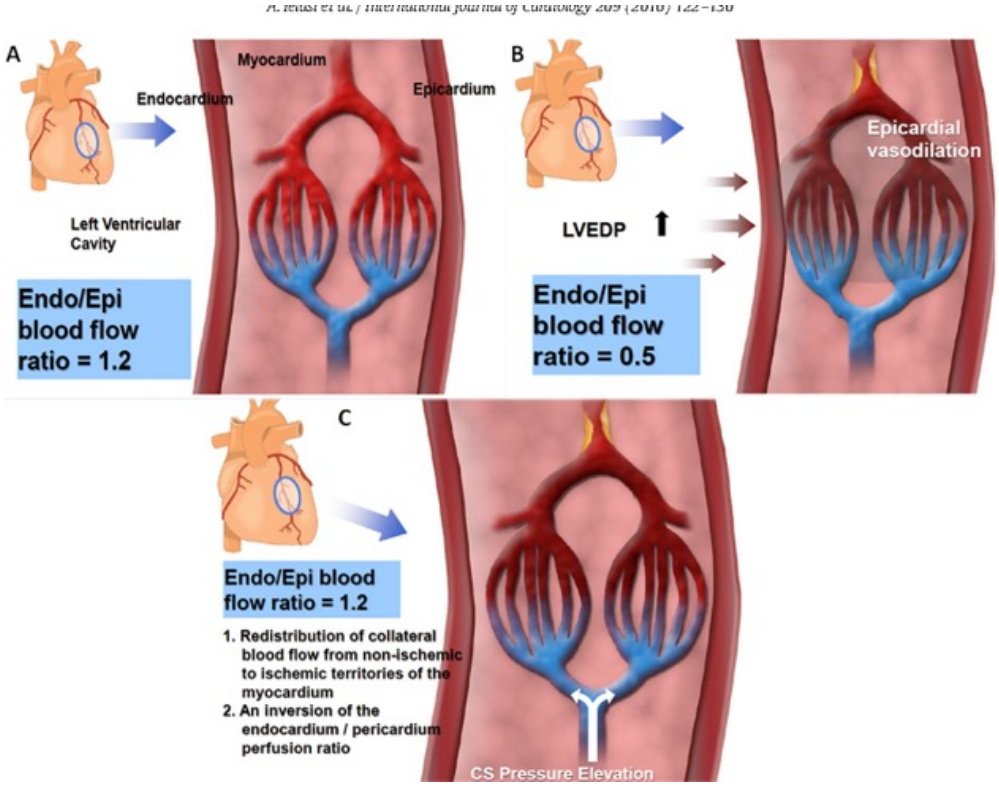

Coronary sinus reducer for the treatment of refractory angina (ORBITA-COSMIC): a randomised, placebo-controlled trial

Summary

Background The coronary sinus reducer (CSR) is proposed to reduce angina in patients with stable coronary artery disease by improving myocardial perfusion. We aimed to measure its efficacy, compared with placebo, on myocardial ischaemia reduction and symptom improvement.

Methods ORBITA-COSMIC was a double-blind, randomised, placebo-controlled trial conducted at six UK hospitals. Patients aged 18 years or older with angina, stable coronary artery disease, ischaemia, and no further options for treatment were eligible. All patients completed a quantitative adenosine-stress perfusion cardiac magnetic resonance scan, symptom and quality-of-life questionnaires, and a treadmill exercise test before entering a 2-week symptom assessment phase, in which patients reported their angina symptoms using a smartphone application (ORBITA-app). Patients were randomly assigned (1:1) to receive either CSR or placebo. Both participants and investigators were masked to study assignment. After the CSR implantation or placebo procedure, patients entered a 6-month blinded follow-up phase in which they reported their daily symptoms in the ORBITA-app. At 6 months, all assessments were repeated. The primary outcome was myocardial blood flow in segments designated ischaemic at enrolment during the adenosine-stress perfusion cardiac magnetic resonance scan. The primary symptom outcome was the number of daily angina episodes. Analysis was done by intention-to-treat and followed Bayesian methodology. The study is registered with ClinicalTrials.gov, NCT04892537, and completed.

Findings Between May 26, 2021, and June 28, 2023, 61 patients were enrolled, of whom 51 (44 [86%] male; seven [14%] female) were randomly assigned to either the CSR group (n=25) or the placebo group (n=26). Of these, 50 patients were included in the intention-to-treat analysis (24 in the CSR group and 26 in the placebo group). 454 (57%) of 800 imaged cardiac segments were ischaemic at enrolment, with a median stress myocardial blood flow of 1·08 mL/min per g (IQR 0·77–1·41). Myocardial blood flow in ischaemic segments did not improve with CSR compared with placebo (difference 0·06 mL/min per g [95% CrI –0·09 to 0·20]; Pr(Benefit)=78·8%). The number of daily angina episodes was reduced with CSR compared with placebo (OR 1·40 [95% CrI 1·08 to 1·83]; Pr(Benefit)=99·4%). There were two CSR embolisation events in the CSR group, and no acute coronary syndrome events or deaths in either group.

Interpretation ORBITA-COSMIC found no evidence that the CSR improved transmural myocardial perfusion, but the CSR did improve angina compared with placebo. These findings provide evidence for the use of CSR as a further antianginal option for patients with stable coronary artery disease.

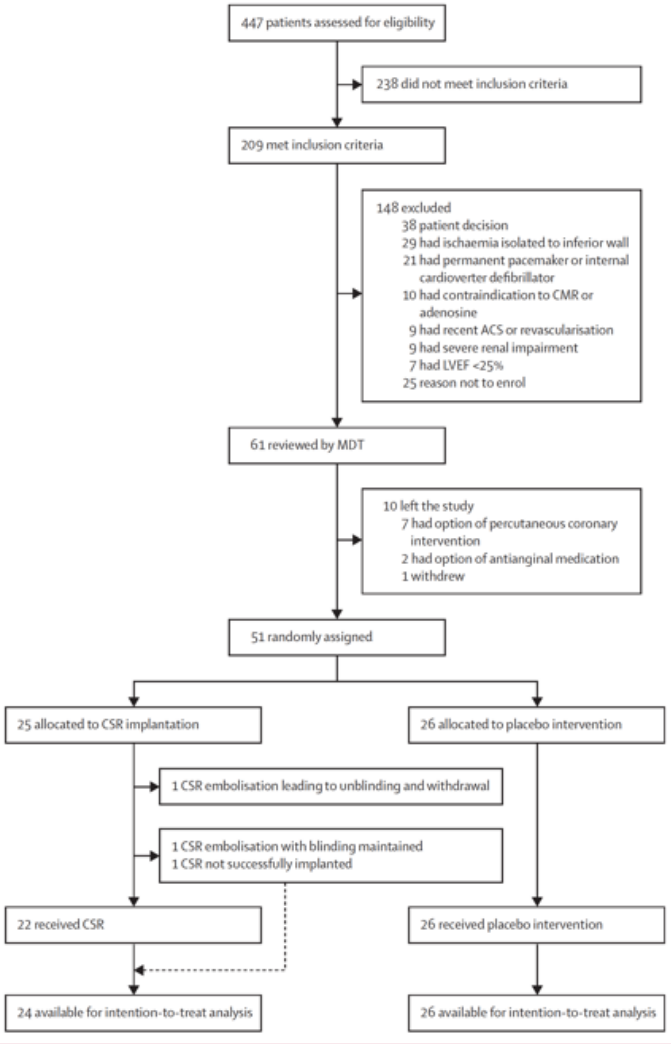

Figure 1: **Trial profile**
ACS=acute coronary syndrome. CMR=cardiac magnetic resonance scan. CSR=coronary sinus reducer. LVEF=left ventricular ejection fraction. MDT=ORBITA-COSMIC multidisciplinary team.

	CSR group (n=25)	Placebo group (n=26)
Median age, years	72 (63–74)	67 (61–72)
Sex		
Male	21 (84%)	23 (88%)
Female	4 (16%)	3 (12%)
Ethnic origin		
White	13 (52%)	12 (46%)
Asian	9 (36%)	9 (35%)
Arab	3 (12%)	4 (15%)
Afro-Caribbean	0	1 (4%)
Hypertension	17 (68%)	23 (88%)
Diabetes		
Non-insulin dependent	13 (52%)	17 (65%)
Insulin-dependent	2 (8%)	2 (8%)
Hyperlipidaemia	16 (64%)	18 (69%)
Previous CABG	21 (84%)	23 (88%)
Previous PCI	14 (56%)	14 (54%)
Smoking status		
Never smoked	18 (72%)	17 (65%)
Ex-smoker*	5 (20%)	7 (27%)
Current smoker	2 (8%)	2 (8%)
Left ventricular systolic function		
Normal	19 (76%)	23 (88%)
Mild impairment	4 (16%)	0
Moderate impairment	2 (8%)	3 (12%)
Canadian Cardiovascular Society class		
II	2 (8%)	1 (4%)
III	19 (76%)	17 (65%)
IV	4 (16%)	8 (31%)
Median angina duration, months	60·0 (22·0–96·0)	36·0 (18·0–60·0)
Median number of antianginal medications	4·0 (3·0–4·0)	3·0 (3·0–4·0)
Median British Cardiovascular Intervention Society Jeopardy	7·0 (6·0–9·0)	5·0 (4·0–6·0)

Data are median (IQR) or n (%). Left ventricular systolic function was defined as normal (≥55%), mildly impaired (45–54%), or moderately impaired (35–44%). CSR=coronary sinus reducer. CABG=coronary artery bypass grafting. PCI=percutaneous coronary intervention. *Ex-smoker was defined by the patient reporting that they had stopped smoking more than 6 months previously.

Table 1: **Baseline characteristics of study participants**

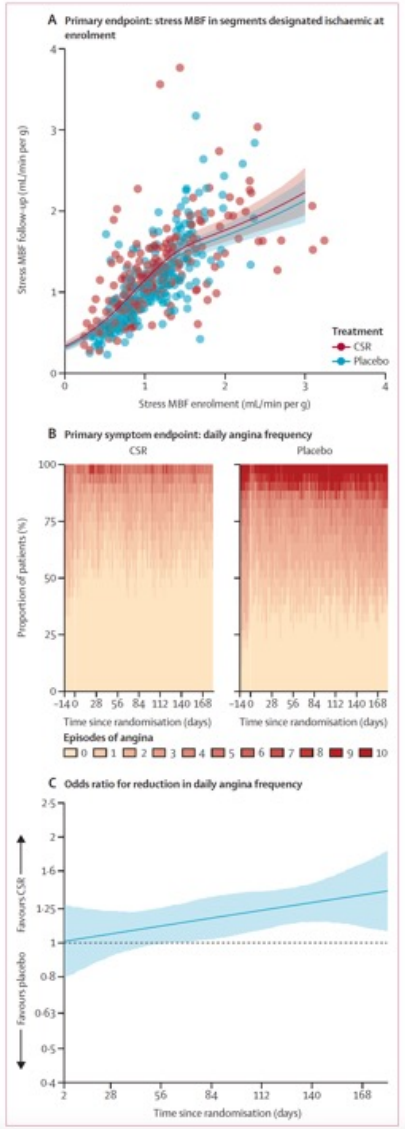

***Figure 2*: Primary outcomes**

(A) Individual patient data for the primary endpoint (stress MBF) in segments designated ischaemic at enrolment. (B) Individual patient data for the primary symptom endpoint (daily angina episodes), reported via the ORBITA smartphone symptom application. (C) Odds ratio for reduction in daily angina episodes for CSR versus placebo. CSR=coronary sinus reducer. MBF=myocardial blood flow.

	Difference at 6-month follow-up for CSR *vs* placebo	Probability of benefit with CSR *vs* placebo*
Quantitative perfusion, stress MBF, mL/min per g		
In ischaemic segments, mL/min per g (primary outcome)	0·06 (−0·09 to 0·20)	78·8%
In non-ischaemic segments, mL/min per g	−0·00 (−0·14 to 0·13)	48·7%
Difference between ischaemic and non-ischaemic segments	0·06 (−0·03 to 0·15)	90·8%
Quantitative perfusion (secondary imaging outcomes)		
Rest MBF, mL/min per g		
In ischaemic segments	0·01 (−0·05 to 0·07)	58·0%
In non-ischaemic segments	−0·01 (−0·07 to 0·05)	33·6%
Difference between ischaemic and non-ischaemic segments	0·02 (−0·01 to 0·05)	89·0%
MPR		
In ischaemic segments	0·06 (−0·17 to 0·27)	69·1%
In non-ischaemic segments	0·06 (−0·15 to 0·27)	72·7%
Difference between ischaemic and non-ischaemic segments	−0·01 (−0·13 to 0·12)	44·1%
Quantitative perfusion, inferior and inferoseptal segments excluded (secondary imaging outcomes)		
Stress MBF, mL/min per g		
In ischaemic segments	0·08 (−0·07 to 0·24)	85·6%
In non-ischaemic segments	−0·00 (−0·14 to 0·13)	47·6%
Difference between ischaemic and non-ischaemic segments	0·09 (−0·03 to 0·19)	93·9%
Rest MBF, mL/min per g		
In ischaemic segments	0·02 (−0·05 to 0·09)	71·2%
In non-ischaemic segments	−0·01 (−0·07 to 0·05)	31·9%
Difference between ischaemic and non-ischaemic segments	0·03 (−0·01 to 0·07)	94·4%
MPR		
In ischaemic segments	0·07 (−0·15 to 0·30)	74·4%
In non-ischaemic segments	0·05 (−0·16 to 0·25)	67·3%
Difference between ischaemic and non-ischaemic segments	0·03 (−0·12 to 0·18)	63·7%
Quantitative perfusion, endocardial to epicardial ratio (secondary imaging outcomes)		
Endocardial to epicardial ratio of stress MBF		
In ischaemic segments	0·09 (0·00 to 0·17)	98·2%
In non-ischaemic segments	−0·02 (−0·10 to 0·07)	35·1%
Difference between ischaemic and non-ischaemic segments	0·10 (0·02 to 0·19)	99·2%
Endocardial to epicardial ratio of rest MBF		
In ischaemic segments	0·03 (−0·04 to 0·10)	81·6%
In non-ischaemic segments	0·10 (0·03 to 0·17)	99·7%
Difference between ischaemic and non-ischaemic segments	−0·07 (−0·13 to −0·01)	1·8%
Endocardial to epicardial ratio of MPR		
In ischaemic segments	0·07 (−0·11 to 0·24)	77·2%
In non-ischaemic segments	−0·13 (−0·33 to 0·06)	8·3%
Difference between ischaemic and non-ischaemic segments	0·20 (0·02 to 0·37)	98·9%

Data are difference (95% credible interval) and percentage. The follow-up and increment values are model-based estimates (to avoid floor and ceiling effects), for an exemplar patient, conditional on the median pre-randomisation value. CSR=coronary sinus reducer. MBF=myocardial blood flow. MPR=myocardial perfusion reserve. *Differences between ischaemic and non-ischaemic segments are shown with an associated probability of interaction (Pr(Interaction)). The secondary outcomes of global MPR, global MBF, and myocardial strain and myocardial scar are shown in the appendix (pp 74, 94–97).

***Table 2*: Cardiac magnetic resonance scan primary and secondary endpoints**

	Odds ratio of transition to fewer angina episodes each day with CSR *vs* placebo	Probability of benefit with CSR *vs* placebo
Day 2 of follow-up	1·01 (0·80–1·28)	53·1%
Day 70 of follow-up	1·15 (1·00–1·30)	98·1%
Day 182 of follow-up	1·40 (1·08–1·83)	99·4%

Data are odds ratio (95% credible interval) or percentage. Results are reported for both the start of the follow-up period (day 2), day 70, and the end (day 182). CSR=coronary sinus reducer.

Table 3: **Primary symptom endpoint (angina episodes)**

	CSR group (n=25)	Placebo group (n=26)
Death	0	0
Myocardial infarction	0	0
Stroke	0	0
Bleeding	0	0
CSR embolisation	2 (8%)	0
Inability to deploy CSR	1 (4%)	0

Data are number of events (%). CSR=coronary sinus reducer.

Table 5: **Adverse events**

	n	Score increment	Score at 6-month follow-up	Benefit from baseline to follow-up	Probability of benefit with CSR *vs* placebo
SAQ angina frequency (baseline median 40·0)					
CSR	24	22·7 (10·6 to 34·6)	62·7 (50·6 to 74·6)	16·0 (5·1 to 27·3)	99·7%
Placebo	26	6·5 (−3·5 to 16·6)	46·5 (36·5 to 56·6)	..	..
SAQ physical limitation (baseline median 44·4)					
CSR	24	10·2 (−0·3 to 21·1)	54·6 (44·1 to 65·5)	4·9 (−5·3 to 15·0)	83·3%
Placebo	26	5·3 (−3·0 to 13·8)	49·7 (41·4 to 58·2)	..	..
SAQ angina stability (baseline median 25·0)					
CSR	24	29·4 (15·4 to 43·2)	54·4 (40·4 to 68·2)	9·2 (−7·0 to 24·7)	86·8%
Placebo	26	20·2 (8·1 to 32·4)	45·2 (33·1 to 57·4)	..	..
SAQ quality of life (baseline median 33·3)					
CSR	24	14·1 (2·1 to 26·2)	47·4 (35·5 to 59·6)	6·1 (−6·1 to 18·5)	83·5%
Placebo	26	7·9 (−1·4 to 18·0)	41·2 (31·9 to 51·4)	..	..
SAQ treatment satisfaction (baseline median 75·0)					
CSR	24	0·6 (−10·3 to 10·1)	75·6 (64·7 to 85·1)	5·7 (−4·2 to 16·2)	86·8%
Placebo	26	−5·0 (−16·7 to 5·0)	69·9 (58·4 to 80·0)	..	..
Treadmill exercise time, s (baseline median 366·8)					
CSR	24	61·4 (−18·1 to 141·8)	428·2 (348·6 to 508·6)	40·7 (−36·1 to 120·2)	84·8%
Placebo	26	20·4 (−58·6 to 104·3)	387·1 (308·2 to 471·1)	..	..
Canadian Cardiovascular Society class (baseline median 3·0)					
CSR	24	−0·8 (−1·1 to −0·4)	2·3 (1·9 to 2·6)	−0·3 (−0·7 to 0·1)	92·3%
Placebo	26	−0·4 (−0·8 to −0·1)	2·6 (2·2 to 2·9)	..	..
EQ-5D-5L index value (baseline median 0·6)					
CSR	24	0·0 (−0·1 to 0·1)	0·6 (0·5 to 0·7)	−0·0 (−0·1 to 0·1)	42·0%
Placebo	26	0·0 (−0·1 to 0·1)	0·6 (0·5 to 0·7)	..	..
EuroQol visual analogue scale (baseline median 55·0)					
CSR	24	4·4 (−4·1 to 12·4)	59·4 (51·0 to 67·4)	7·3 (−2·0 to 17·2)	93·3%
Placebo	26	−3·1 (−12·5 to 5·8)	52·0 (42·5 to 60·8)	..	..
MacNew Heart Disease Health-Related Quality of Life questionnaire (baseline median 3·8)					
CSR	24	0·5 (−0·0 to 1·0)	4·3 (3·8 to 4·8)	0·6 (0·2 to 1·1)	99·4%
Placebo	26	−0·1 (−0·6 to 0·3)	3·7 (3·3 to 4·1)	..	..

Data are score values (95% credible interval) and percentages. Treadmill exercise is presented for the patients who had both enrolment and follow-up scores. The follow-up and increment values are model based estimates (to avoid floor and ceiling effects), for an exemplar patient, conditional on the median pre-randomisation value. CSR=coronary sinus reducer. SAQ=Seattle Angina Questionnaire.

Table 4: **Secondary symptom endpoints**

Research in context

Evidence before this study

The coronary sinus reducer (CSR) device is believed to reduce angina by diverting blood flow from more perfused to less perfused areas of the myocardium. We did a literature search on PubMed, on Oct 20, 2019 (before the start of this trial), using the search terms "coronary sinus reducer" and "randomised controlled trial". This search confirmed that only one randomised trial of the coronary sinus reducer—the COSIRA trial—has been reported so far. This trial showed no improvement in patient-reported angina, but a distinct improvement in physician-assessed angina status. An additional search on the same date, using the terms "coronary sinus narrowing", "coronary sinus reducer", and "mechanism", showed that the effect of coronary sinus narrowing has been investigated in dogs and pigs, and that the mechanism of action of the CSR has only been investigated in observational single-arm registries. The mechanism of action of the CSR remains unclear. The literature search was updated annually.

Added value of this study

ORBITA-COSMIC is a double-blind, placebo-controlled trial of CSR in patients with angina, stable coronary artery disease, ischaemia, and no further antianginal medication or revascularisation options available. To our knowledge, it is the only trial of the CSR to mandate procedural auditory isolation, a deep level of conscious sedation during the randomisation procedure, and reporting of blinding fidelity for patients and research staff. It is also the only trial of the CSR to quantify perfusion in all myocardial segments at enrolment and follow-up by means of a bias-resistant cardiac magnetic resonance sequence, and to collect patient-reported angina episodes every day for the duration of the trial. We did not find strong evidence of an increase in perfusion of ischaemic areas. However, we found clear evidence of reduction in patient-reported angina episodes. This reduction developed gradually over a period of weeks and was sustained at 6 months.

Implications of all the available evidence

Physicians should favour placebo-controlled data when making symptom-focused treatment recommendations to patients. Although the mechanism of action of the CSR remains uncertain, ORBITA-COSMIC produced placebo-controlled data showing an improvement in patient-reported angina in a population with stable coronary artery disease, ischaemia, and no further options for antianginal therapy. The results of this trial provide evidence supporting the use of CSR as an additional treatment option for patients with stable coronary artery disease.

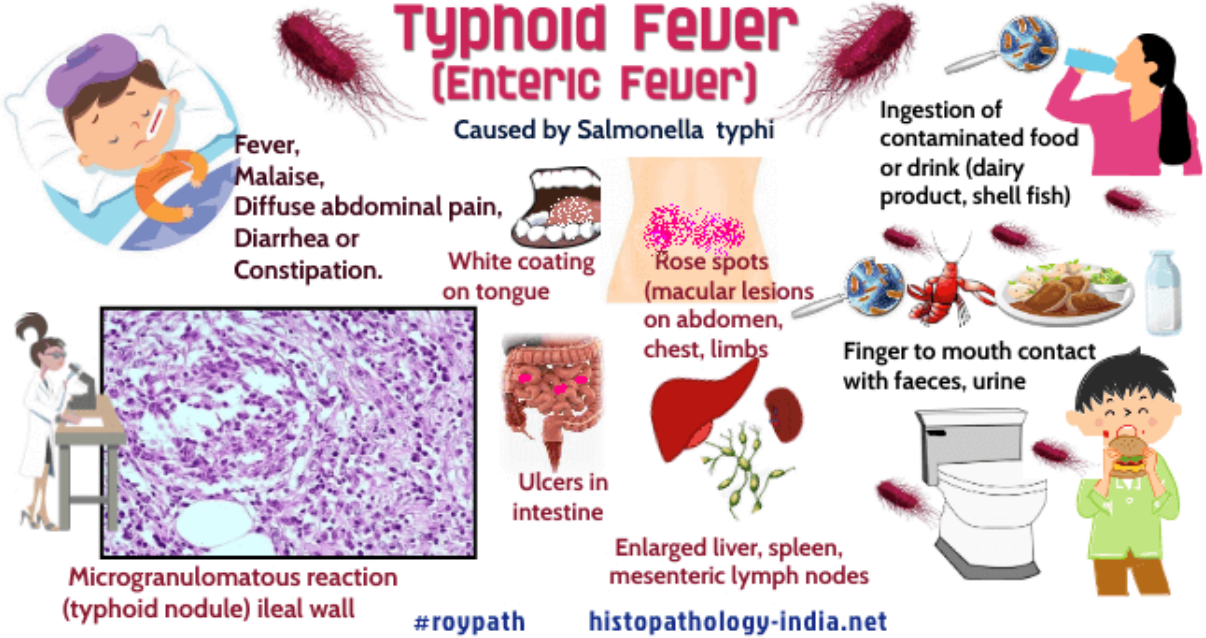

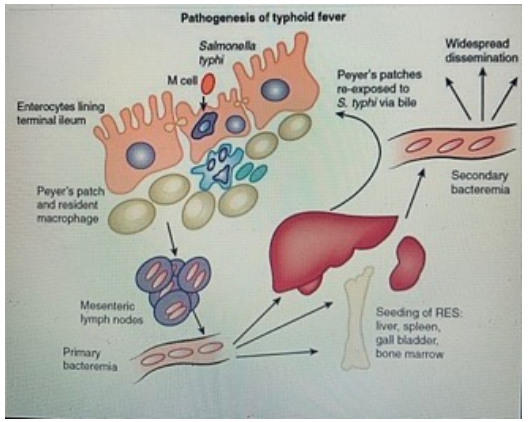

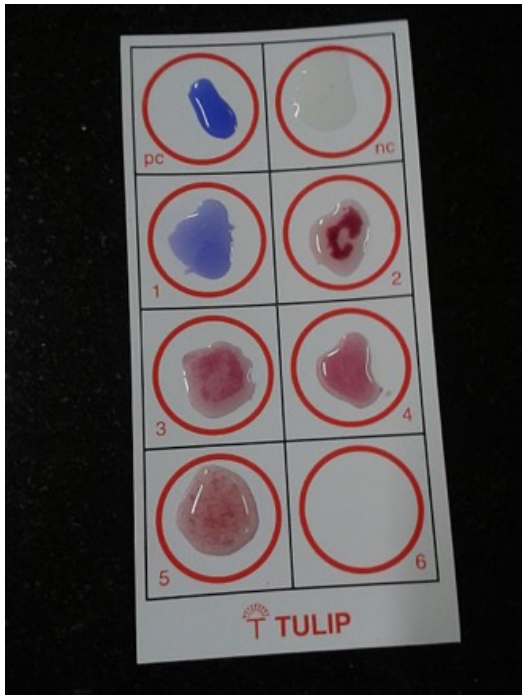


Tubercular ulcer


Typhoid ulcer

Table Comparing

Typhoid & Paratyphoid

	Typhoid	Paratyphoid
Prevalence	Typhoid is more prevalent, annually diagnosed in 26 million people worldwide.	Paratyphoid is less prevalent, with around 5.6 million cases reported annually.
Pathology	It is more contagious and the primary hosts are humans only.	Less contagious and primary hosts can be both humans and domestic animals.
Causative organism	Salmonella Typhi	Salmonella Paratyphi A, B, and C.
Symptoms	Symptoms are more severe and can cause debilitating effects in typhoid.	Symptoms are less severe in paratyphoid.
Treatment	Vaccine and immunization is available to prevent the disease.	No known vaccine or immunization is currently available.
Incubation period	2-14 days	10 days

DB Difference Between.net

Typhoid and paratyphoid fevers are diseases affecting the whole body and are caused by the bacteria *Salmonella* Typhi and *Salmonella* Paratyphi, respectively. In Europe, the disease is mainly associated with travel to endemic countries outside of the EU/EEA.

Humans are the only hosts and can carry the bacteria in their intestines for a long time and transmit it to others.

Symptoms take 1-2 weeks to appear and include

- Sustained fever
- headache
- malaise
- cough
- skin rash
- enlarged spleen or liver
- diarrhoea or constipation

Perforation of the intestines and bleeding can occur, which can lead to infections in all organs.

The untreated mortality rate is around 10%, but it has been greatly reduced by antibiotics. Antibiotic resistance is however becoming a problem, particularly in *Salmonella* Typhi.

The best way to prevent the disease is vaccination, which is currently only available for typhoid fever, together with proper personal and food hygiene.

The safety and immunogenicity of a bivalent conjugate vaccine against *Salmonella enterica* Typhi and Paratyphi A in healthy Indian adults: a phase 1, randomised, active-controlled, double-blind trial

Summary

Background Enteric fever caused by *Salmonella enterica* Typhi and *Salmonella* Paratyphi A is an important public health problem, especially in low-income and middle-income countries with limited access to safe water and sanitation. We present results from, to our knowledge, the first ever human study of a bivalent paratyphoid A-typhoid conjugate vaccine (Sii-PTCV).

Methods In this double-blind phase 1 study, 60 healthy Indian adults were randomly assigned (1:1) to receive a single intramuscular dose of either Sii-PTCV or typhoid conjugate vaccine (Typbar-TCV). Safety was assessed by observing solicited adverse events for 1 week, unsolicited events for 1 month, and serious adverse events (SAEs) over 6 months. Immunogenicity at 1 month and 6 months was assessed by measuring anti-capsular polysaccharide antigen Vi (anti-Vi) IgG and IgA against *Salmonella* Typhi and anti-lipopolysaccharide (LPS) IgG against *Salmonella* Paratyphi A by ELISA, and functional antibodies using serum bactericidal assay (SBA) against *Salmonella* Paratyphi A. This study is registered with Clinical Trial Registry–India (CTRI/2022/06/043608) and is completed.

Findings 60 participants were enrolled. Of these 60 participants, 57 (95%) participants were male and three (5%) participants were female. Solicited adverse events were observed in 27 (90%) of 30 participants who received Sii-PTCV and 26 (87%) of 30 participants who received Typbar-TCV. The most common local solicited event was pain in 27 (90%) participants who received Sii-PTCV and in 23 (77%) participants who received Typbar-TCV. The most common solicited systemic event was myalgia in five (17%) participants who received Sii-PTCV, whereas four (13%) participants who received Typbar-TCV had myalgia and four (13%) had headache. No vaccine-related unsolicited adverse events or SAEs were reported. The seroconversion rates on day 29 were 96·7% (95% CI 82·8–99·9) with Sii-PTCV and 100·0% (88·4–100·0) with Typbar-TCV for anti-Vi IgG; 93·3% (77·9–99·2) with Sii-PTCV and 100·0% (88·4–100·0) with Typbar-TCV for anti-Vi IgA; 100·0% (88·4–100·0) with Sii-PTCV and 3·3% (0·1–17·2) with Typbar-TCV for anti-LPS (paratyphoid); and 93·3% (77·9–99·2) with Sii-PTCV and 0% (0·0–11·6) with Typbar-TCV for SBA titres (paratyphoid). Paratyphoid anti-LPS immune responses were sustained at day 181.

Interpretation Sii-PTCV was safe and immunogenic for both typhoid and paratyphoid antigens indicating its potential for providing comprehensive protection against enteric fever.

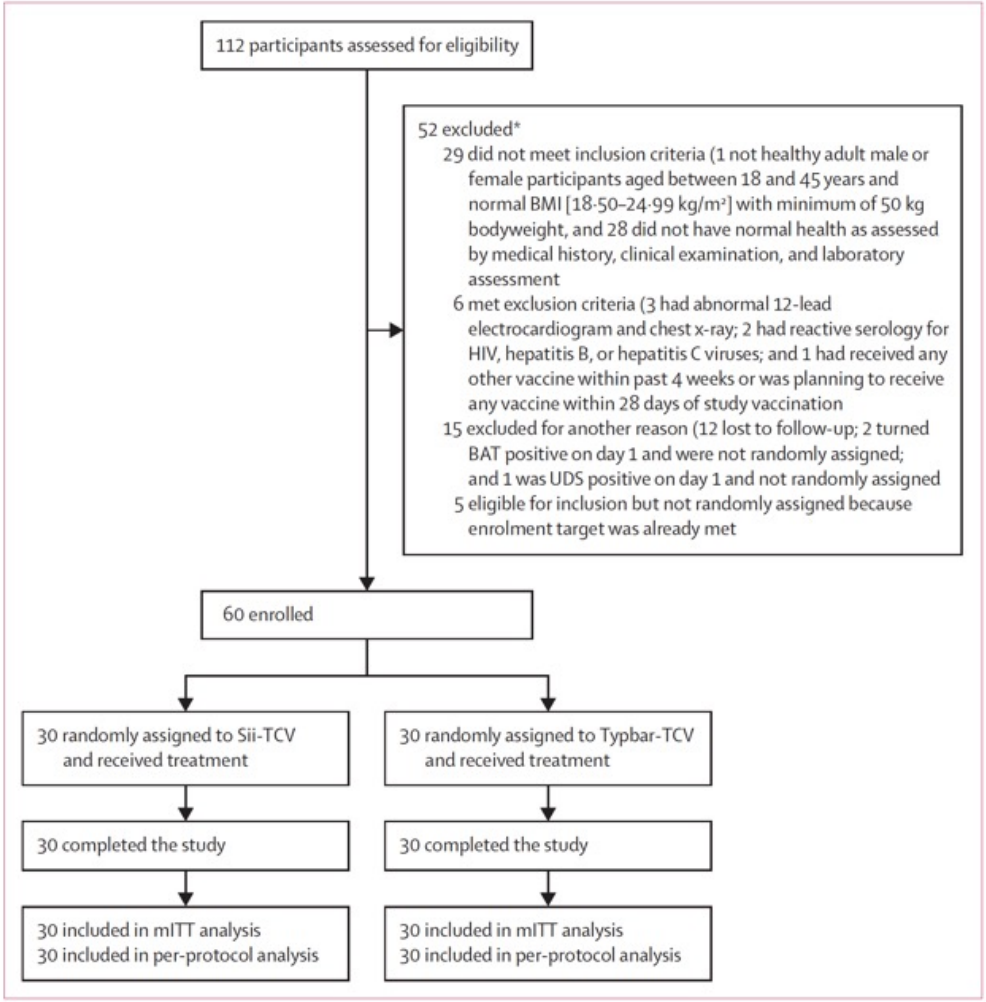

Figure: **Trial profile**

BAT=breath alcohol test. mITT=modified intention to treat. Sii-PTCV=bivalent paratyphoid A-typhoid conjugate vaccine. TCV=typhoid conjugate vaccine. UDS=urine drug screen for drugs that are abused. *Three participants both did not meet inclusion criteria and met the exclusion criteria.

	Sii-PTCV (n=30)	Typbar-TCV (n=30)
Age, years	30·7 (5·6)	30·9 (5·8)
Sex		
Male	29 (97%)	28 (93%)
Female	1 (3%)	2 (7%)
Weight, kg	65·3 (5·3)	60·2 (6·3)
Height, cm	169·0 (5·8)	167·0 (6·7)
BMI, kg/m²	22·9 (1·5)	21·6 (1·9)

Data are mean (SD) or n (%). TCV=typhoid conjugate vaccine.

Table 1: **Baseline demographics**

	Sii-PTCV (n=30)	Typbar-TCV (n=30)
Solicited adverse events	27 (90%), 27	26 (87%), 40
Solicited local events	27 (90%), 27	23 (77%), 26
Pain	27 (90%), 27	23 (77%), 23
Redness	..	2 (7%), 2
Swelling	..	1 (3%), 1
Solicited systemic events	7 (23%), 20	9 (30%), 14
Fever	1 (3%), 1	1 (3%), 1
Headache	3 (10%), 4	4 (13%), 4
Malaise	3 (10%), 4	2 (7%), 2
Anorexia	2 (7%), 2	2 (7%), 2
Myalgia	5 (17%), 6	4 (13%), 4
Arthralgia	2 (7%), 3	1 (3%), 1
Unsolicited adverse events	1 (3%), 1	5 (17%), 6
Lymphadenitis	1 (3%), 1	..
Vomiting	..	1 (3%), 1
Limb injury	..	1 (3%), 1
γ-glutamyl transferase increased	..	1 (3%), 1
Glucose present in urine	..	1 (3%), 1
Aminotransferases increased	..	2 (7%), 2

Data are n (%), number of events. Sii-PTCV=bivalent paratyphoid A-typhoid conjugate vaccine. TCV=typhoid conjugate vaccine.

Table 2: **Reported solicited and unsolicited events**

	Sii-PTCV (n=30)			Typbar-TCV (n=30)		
	GMT (95% CI)	GMFR (95% CI)	Seroconversion, n (%, 95% CI)	GMT (95% CI)	GMFR (95% CI)	Seroconversion, n (%, 95% CI)
Anti-Vi IgG (typhoid)						
Day 1	6·97 (4·75–10·22)	..	..	5·82 (4·13–8·20)	..	..
Day 29	1477·00 (867·80–2513·89)	211·96 (121·69–369·20)	29 (96·7%, 82·8–99·9)	996·38 (676·58–1467·35)	171·25 (103·13–284·38)	30 (100·0%, 88·4–100·0)
Day 181	480·46 (297·94–774·79)	68·95 (43·18–110·10)	29 (96·7%, 82·8–99·9)	482·54 (327·32–711·36)	82·93 (53·25–129·16)	30 (100·0%, 88·4–100·0)
Anti-Vi IgA (typhoid)						
Day 1	1·75 (1·48–2·07)	..	..	1·70 (1·43–2·01)	..	..
Day 29	75·66 (53·25–107·51)	43·27 (28·42–65·87)	28 (93·3%, 77·9–99·2)	85·19 (57·93–125·28)	50·15 (34·82–72·23)	30 (100·0%, 88·4–100·0)
Day 181	27·75 (18·90–40·74)	15·89 (10·51–23·95)	27 (90·0%, 73·5–97·9)	40·59 (27·2–60·59)	23·90 (16·74–34·12)	30 (100·0%, 88·4–100·0)
Anti-LPS (paratyphoid A)						
Day 1	360·46 (237·07–548·07)	..	..	181·04 (126·08–259·96)	..	..
Day 29	28 845·24 (19 679·44–42 280·06)	80·02 (54·93–116·58)	30 (100·0%, 88·4–100·0)	236·81 (169·24–331·37)	1·31 (1·09–1·58)	1 (3·3%, 0·1– 17·2)
Day 181	9535·52 (6281·40– 14 475·46)	26·45 (19·31–36·25)	30 (100·0%, 88·4–100·0)	222·86 (159·58– 311·22)	1·23 (1·05–1·44)	0
SBA (paratyphoid A)						
Day 1	8044·60 (5326·37– 12 150·05)	..	..	6765·70 (4672·43– 9796·85)	..	..
Day 29	155 737·80 (102 803·95–235 927·33)	19·40 (12·61–29·73)	28 (93·3%, 77·9–99·2)	5993·70 (4047·46–8875·91)	0·90 (0·66–1·19)	0 (NC)
Day 181	56 367·40 (33 580·12–94 617·93)	7·00 (3·98–12·32)	20 (66·7%, 47·2–82·7)	1782·30 (520·64–6101·18)	0·30 (0·09–0·81)	1 (3·3%, 0·1–17·2)

GMTs were calculated by taking the anti-log of the arithmetic mean of the log10-transformed titres. GMFR was calculated by taking the arithmetic mean of the difference in the log10-transformed titres, where difference was post-vaccination $\log_{10}$ titre minus baseline vaccination log10 titre. Seroconversion is defined as four-fold or higher rise in post-vaccination titres compared with pre-vaccination titres. GMFR=geometric mean fold rise from baseline. GMT=geometric mean titre. LPS=lipopolysaccharide. NC=not calculable. SBA=serum bactericidal assay. Sii-PTCV=bivalent paratyphoid A-typhoid conjugate vaccine. TCV=typhoid conjugate vaccine. Vi=capsular polysaccharide.

Table 3: **Immune response to typhoid and paratyphoid A antigen**

	Sii-PTCV (n=30)	Sii-PTCV (n=30)	Typbar-TCV (n=30)	Typbar-TCV (n=30)
Pre-existing anti-TT antibodies, n (%)	Yes, 29 (96·7%)	No, 1 (3·3%)	Yes, 26 (86·7%)	No, 4 (13·3%)
Geometric mean titres (95% CI)				
Anti-Vi IgG	1427·51 (826·42–2465·78)	3968·82 (NC)	875·23 (584·90–1309·69)	2314·13 (472·38–11 336·64)
Anti-Vi IgA	71·91 (50·79–101·82)	330·80 (NC)	74·44 (50·18–110·42)	204·71 (36·14–1159·49)
Seroconversion, n/N (%, 95% CI)				
Anti-Vi IgG	28/29 (96·7%, 82·2–99·9)	1/1 (100·0%, NC)	26/26 (100·0%, 86·8–100·0)	4/4 (100·0%, 39·8–100·0)
Anti-Vi IgA	27/29 (93·1%, 77·2–99·2)	1/1 (100·0%, NC)	26/26 (100·0%, 86·8–100·0)	4/4 (100·0%, 39·8–100·0)
Pre-existing anti-DT antibodies, n (%)	Yes, 15 (50%)	No, 15 (50%)	Yes, 21 (70%)	No, 9 (30%)
Geometric mean titres (95% CI)				
Anti-LPS	38 697·07 (23 013·65–65 068·49)	21 501·58 (12 008·45–38 499·37)	237·29 (158·56–355·10)	235·70 (110·38–503·31)
SBA	149 754·50 (84 354·52–265 858·88)	161 960·20 (82 468·68–318 073·54)	6699·90 (4147·07–10824·27)	4622·00 (2046·84–10436·91)
Seroconversion, n/N (%, 95% CI)				
Anti-LPS	15/15 (100·0%, 78·2–100·0)	15/15 (100·0%, 78·2–100·0)	0/21 (NC)	1/9 (11·1%, NC)
SBA	14/15 (93·0%, 68·1–99·8)	14/15 (93·3%, 68·1–99·8)	0/21 (NC)	0/9 (NC)

DT=diphtheria toxoid. LPS=lipopolysaccharide. NC=not calculable. SBA=serum bactericidal assay. Sii-PTCV=bivalent paratyphoid A-typhoid conjugate vaccine. TCV=typhoid conjugate vaccine. TT=tetanus toxoid. Vi=capsular polysaccharide.

***Table 4*: Effect of pre-existing tetanus and diphtheria antibodies on immune response on day 29 to typhoid and paratyphoid A antigens**

Research in context

Evidence before this study

We searched PubMed and WHO's website on May 17, 2021 using the search terms 'typhoid conjugate vaccine', 'paratyphoid vaccine', 'paratyphi A' with no date restrictions or language restrictions. We identified 25 articles relevant for a clinical trial of typhoid conjugate vaccines (TCVs) on PubMed. We identified one trial of a candidate paratyphoid conjugate vaccine. Previous phase 1 and phase 2 studies in Viet Nam showed that a *Salmonella enterica* Paratyphi A conjugate vaccine was safe and immunogenic. WHO recognises the need for development of an efficacious paratyphoid vaccine. WHO mentions seven paratyphoid vaccines that are in various stages of clinical development. CVD 1902, an oral paratyphoid vaccine, has completed a phase 1 study and is undergoing a human challenge study to assess the efficacy against paratyphoid A infection.

Added value of this study

This Article describes a phase 1 study of a bivalent paratyphoid A-typhoid conjugate vaccine (Sii-PTCV) to evaluate its safety and immunogenicity. Sii-PTCV was well tolerated by all recipients and no serious adverse events were reported over a 6-month period. Sii-PTCV showed robust immune responses to the paratyphoid A component at 4 weeks after vaccination, measured by anti-lipopolysaccharide IgG and serum bactericidal assay. Sii-PTCV also showed a comparable post-vaccination immune response for the typhoid component of an already licensed and WHO-prequalified TCV.

Implications of all the available evidence

Current TCVs provide protection against typhoid fever only and there is no vaccine against paratyphoid fever. Thus, comprehensive protection against enteric fever remains an unmet need. An effective bivalent vaccine would provide protection against enteric fever caused by *Salmonella* Typhi and *Salmonella* Paratyphi A, helping to mitigate increasing antimicrobial resistance. Sii-PTCV was safe and immunogenic in a phase 1 study. These findings warrant further evaluation in phase 2 and phase 3 studies.

RGX-314 Uses a Novel AAV8 Vector to Deliver an anti-VEGF Fab

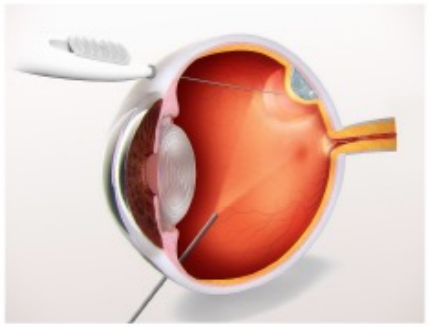

Subretinal Procedure

AAV8

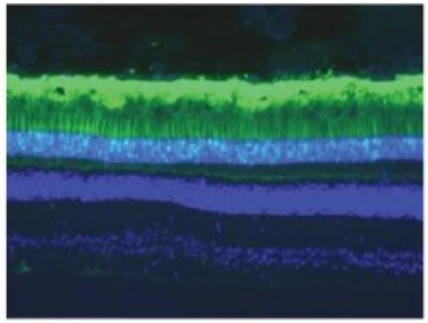

Efficient Gene Delivery to the RPE[1]

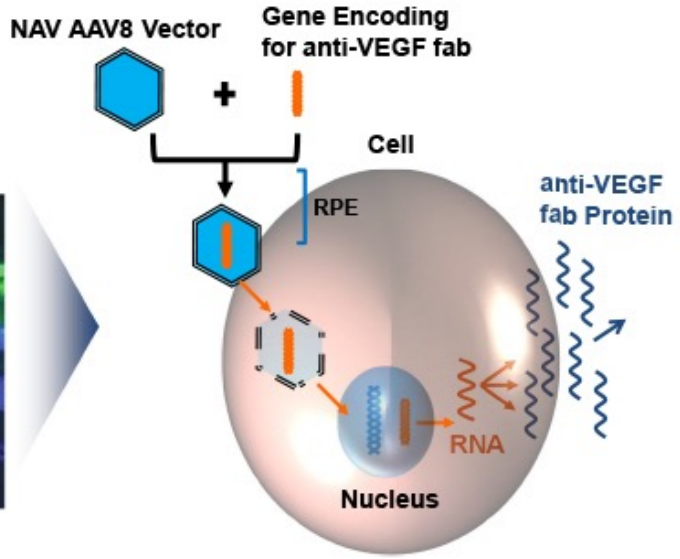

RGX-314 is Designed to Deliver a Gene Encoding for an Anti-VEGF Fab Protein

[1]Vandenberghe et al. 2011 *Science Translational Medicine*

Gene therapy for neovascular age-related macular degeneration by subretinal delivery of RGX-314: a phase 1/2a dose-escalation study

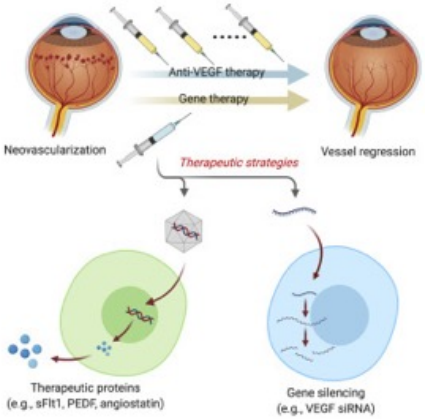

Summary

Background Frequent anti-vascular endothelial growth factor A (VEGF-A) injections reduce the risk of rapid and severe vision loss in patients with neovascular age-related macular degeneration (nAMD); however, due to undertreatment, many patients lose vision over time. New treatments that provide sustained suppression of VEGF-A are needed. RGX-314 (currently known as ABBV-RGX-314) is an adeno-associated virus serotype 8 vector that expresses an anti-VEGF-A antigen-binding fragment, which provides potential for continuous VEGF-A suppression after a single subretinal injection. We report results on the safety and efficacy of subretinal injection of RGX-314 in patients with nAMD.

Methods For this open-label, multiple-cohort, multicentre, phase 1/2a, dose-escalation study conducted at eight sites in the USA, we enrolled participants with nAMD aged 50–89 years who had previously been treated with anti-VEGF injections into five cohorts (with five different doses of RGX-314). To be eligible, participants had to have macular neovascularisation secondary to nAMD with subretinal or intraretinal fluid in the centre subfield, be pseudophakic (after cataract removal), and have a best-corrected visual acuity (BCVA) in the study eye between 20/63 and 20/400 for the first participant in each cohort and between 20/40 and 20/400 for others. Subretinal injection of RGX-314 was done without a pre-bleb by a wet-laboratory-trained vitreoretinal surgeon. Cohort 1 received 3×10^{9} genome copies per eye, cohort 2 received 1×10^{10}, and cohort 3 received 6×10^{10}. Two additional dose cohorts (cohort 4: $1{\cdot}6\times10^{11}$; cohort 5: $2{\cdot}5\times10^{11}$) were added. Participants were seen 1 day and 1 week after administration of RGX-314, and then monthly for 2 years (up to week 106). The primary outcome was safety of RGX-314 delivered by subretinal injection up to week 26. This analysis includes all 42 patients enrolled in the study. This study is registered with ClinicalTrials.gov, NCT03066258.

Findings Between May 12, 2017, and May 21, 2019, we screened 110 patients for eligibility and enrolled 68. 42 participants demonstrated the required anatomic response to intravitreal ranibizumab and then received a single RGX-314 injection (dose range 3×10^{9} to $2{\cdot}5\times10^{11}$ genome copies per eye) and were followed up for 2 years. There were 20 serious adverse events in 13 participants, of which one was possibly related to RGX-314: pigmentary changes in the macula with severe vision reduction 12 months after injection of RGX-314 at a dose of $2{\cdot}5\times10^{11}$ genome copies per eye. Asymptomatic pigmentary changes were seen in the inferior retinal periphery several months after subretinal injection of RGX-314 most commonly at doses of 6×10^{10} genome copies per eye or higher. There were no clinically determined immune responses or inflammation beyond that expected following routine vitrectomy. Doses of 6×10^{10} genome copies or higher resulted in sustained concentrations of RGX-314 protein in aqueous humour and stable or improved BCVA and central retinal thickness with few or no supplemental anti-VEGF-A injections in most participants.

Interpretation Subretinal delivery of RGX-314 was generally well tolerated with no clinically recognised immune responses. RGX-314 gene therapy provides a novel approach for sustained VEGF-A suppression in patients with nAMD that has potential to control exudation, maintain vision, and reduce treatment burden after a single administration. Results from this study informed the pivotal programme to evaluate RGX-314 in patients with nAMD.

Procedures

The study evaluated five doses of RGX-314 administered by subretinal injection in one eye per patient. To determine anti-VEGF-A responsiveness, patients received an intravitreal injection of 0·5 mg ranibizumab at visit 1; 7 days later (ie, at visit 2), their SD-OCT had to show a response (defined as a central retinal thickness [CRT; a biomarker for exudation] reduction >50 µm or central fluid reduction >30% from the initial value) for eligibility before subretinal injection of RGX-314 about 14 days later (ie, at visit 3).

Under local anaesthesia in an operating room, a small-gauge vitrectomy was performed with removal of posterior hyaloid aided by injection of triamcinolone acetonide to visualise the hyaloid. Subretinal injection of RGX-314 was done without a pre-bleb by a wet laboratory-trained vitreoretinal surgeon who was supervised by a surgical proctor (appendix p 4).

The original design included evaluation of 18 participants, six sequentially enrolled in three ascending dose cohorts. Cohort 1 received 3×10^9 genome copies per eye ($1\cdot2\times10^{10}$ genome copies per mL), cohort 2 received 1×10^{10} genome copies per eye (4×10^{10} genome copies per mL), and cohort 3 received 6×10^{10} genome copies per eye ($2\cdot4\times10^{11}$ genome copies per mL). Two additional dose cohorts (cohort 4: $1\cdot6\times10^{11}$ genome copies per eye [$6\cdot2\times10^{11}$ genome copies per mL]; cohort 5: $2\cdot5\times10^{11}$ genome copies per eye [1×10^{12} genome copies per mL]) were added with 12 participants per cohort (protocol version 7 and 8; appendix p 5). Participants were seen 1 day and 1 week after administration of RGX-314, and then monthly for 2 years (up to week 106) after RGX-314 administration. After each cohort reached a predesignated timepoint, safety review preceded the next cohort enrolment.

	Cohort 1 (RGX-314 3×10^9 GC/eye; n=6)	Cohort 2 (RGX-314 1×10^{10} GC/eye; n=6)	Cohort 3 (RGX-314 6×10^{10} GC/eye; n=6)	Cohort 4 (RGX-314 $1{\cdot}6 \times 10^{11}$ GC/eye; n=12)	Cohort 5 (RGX-314 $2{\cdot}5 \times 10^{11}$ GC/eye; n=12)	Total (n=42)
At least one event	6 (100%)	6 (100%)	6 (100%)	12 (100%)	12 (100%)	42 (100%)
At least one RGX-314-related event*	0	2 (33%)	3 (50%)	12 (100%)	10 (83%)	27 (64%)
At least one ranibizumab-related event*	0	0	0	0	0	0
At least one subretinal procedure-related event*	4 (67%)	6 (100%)	6 (100%)	12 (100%)	11 (92%)	39 (93%)
At least one study procedure-related event*†	2 (33%)	1 (17%)	1 (17%)	7 (58%)	5 (42%)	16 (38%)
At least one event of grade 3 or higher‡	1 (17%)	2 (33%)	0	3 (25%)	6 (50%)	12 (29%)
At least one APTC event	0	0	0	0	0	0
At least one serious event§	2 (33%)	2 (33%)	1 (17%)§	3 (25%)	4 (33%)	12 (29%)§¶
At least one RGX-314-related serious event*§	0	0	0	0	1 (8%)	1 (2%)
Death (grade 5‡)	1 (17%)	0	0	0	1 (8%)	2 (5%)

Data are presented as n (%). Participants were counted once for each category regardless of the number of events. APTC=Anti-Platelet Trialists' Collaboration. GC=genome copy. *Related events were those considered by the investigator to be probably or possibly related. †Excluding the subretinal procedure. ‡Grade 3 represents severe, grade 4 represents life-threatening, and grade 5 represents fatal. §Serious events included events meeting the protocol-specified definition of serious, along with Hy's law events and other important medical events. ¶One participant in cohort 3 experienced a grade 2 event of recurrent transitional cell carcinoma that was assessed by the investigator as non-serious and not related to RGX-314, but the sponsor considered it a medically important event and upgraded it to serious. Thus, the event appears in the clinical database (and the source for this table) as non-serious. However, with the inclusion of this event, there were two (33%) participants in cohort 3 who experienced at least one serious event, and a total across cohorts of 13 (31%) participants who experienced at least one serious event. The event was not related to RGX-314.

Table 1: **Treatment-emergent adverse events reported over the course of the study (as-treated population)**

	Cohort 1 (RGX-314 3×10^9 GC/eye; n=6)	Cohort 2 (RGX-314 1×10^{10} GC/eye; n=6)	Cohort 3 (RGX-314 6×10^{10} GC/eye; n=6)	Cohort 4 (RGX-314 $1{\cdot}6 \times 10^{11}$ GC/eye; n=12)	Cohort 5 (RGX-314 $2{\cdot}5 \times 10^{11}$ GC/eye; n=12)	Total (n=42)
Conjunctival haemorrhage	2 (33%)	3 (50%)	4 (67%)	9 (75%)	11 (93%)	29 (69%)
Retinal pigmentary changes*	0	3 (50%)	3 (50%)	12 (100%)	11 (93%)	29 (69%)
Inflammation†	4 (67%)	3 (50%)	3 (50%)	3 (25%)	2 (17%)	15 (36%)
Retinal haemorrhage	4 (67%)	0	1 (17%)	3 (25%)	3 (25%)	11 (26%)
Reduced or impaired visual acuity	3 (50%)	3 (50%)	1 (17%)	1 (8%)	1 (8%)	9 (21%)
Intraocular pressure increased	1 (17%)	1 (17%)	2 (33%)	0	4 (33%)	8 (19%)
Eye irritation	0	0	0	3 (25%)	4 (33%)	7 (17%)
Eye pain	1 (17%)	1 (17%)	0	3 (25%)	2 (17%)	7 (17%)
Retinal degeneration	0	0	1 (17%)	2 (17%)	4 (33%)	7 (17%)
Photopsia	2 (33%)	1 (17%)	0	1 (8%)	2 (17%)	6 (14%)
Vision blurred	1 (17%)	1 (17%)	0	0	3 (25%)	5 (12%)
Conjunctival hyperaemia	0	1 (17%)	2 (33%)	0	2 (17%)	5 (12%)

Data are presented as n (%). Participants are counted once for each preferred term regardless of the number of events. Preferred terms are sorted by decreasing frequency in the total group. Adverse event reported terms were coded using the Medical Dictionary for Regulatory Activities dictionary, version 20.0. GC=genome copy. *Retinal pigmentary changes includes retinal depigmentation, retinal pigment epitheliopathy, and retinal pigmentation. †Inflammation includes anterior chamber cell, anterior chamber flare, and anterior chamber inflammation.

Table 2: **RGX-314-emergent ocular adverse events in the study eye by preferred term**

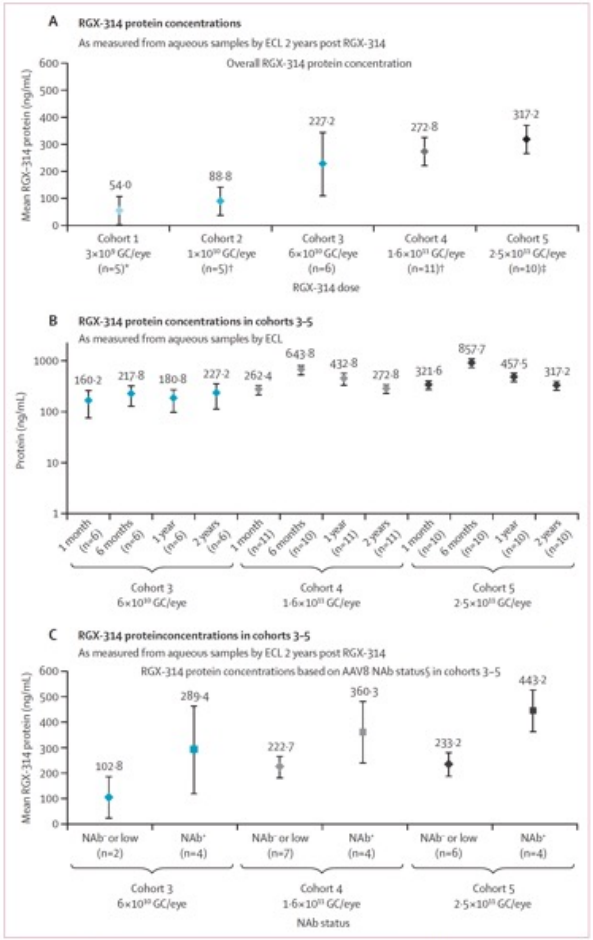

Figure 1: RGX-314 protein expression measured in aqueous humour samples by ECL
(A) Mean (SEM) aqueous RGX-314 protein concentrations (ng/mL) displayed for all five cohorts 2 years after subretinal injection of RGX-314. (B) Mean (SEM) aqueous RGX-314 protein concentration (ng/mL) displayed for cohorts 3–5 at 1 and 6 months, and 1 and 2 years after subretinal injection of RGX-314. (C) Mean (SEM) aqueous RGX-314 protein concentrations displayed for cohorts 3–5, by baseline presence of AAV8 serum neutralising antibodies (neutralising antibody-negative or low and neutralising antibody-positive) 2 years after subretinal injection of RGX-314. AAV8=adeno-associated virus serotype 8. ECL=electrochemiluminescence. NAb=neutralising antibodies. *One patient in cohort 1 discontinued before the week 22 visit. †One patient did not have a year 2 sample. ‡One patient in cohort 5 discontinued before week 22; another patient did not have a year 2 sample. §Baseline serum Nab⁻ is defined as day 8 titer value of >1:10 and baseline serum Nab⁻ is defined as day 8 titer value of <1:5, 1:5, or 1:10.

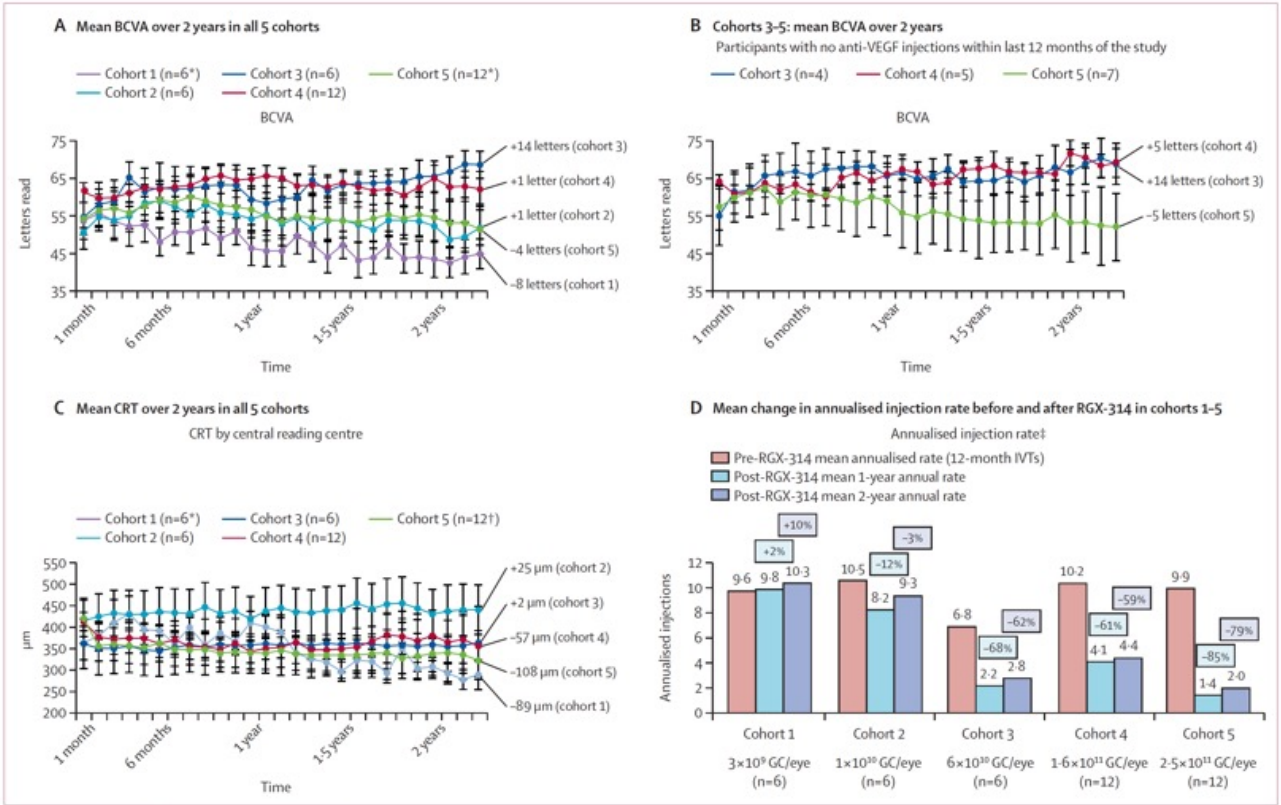

***Figure 2*: Longitudinal efficacy measures of RGX-314**
(A) Mean (SEM) baseline BCVA by ETDRS letters read displayed for all five cohorts from baseline (day 1) up to 2 years after subretinal injection of RGX-314. (B) Mean (SEM) baseline BCVA by ETDRS letters read displayed for participants in cohorts 3–5 that did not receive any supplemental anti-VEGF-A injections over the last 12 months of the study period. (C) Mean (SEM) CRT including height of PEDs (µm), as graded by independent reading centre, displayed for all five cohorts from baseline (day 1) up to 2 years after subretinal injection of RGX-314. (D) Mean change in annualised injection rate for all five cohorts, for the period beginning 12 months before receiving RGX-314, the 1-year period following RGX-314, and the period from 1 year to 2 years following RGX-314 administration. BCVA=best-corrected visual acuity. CRT=central retinal thickness. ETDRS=Early Treatment Diabetic Retinopathy Study. PED=pigment epithelial detachment. IVT=intravitreal injection. VEGF=vascular endothelial growth factor. *One patient in cohort 1 and one patient in cohort 5 discontinued the study, both before the visits at week 22, and missing data after discontinuation were not used in the analysis. Another patient in cohort 5 missed the visits due to COVID-19 from week 50 up to week 74 and from week 86 up to week 94. For this patient, missing visits were imputed using the last observation carried forward. 12 additional missing BCVA results were interpolated. †One patient in cohort 1 and one patient in cohort 5 discontinued the study, both before the visits at week 22, and missing data after discontinuation was not imputed. Another patient in cohort 5 missed the visits due to COVID-19 from week 50 up to week 74 and from week 86 up to week 94. For this patient, missing visits were imputed using the last observation carried forward; 15 additional missing CRT results were interpolated. ‡Previous annual rate=(total number of previous IVTs)/(minimum(366 days or duration between first ever IVT and day 1)/365·25); post-RGX-314 annual rate=(total number of IVTs on study)/(duration on study/365·25), for which on study is defined from RGX-314 administration to a specified cutoff date.

Best corrected visual acuity, kurz BCVA, steht für die Sehschärfe bei bestmöglicher Korrektur durch eine Sehhilfe (z.B.Brille).

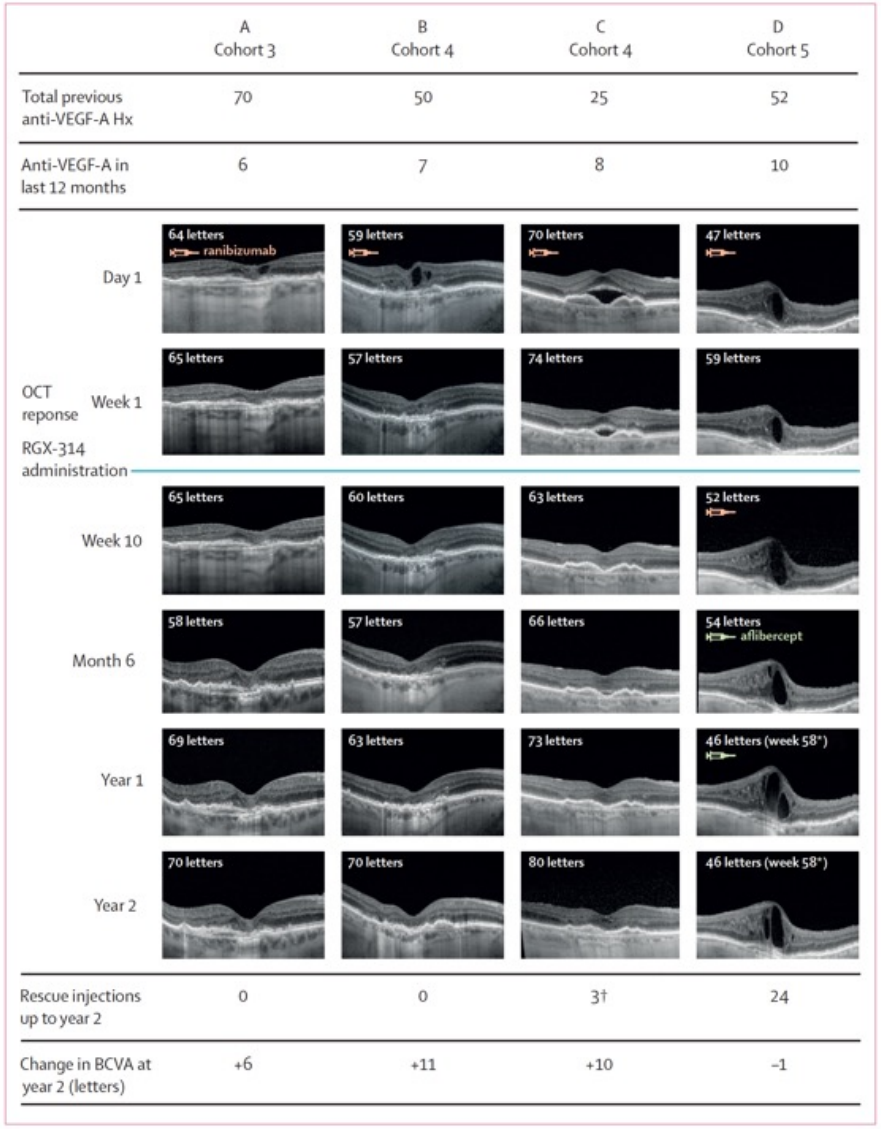

Figure 3: **Longitudinal OCT scans and BCVA (ETDRS letters) of four participants treated with RGX-314**
(A) Male aged 79 years in cohort 3 (dose 6×10^{10} genome copies per eye). This participant received 70 anti-VEGF-A injections since neovascular AMD diagnosis, six within the 12 months before RGX-314 administration, did not require any supplemental anti-VEGF-A intravitreal injections, and has a change in BCVA of +6 letters. (B) Male aged 88 years in cohort 4 (dose $1{\cdot}6 \times 10^{11}$ genome copies per eye). This participant received 50 anti-VEGF-A injections since neovascular AMD diagnosis, seven within the 12 months before RGX-314 administration, did not require any supplemental anti-VEGF-A intravitreal injections, and had a change in BCVA of +11 letters. (C) Male aged 89 years in cohort 4 (dose $1{\cdot}6 \times 10^{11}$ genome copies per eye). This participant received 25 anti-VEGF-A injections since neovascular AMD diagnosis, eight within the 12 months before RGX-314 administration, required three supplemental anti-VEGF-A intravitreal injections, and had a change in BCVA of +10 letters. (D) Male aged 88 years in cohort 5 (dose $2{\cdot}5 \times 10^{11}$ genome copies per eye). This participant received 52 anti-VEGF-A injections since neovascular AMD diagnosis, ten within the 12 months before RGX-314 administration, required 24 supplemental anti-VEGF-A intravitreal injections, and had a change in BCVA of –1 letter. AMD=age-related macular degeneration. BCVA=best-corrected visual acuity. ETDRS=Early Treatment Diabetic Retinopathy Study. OCT=optical coherence tomography. VEGF=vascular endothelial growth factor. *Week 54 not available. †Rescue injections were at weeks 6, 14, and 22.

Research in context

Evidence before this study

Vascular endothelial growth factor A (VEGF-A) plays a crucial role in neovascular age-related macular degeneration (nAMD) by stimulating neovascularisation and exudation, resulting in collection of fluid in the macula, which reduces vision. We searched the PubMed database for articles published in English with no date restriction, using the terms "nAMD", "treatments", "interventional trials", "observational trials", vascular endothelial growth factor", and "gene therapy". A few randomised clinical trials have shown that intraocular injections of anti-VEGF-A proteins block exudation, allowing resorption of fluid and improvement in vision. However, observational studies published in the past 10 years have shown that visual outcomes are much worse in clinical practice than in clinical trials because the frequency of injections needed to control exudation are often not maintained. Meanwhile, at least four previous attempts to use gene therapy for sustained delivery of an anti-VEGF-A protein have not worked, probably due to insufficient transgene expression or absence of transgene activity.

Added value of this study

This study tested the safety and efficacy of subretinal injection of RGX-314, an adeno-associated virus serotype 8 vector expressing an anti-VEGF-A antigen-binding fragment, and measured anti-VEGF-A antigen-binding fragment concentrations in the aqueous, which is crucial for the interpretation of efficacy outcomes. We showed that subretinal injections of RGX-314 in doses less than 6×10^{10} genome copies per eye resulted in little or no expression of anti-VEGF-A protein and no suppression of exudation, whereas doses of 6×10^{10} genome copies per eye or higher resulted in sustained anti-VEGF-A protein expression, control of exudation, and maintenance of vision in many patients. Doses smaller than $2{\cdot}5 \times 10^{11}$ genome copies per eye showed a good safety profile with little or no intraocular inflammation or a clinically evident immune response.

Implications of all the available evidence

This study provided the proof of concept for treatment of patients with nAMD with subretinal RGX-314 and identified doses that have the potential to control exudation without drug-related vision-threatening adverse events. These findings have guided the design of ongoing, pivotal, phase 3 clinical trials.

Swollen eyelids caused by polyvinylpyrrolidone histiocytosis with intravenous methylphenidate

A 26-year-old woman with a 2-year history of swelling of her eyelids and reduced vision was referred to our clinic by an ophthalmologist because of increased myopia, decreased visual acuity, scattered pale dots of the maculae, and suspected angioedema.

The patient had been diagnosed with attention deficit disorder and had been prescribed methylphenidate since adolescence. 5 years before we saw her, she reported having occasional episodes of dizziness thought to be caused by anaemia—investigations at that stage had found an elevated erythrocyte sedimentation rate (ESR; 134 mm/h; typical rate 0–20) and a normocytic anaemia (haemoglobin concentration 9·5 g/dL; typical range 11·7–15·5). The patient had been found to have hepatitis C genotype 3 but was temporarily lost to follow-up.

On examination, we found the patient to be generally well but lethargic; she was thin with a BMI of 13·9 kg/m² (typical range 18·5–25·0). She had bilateral upper and lower palpebral oedema (figure 1) and diminished visual acuity. Oedema was noted also in the face and lips; but despite slight distal lower extremity hyperalgesia and uncertainty of balance and side steps in tandem walk, there were no other abnormalities found.

Fundoscopic examination showed abundant pale dots around the maculae and peripherally in the retinae (figure 2) indicating a crystal retinopathy; optical coherence tomography confirmed the diagnosis showing numerous retinal white dots, oedema of both fovea, and submacular cysts (figure 2).

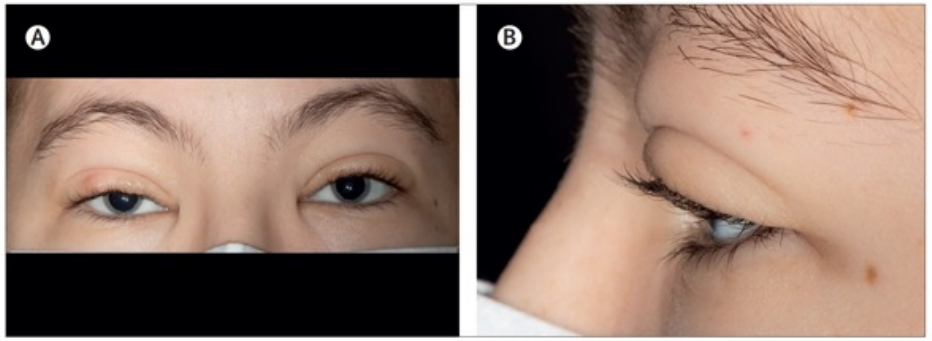

Figure 1: **Swollen eyelids caused by polyvinylpyrrolidone histiocytosis with intravenous methylphenidate**
Photographs (A; B) show bilateral upper and lower palpebral oedema.

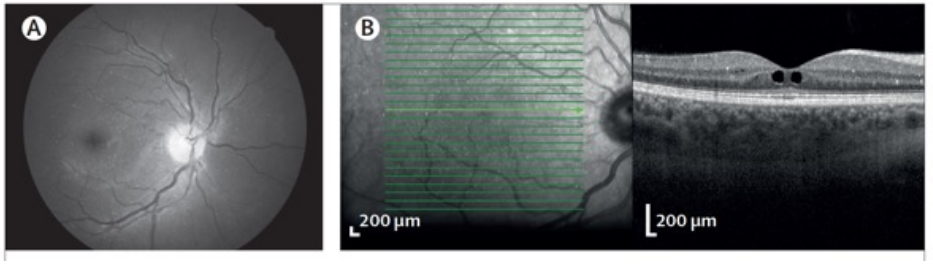

Crystal retinopathy and submacular cysts

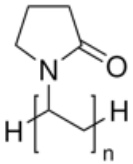

Crystalline retinopathies are a heterogenous group of disorders associated with crystal deposits in any layer and/or region of the retina

Polyvinylpyrrolidon wird als Hilfsstoff in der pharmazeutischen Industrie eingesetzt. Es dient in Medikamenten (speziell Tabletten) in der Regel als Bindemittel und kann die Freisetzung des Wirkstoffs in den Körper beeinflussen. Die quervernetzten Produkte steuern den Zerfall der Tablette.

Laboratory investigations found that both the anaemia (haemoglobin concentration 8·2 g/dL) and the elevated ESR (129 mm/h) persisted. A comprehensive metabolic panel—which included tests for plasma C-reactive protein concentration, sodium concentration, potassium concentration, creatinine concentration, calcium concentration, glucose concentration, alanine aminotransferase, alkaline phosphatase, bilirubin, thromboplastin time, amylase, cortisol, free thyroxine, thyroid stimulating hormone, angiotensin converting enzyme, and immunoglobulin subclass analysis—and urinalysis found no abnormalities. Tests for infectious mononucleosis and HIV were negative; plasma albumin was 31 g/L (normal range 36–48) and prealbumin 0·13 g/L (normal range 0·23–0·37).

^{18}fluorodeoxyglucose PET/CT of the whole body showed no signs of systemic disease, infection, or cancer. An electrocardiogram showed inverted T waves in the anterior leads; an echocardiogram showed mild enlargement of the right heart with a small pericardial effusion. Systolic flattening of the interventricular septum was present. Trace tricuspid regurgitation was seen. Right heart catheterisation confirmed precapillary pulmonary hypertension.

Histopathological analysis of a sample of a bone marrow biopsy showed abundant foamy macrophage infiltration characterised by clear cytoplasm (figure 2); additionally, histiocytes in the bone marrow contained dark pigmented fragments—consistent with titanium deposits that can be associated with intravenous substance use. Furthermore, serum chitotriosidase activity was elevated (1036 nmol/h per mL; typical range 0–195), indicating possible increased macrophage activity or any of several lysosomal storage disorders. Neuropsychiatric assessment showed the patient had impairments of both short-term memory and executive functioning.

Brain MRI with contrast showed diffuse dural thickening and enhancement without any focal pathology of the brain (figure 2). Histopathologic examination of a sample obtained from dural biopsy indicated clusters of CD68-positive macrophages (figure 2); analyses of samples of biopsies from the skin and of biopsies obtained during a gastroscopy were normal.

At this stage our working diagnoses included chronic hepatitis C, severe protein energy malnutrition, secondary pulmonary hypertension, talc retinopathy, secondary histiocytosis, pachymeningitis, amyloidosis, and IgG4 disease.

Whole exome sequencing ruled out inherited causes of primary or secondary histiocytosis. On closer questioning, the patient said she had been intravenously injecting methylphenidate hydrochloride by dissolving the core of the tablets in water. Methylphenidate tablets contain titanium and high molecular weight polyvinylpyrrolidone (PVP) as an adjuvant—a substance associated with histiocytosis when used parenterally. A diagnosis of PVP histiocytosis was made. The patient was counselled and informed of the diagnosis and advised to avoid intravenous substance use. At follow-up 1 year later, she was more alert than before, and her appetite had improved; ESR had decreased ranging from 26 mm/h to 38 mm/h suggesting discontinuation of active intravenous substance use.

Bilateral swelling of the eyelids or periorbital oedema can be caused by nephrotic syndrome, thyroid eye disease, systemic infections such as mononucleosis, atopic or allergic swelling, sarcoidosis, dermatomyositis, lymphoma, IgG4 disease, and various histiocytoses. PVP is widely used in prescription drugs. Moderate and high molecular weight PVP is only used in oral preparations; when used intravenously patients may have renal insufficiency, anaemia, pathological fractures, and abdominal complaints. PVP can be deposited in most organs leading to severe dysfunction. Earlier intravenous abuse of oral PVP containing buprenorphine and methadone preparations, for maintenance therapy for opioid dependence, has been reported to cause severe, and even lethal PVP histiocytosis.

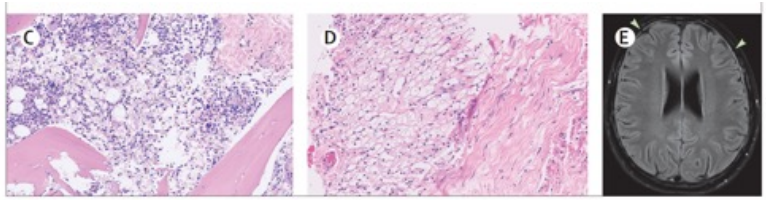

Figure 2: **Fundoscopy, optical coherence tomography, histopathology, and MRI with intravenous methylphenidate**
(A) Fundoscopy shows crystal retinopathy. (B) Optical coherence tomography shows crystal retinopathy and submacular cysts. Histopathological analysis of samples of biopsies containing foamy macrophages from the bone marrow shows intracytoplasmic fragments of dark pigmentation (C) compared to dural macrophages (D) which are without the fragments. Haematoxylin and eosin stain. x100 magnification. (E) MRI brain shows dural thickening (arrows).

The History of operative interventions on the heart.

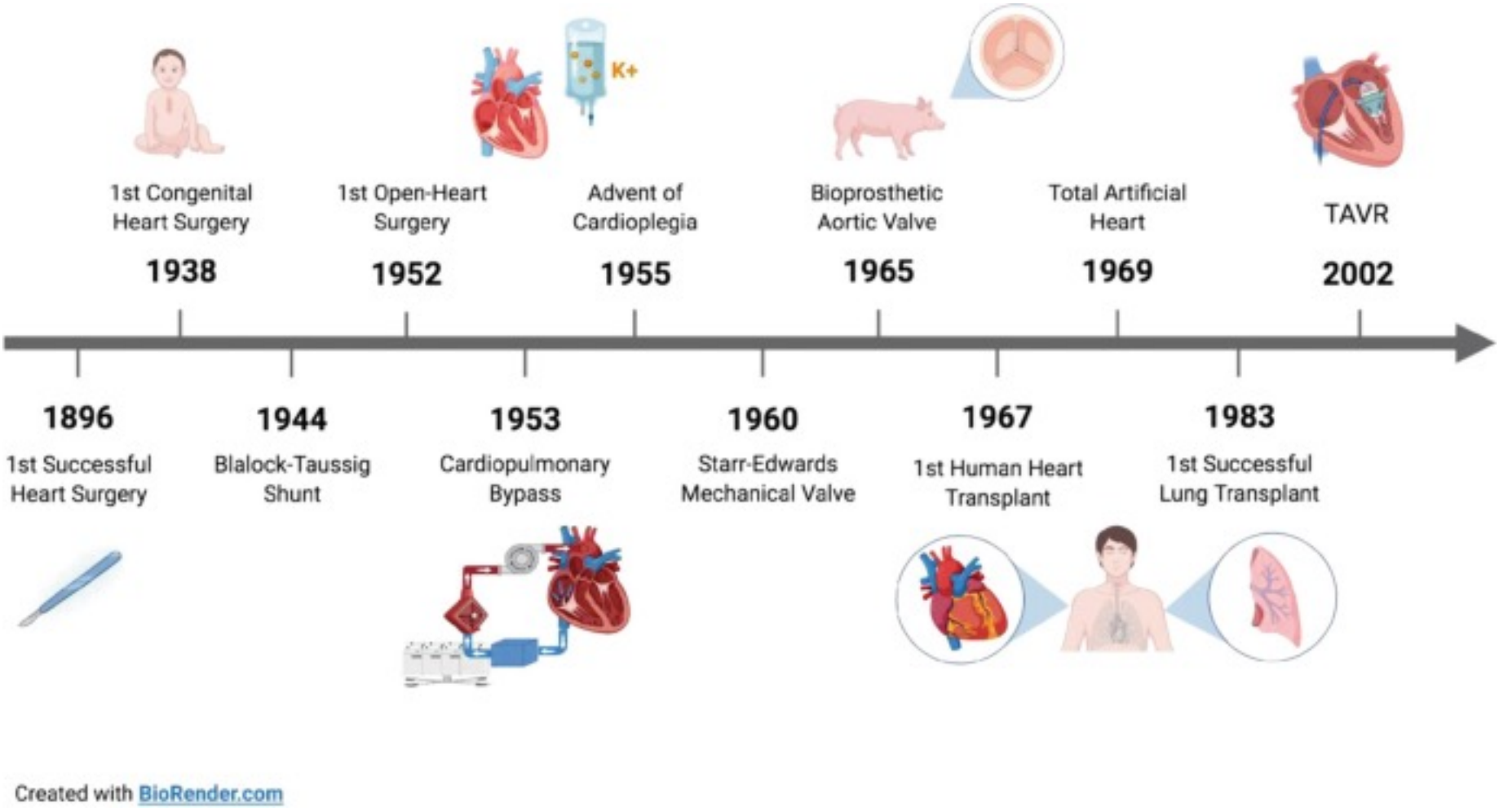

Valvular Heart Disease 1

Valvular heart disease: from mechanisms to management

Valvular heart disease is common and its prevalence is rapidly increasing worldwide. Effective medical therapies are insufficient and treatment was historically limited to the surgical techniques of valve repair or replacement, resulting in systematic underprovision of care to older patients and those with substantial comorbidities, frailty, or left ventricular dysfunction. Advances in imaging and surgical techniques over the past 20 years have transformed the management of valvular heart disease. Better understanding of the mechanisms and causes of disease and an increasingly extensive and robust evidence base provide a platform for the delivery of individualised treatment by multidisciplinary heart teams working within networks of diagnostic facilities and specialist heart valve centres. In this Series paper, we aim to provide an overview of the current and future management of valvular heart disease and propose treatment approaches based on an understanding of the underlying pathophysiology and the application of multidisciplinary treatment strategies to individual patients.

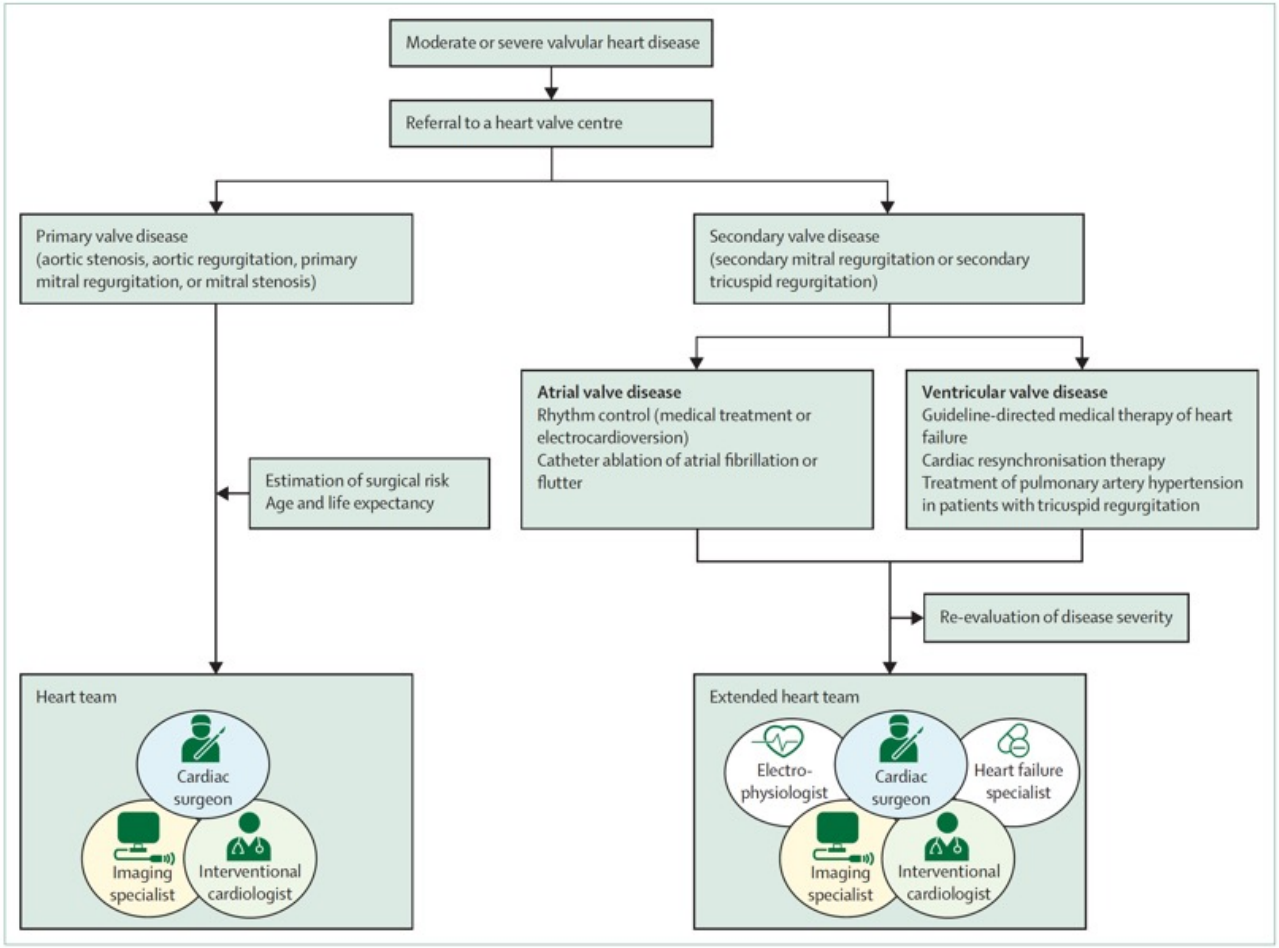

Figure 1: **Diagrammatic representation of clinical management pathways for patients with valvular heart disease**

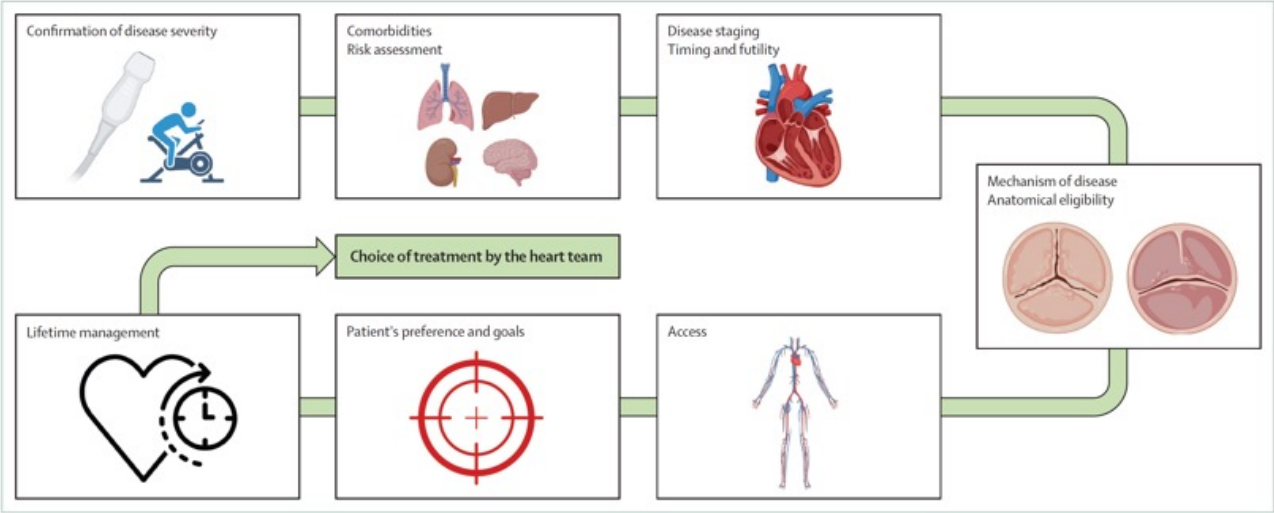

Figure 2: Key steps for clinical decisions by the multidisciplinary heart team

Panel 1: Surgical innovations for the treatment of valvular heart disease

Aortic valve disease

- Rapid-deployment and sutureless valves
- Totally endoscopic surgery
- Robotic surgical platforms
- Hemisternotomy or right anterior minithoractomy
- Valve repair for aortic regurgitation
- More frequent use of the Ross procedure
- Novel leaflet treatment improving tissue valve durability

Mitral valve disease

- Right lateral minithoractomy
- Totally endoscopic surgery
- Robotic surgical platforms

Tricuspid valve disease

- Right lateral minithoractomy
- Early patient referral
- Dedicated risk assessment (eg, by TRI-SCORE)
- Liberal use of concomitant tricuspid valve repair during left-sided cardiac surgery

	Transcatheter aortic valve implantation preferable	Surgical aortic valve replacement preferable
Transfemoral approach feasible	Yes	No
Transfemoral approach challenging but surgical aortic valve replacement feasible	No	Yes
Alternative access feasible; increased surgical risk	Yes	No
Sequelae of chest radiation	Yes	No
Porcelain aorta	Yes	No
High likelihood of severe patient–prosthesis mismatch (aortic valve area <0·65 cm^2/m^2 body surface area)	Yes	No
Severe chest deformation or scoliosis	Yes	No
Annular dimensions unsuitable for current transcatheter aortic valve implantation devices	No	Yes
Bicuspid aortic valve	No	Yes
Severe left ventricular outflow tract or leaflet calcification	No	Yes
High risk of coronary artery obstruction	No	Yes
Thrombus in aorta or left ventricle	No	Yes

Adapted from the European Society of Cardiology and European Association for Cardio-Thoracic Surgery guidelines for the management of valvular heart disease.[35]

Table: **Anatomical and procedural factors that guide choice of treatment methods for isolated aortic stenosis**

Panel 2: Key considerations for lifetime management of severe aortic stenosis

- Age and life expectancy (which influence the likelihood of future interventions)
- Previous aortic valve interventions (ie, surgical aortic valve replacement, transcatheter aortic valve implantation, or Ross procedure)
- Patient and physician acceptance of the need for anticoagulation therapy
- Concomitant cardiac disease
- Aortopathy
- Other valve lesions
- Coronary artery disease
- Atrial fibrillation
- Comorbidities and frailty (which affect the feasibility of surgery)
- Aortic valve and root anatomy
- Bicuspid or tricuspid aortic valve
- Low coronary ostia (which affects the likelihood of occlusion related to transcatheter aortic valve implantation)
- Annular dimensions (which affects the likelihood of patient–prosthesis mismatch)
- Feasibility of future valve-in-valve procedures
- Likelihood of the need for permanent pacemaker implantation
- Future coronary access

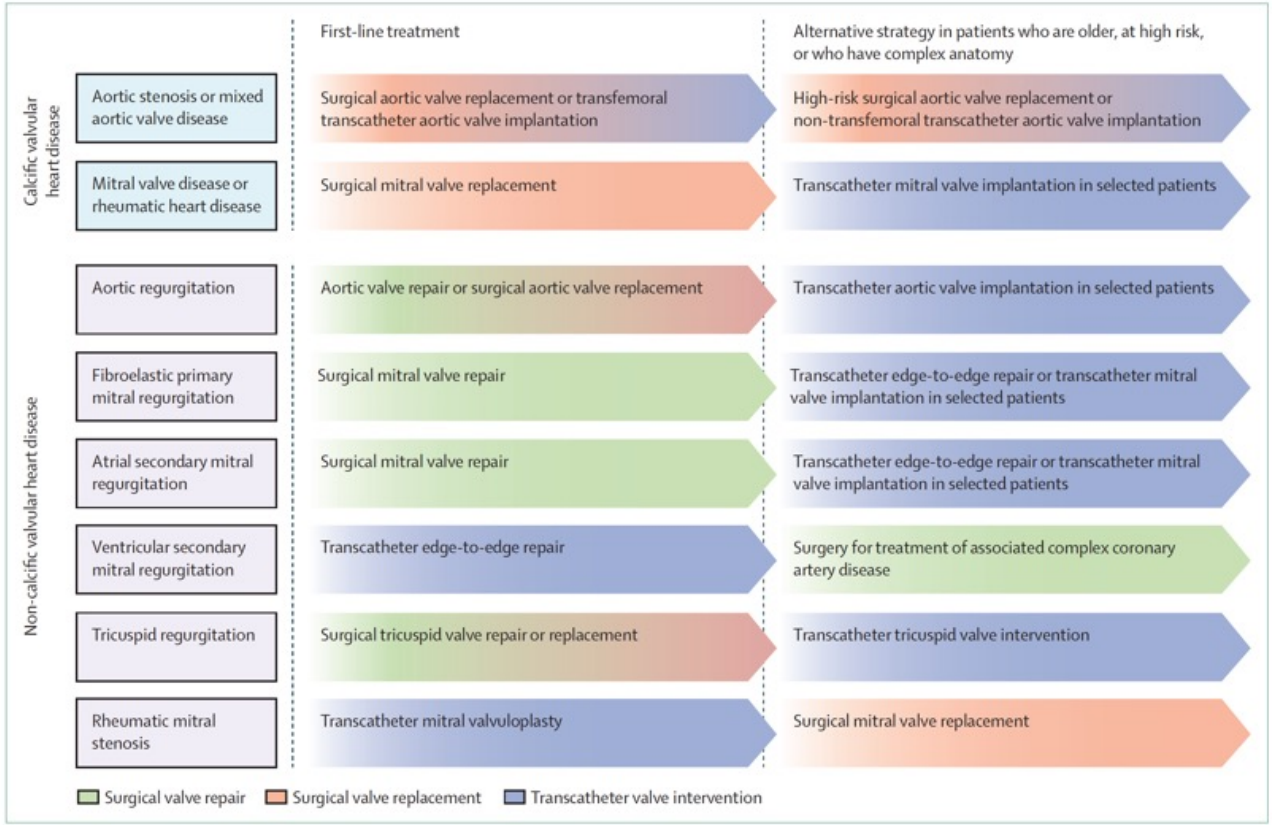

***Figure 3*: Management of valvular heart disease according to underlying disease mechanism**

***Panel 3*: Advantages and disadvantages of transcatheter replacement of the mitral and tricuspid valves, with anatomical criteria favouring replacement**

Advantages of transcatheter valve replacement

- More effective than valve repair in reducing regurgitation
- Durability likely (although largely unknown)

Disadvantages of transcatheter valve replacement

- Higher risk of procedural complications than with valve repair
- Risk of left ventricular outflow tract obstruction (mitral valve)
- Risk of need for new pacemaker implantation (tricuspid valve)
- Interaction with the subvalvular apparatus or right ventricular lead
- Risk of valve thrombosis
- Risk of haemolysis associated with paravalvular leakage

Criteria favouring mitral valve replacement[108]

- Concentric mitral annular calcification with stenosis
- Mitral valve area <3 cm^2
- Clinically relevant mitral stenosis (mean gradient >5 mm Hg)
- Posterior leaflet <5 mm
- Calcification in the grasping zone
- Deep regurgitant cleft
- Leaflet perforation
- Multiple or wide jets
- Rheumatic mitral stenosis
- Failed surgical or transcatheter repair

Criteria favouring orthotopic tricuspid valve replacement[109]

- Large coaptation gap and predominantly central gap
- Severe leaflet tethering
- Tricuspid regurgitation related to cardiac implantable electronic device leads
- Complex leaflet morphology (more than three valve leaflets)
- Leaflet thickening or perforation (eg, rheumatic, carcinoid, or post-endocarditis)
- Previous surgical repair or bioprosthetic valve replacement

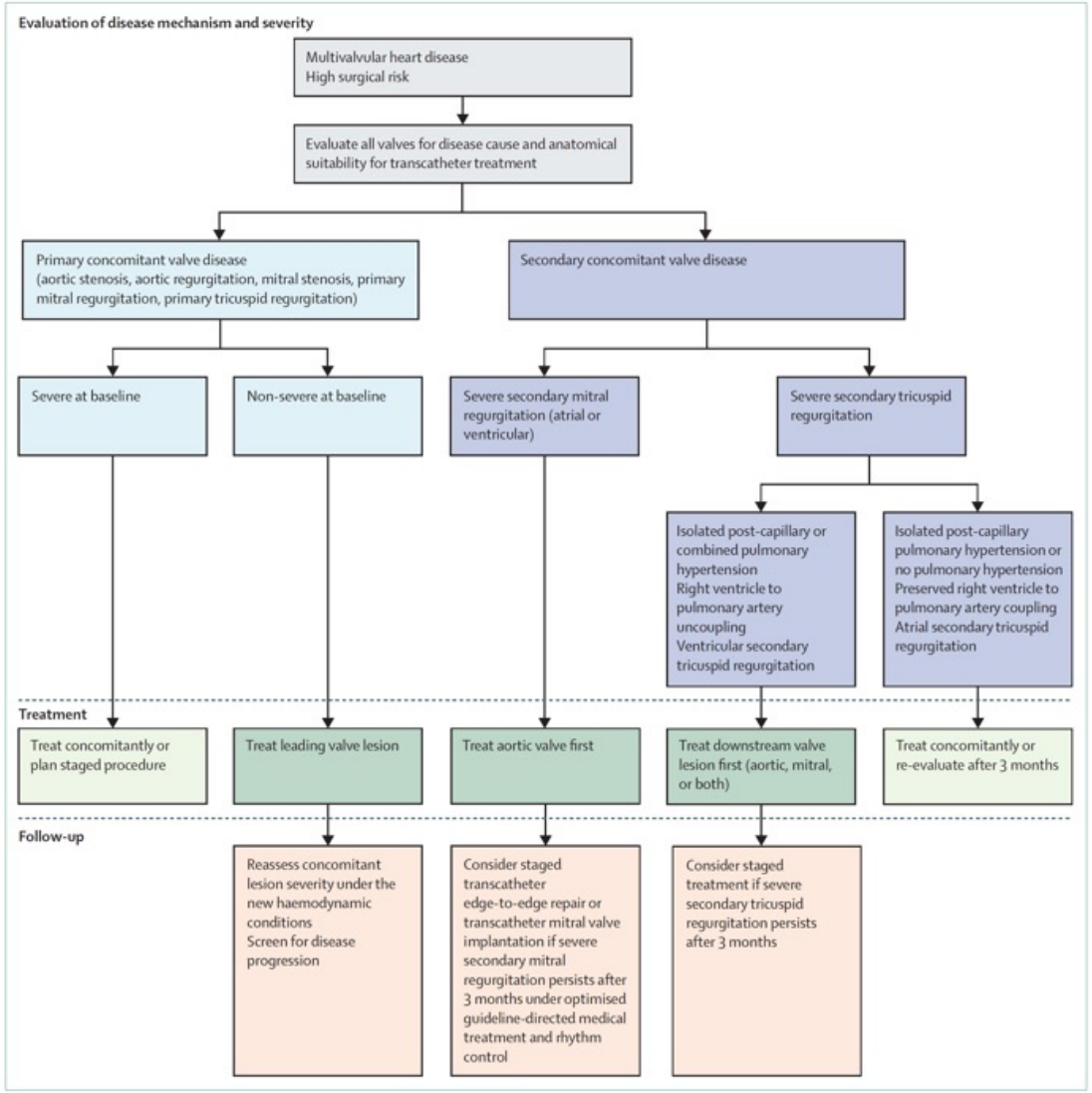

Figure 4: **Proposed strategies for the transcatheter treatment of multiple valvular heart disease according to cause**

Conclusions

The management of valvular heart disease is strongly dependent on a sound understanding of the cause and mechanisms of disease, which should be thoroughly assessed in individual patients before consideration of the most appropriate treatment options by a multidisciplinary heart team. This approach is strongly endorsed by current international guidelines, but requires research. Despite a major surge in the awareness of valvular heart disease and the availability of resources to improve understanding and outcomes of this often-complex condition over the past 20 years, important evidence gaps remain regarding new avenues for medical therapy, the optimal timing of surgical and transcatheter interventions, standardised antithrombotic treatment after mitral and tricuspid procedures, and management of multivalvular disease (including right-sided lesions). Meanwhile, an immediate challenge is to ensure that advances in diagnosis, surgical and transcatheter intervention, and access to treatments that have been established in high-income settings are extended to low-income and middle-income countries, where awareness of valvular heart disease is lower and treatments are largely underused.

Valvular Heart Disease 2

The future of valvular heart disease assessment and therapy

Valvular heart disease (VHD) is becoming more prevalent in an ageing population, leading to challenges in diagnosis and management. This two-part Series offers a comprehensive review of changing concepts in VHD, covering diagnosis, intervention timing, novel management strategies, and the current state of research. The first paper highlights the remarkable progress made in imaging and transcatheter techniques, effectively addressing the treatment paradox wherein populations at the highest risk of VHD often receive the least treatment. These advances have attracted the attention of clinicians, researchers, engineers, device manufacturers, and investors, leading to the exploration and proposal of treatment approaches grounded in pathophysiology and multidisciplinary strategies for VHD management. This Series paper focuses on innovations involving computational, pharmacological, and bioengineering approaches that are transforming the diagnosis and management of patients with VHD. Artificial intelligence and digital methods are enhancing screening, diagnosis, and planning procedures, and the integration of imaging and clinical data is improving the classification of VHD severity. The emergence of artificial intelligence techniques, including so-called digital twins—eg, computer-generated replicas of the heart—is aiding the development of new strategies for enhanced risk stratification, prognostication, and individualised therapeutic targeting. Various new molecular targets and novel pharmacological strategies are being developed, including multiomics—ie, analytical methods used to integrate complex biological big data to find novel pathways to halt the progression of VHD. In addition, efforts have been undertaken to engineer heart valve tissue and provide a living valve conduit capable of growth and biological integration. Overall, these advances emphasise the importance of early detection, personalised management, and cutting-edge interventions to optimise outcomes amid the evolving landscape of VHD. Although several challenges must be overcome, these breakthroughs represent opportunities to advance patient-centred investigations.

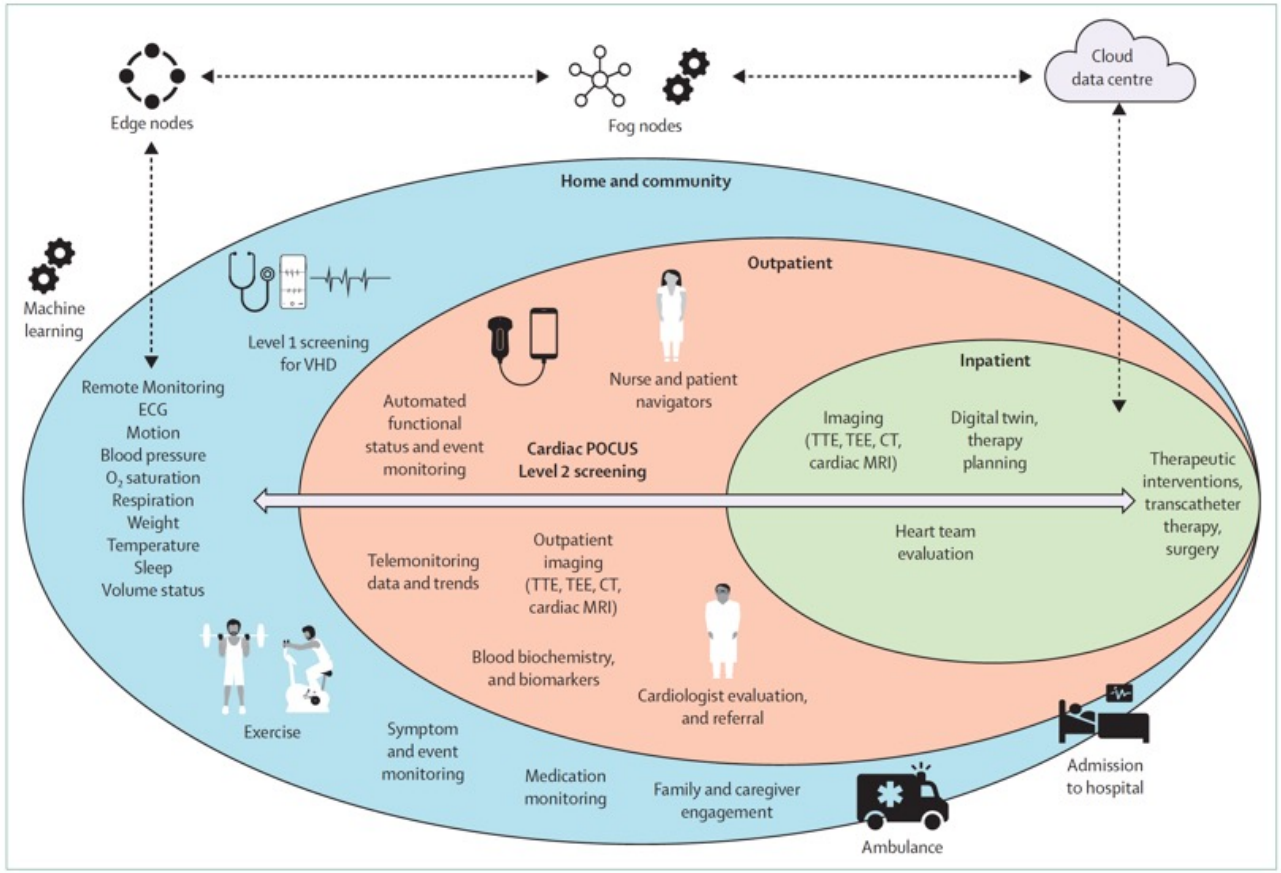

Figure 1: **Digital innovations in care delivery for valvular heart disease**

The schematic conceptualises machine learning techniques using ECG, wearable devices, and physiological sensor-based data for screening, individualised care coordination, and follow-up strategies. Screening in communities can be triggered with the use of wearables, devices, and remote patient monitoring systems. The appropriate triggers can lead to specialised consultations, with additional screening (using cardiac POCUS imaging techniques) and optimisation of downstream testing, evaluation, and timing of interventions. ECG=electrocardiogram. VHD=valvular heart disease. POCUS=point-of-care ultrasound. TTE=transthoracic echocardiogram. TEE=transesophageal echocardiogram.

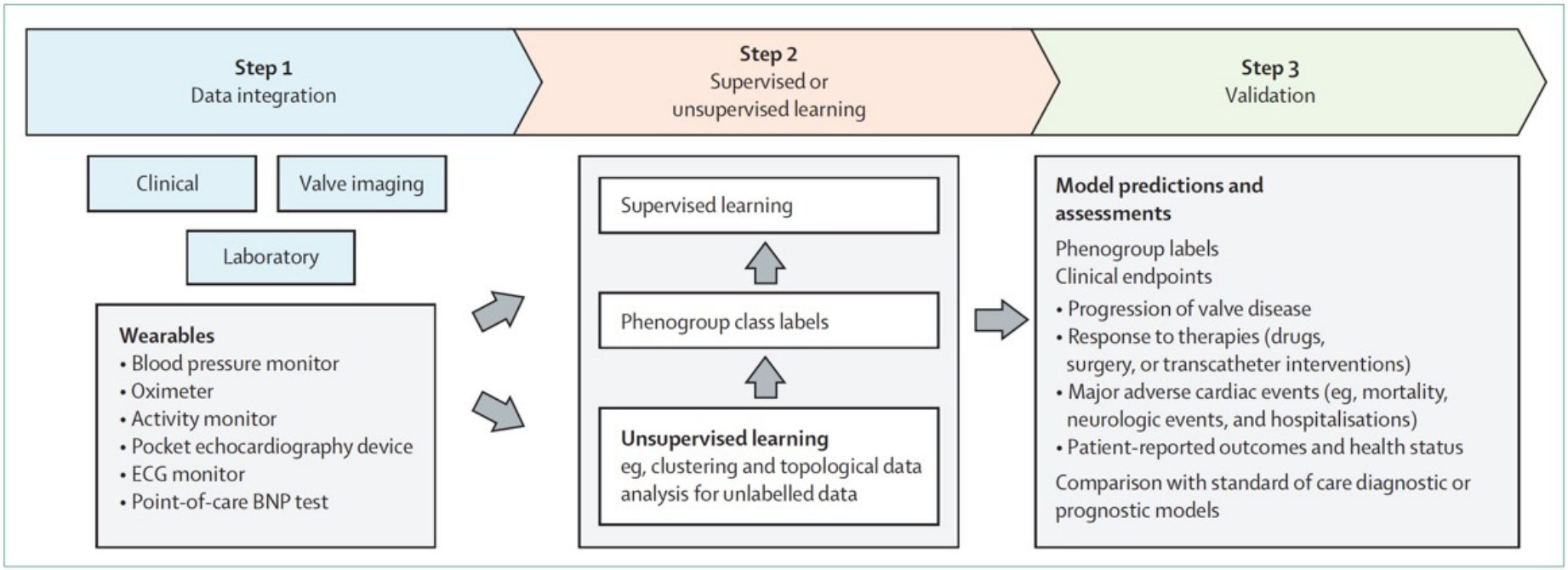

Figure 2: **Use of machine-learning approaches to refine the taxonomy of valvular heart diseases**

Unlike the conventional description of heart valve lesion severity (eg, mild, moderate, or severe), which uses a small number of imaging features, unsupervised machine-learning approaches integrate diverse data to develop meaningful subgroups (clusters) and biological networks (topological maps) associating disease severity with distinct outcomes. After the unsupervised learning is used to develop phenogroup labels, a supervised machine-learning classifier can assign a new patient to the phenogroup class label, which might be particularly useful when patients have conflicting clinical data or imaging measurements. ECG=electrocardiogram. CNN=convolutional neural network. AVR=aortic valve replacement.

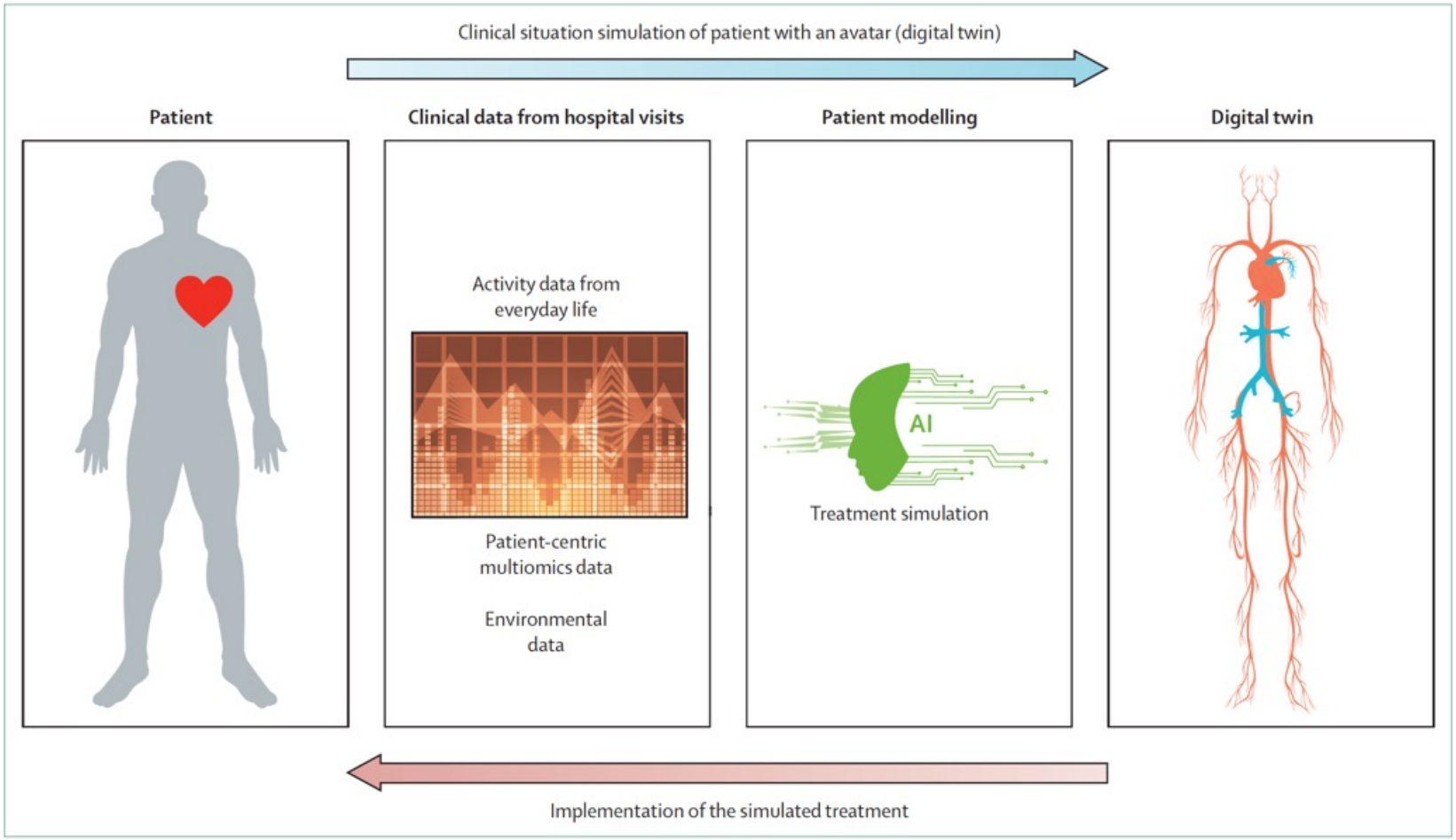

Figure 3: **Suggested pipeline for developing, planning, and predicting the efficacy of therapy for valvular heart disease before real-world implementation**
A digital twin of an individual can be constructed using patient-centred multimodal data and used to simulate treatment outcomes, making it possible to predict the efficacy of therapy (blue arrow). Simulation results from the digital twin make it possible to implement the most effective treatment (red arrow), thereby maximising cost-effectiveness and efficacy. AI=artificial intelligence.

Panel 1: Digital twins in valvular heart disease: opportunities and challenges

Digital twins offer a promising solution for clinicians and patients in precision cardiovascular medicine, especially when dealing with complex valvular conditions and individual treatment strategies. Digital twins are computational models that serve as avatars of patients and can aid clinicians in optimising treatment options. Digital twins can be constructed by leveraging various imaging technologies, providing insights into valve structure, haemodynamics, and the systemic milieu. Digital twins can facilitate virtual procedures, such as transcatheter aortic valve replacement in severe aortic stenosis, enabling clinicians to establish the optimal placement and sizing of valves and identify potential post-procedure complications, including paravalvular regurgitation.[51] Cloud-based simulation software creates digital copies of the heart and its valves to optimise procedural outcomes.

Digital twins can be used to evaluate borderline cases, such as asymptomatic older patients with severe mitral regurgitation who might or might not benefit from the MitraClip procedure. Using more expansive models of the heart, such as those developed by The Living Heart Project, digital twins can simulate and forecast potential cardiac failure, enabling early valve repair and personalised treatment strategies.[52] This approach ensures that only patients who require intervention undergo procedures, avoiding unnecessary risks for those who tolerate their condition well.

Although digital twins show great potential, the current models have limitations. These models primarily focus on the structural aspects of the heart and some haemodynamic factors while neglecting the systemic milieu, which can substantially influence valve function. Additionally, the slow evolution of most valvular heart diseases (VHDs) requires serial follow-ups for accurate twin creation, which might not be feasible in the near future. The reliability of digital twins heavily depends on the data used to create them, making them potentially biased, particularly in under-represented populations.

Despite these challenges, digital twins offer considerable room for improvement and development. Digital twins can be valuable tools in clinical practice, especially as technology advances, allowing for more comprehensive and accurate models of VHD. The complexity of cardiovascular structures and patients' unique characteristics highlight the need for personalised treatment strategies, with digital twins potentially playing a vital role in guiding clinicians' decisions.

Although it remains uncertain whether digital twins provide a clear advantage over conventional models in predicting outcomes for diverse populations, ongoing developments and research in this area are promising. As technology evolves and more data become available, digital twins could revolutionise precision medicine and improve individualised cardiovascular care for patients in the coming years.

Panel 2: Barriers to digital and artificial intelligence techniques in valvular heart disease care

Wearable tools and digital health

Wearable technology studies have shown promising results in valvular heart disease (VHD) care but have limitations due to the under-representation of particular populations, study design heterogeneity, and the need for long-term, meaningful clinical results. The COVID-19 pandemic highlighted disparities in telemedicine access, particularly for older individuals, Asian people, Black people, Latinx individuals, non-English speakers, women, and individuals on low incomes. Reproducibility is hindered by varied interventions, differing devices, and evolving technology. Additionally, data quality from wearables faces challenges from technical issues, user-related factors, and the absence of standardisation. Moreover, the digital divide—the growing gap between groups due to unequal access to digital technologies—disproportionately affects older people, disabled people, people with low socioeconomic status, and people living in rural communities. To address these disparities, efforts are needed to improve broadband internet access, the affordability of digital tools, language accessibility, and form accessibility. Tailoring digital health solutions to patient context and communication preferences, promoting digital literacy, and recognising the digital divide as a social determinant of health are essential steps toward achieving health equity. Future clinical studies should focus on under-represented populations and assess the accuracy and validity of wearable devices through structured frameworks to enhance the equitability of digital health.

Artificial intelligence techniques

Machine learning algorithms are inherently susceptible to biases, and the scarcity of high-quality data that include specific patient groups, such as women and people from minoritised ethnic groups, presents a considerable obstacle to patient-centred machine learning research and decision making. Additionally, the black box nature of artificial intelligence algorithms raises concerns about transparency in the decision-making process. Although explainable artificial intelligence methods can provide reasoning for artificial intelligence predictions, these explanations might only focus on specific aspects of the model's decision. In complex cases, the explanations might not be comprehensive enough to fully capture the reasoning behind a diagnosis or classification. For example, imagers might need to rely on their own expertise to validate or interpret artificial intelligence-generated explanations, adding an additional layer of complexity. Moreover, the successful implementation of artificial intelligence requires skilled professionals who can develop, implement, and maintain artificial intelligence solutions, but health-care organisations might face challenges in recruiting and training staff with the necessary expertise. Finally, the integration of artificial intelligence raises ethical considerations about the potential impact of this technology on patient autonomy and the question of who takes responsibility for artificial intelligence-driven decisions. Ensuring that artificial intelligence adheres to ethical guidelines and regulatory requirements is crucial for building trust in artificial intelligence-driven solutions.

Specific strategies for VHD

The development of robust artificial intelligence tools will require the prospective collection of high-quality data for various heart valve patient groups, including detailed valve-specific data (eg, valve characteristics during surgical valve analysis and imaging data) and complete follow-up. Validations need to be performed in diverse settings, with the inclusion of mortality, morbidity, and valve-specific outcomes (eg, reoperation, recurrent regurgitation, and structural valve deterioration). Furthermore, methods for ethical data collection, data governance, patient permission, and data sharing between institutions with additional privacy and data safety issues are important considerations.[55] Currently, the EU medical device regulation mandates medical device companies to assess the clinical outcomes of their devices. For example, the Heart Valve Society AVIATOR registry, a network that includes patients with regurgitant aortic valves or root aneurysms, allows clinicians to collaborate with medical device companies to collect high-quality data. If data inclusion in large prospective registries (that include patient-reported outcome measures) becomes a prerequisite for reimbursement, there could be meaningful opportunities to improve real-time clinical decision making for patients with VHD.

Panel 3: Multiomics in valvular heart disease: projections and pitfalls

To date, haemodynamic and structural research have been the main ways of understanding valvular heart disease (VHD). Recent large-scale omics research has provided biochemical and molecular insights into VHD, mainly focusing on aortic stenosis. Proteomics and metabolomics have shown promising potential for stratifying risk and identifying therapeutic targets for VHD. For example, in patients with aortic stenosis who have diabetes, plasma proteomics revealed a pro-inflammatory and pro-fibrotic milieu that might worsen their condition.[82] Metabolomics showed that higher lysophosphatidic acid concentrations in stenotic valves correlated with faster haemodynamic progression.[83] Such findings can help predict which individuals are at higher risk of future adverse events. Moreover, omics studies have identified novel molecular targets for aortic stenosis. Transcriptomics revealed increased *DPP4* transcription in stenotic aortic valves, suggesting the potential of this molecule as a therapeutic target.[71] Inhibition of DPP4 has shown promise in treating aortic stenosis.[74]

The use of multiple omics domains, known as multiomics, enables a comprehensive understanding of valvular disease, revealing the distinct pathways driving aortic stenosis and carotid atherosclerosis. Recent research using proteomics and vesiculomics (extracellular vesicle proteomics) to analyse biospecimens of human carotid arteries and stenotic aortic valves showed that although atherosclerosis and aortic stenosis share common pathophysiology, distinct pathways drive each condition (eg, Notch signalling in carotid atherosclerosis and Wnt signalling in aortic stenosis).[84] These findings suggest that although some drugs might work on both atherosclerosis and aortic stenosis, others might only be effective in one of these disease processes. Vesiculomics also provides a basis for developing novel diagnostic strategies, as extracellular vesicles are now the focus of disease monitoring and therapeutic material delivery.

Genomics, the typical starting point of multiomics studies, has also provided new tools for the development of therapeutic targets of VHD, such as the use of genome-wide association studies to predict the results of randomised clinical trials. Human genotypes are inherently randomised as individuals can receive one of two alleles for each gene from their parents. These genotypes can be used as proxies for independent variables in randomised clinical trials, a process named Mendelian randomisation, which can then be used to assess causality. For example, if the effect of statins on aortic stenosis is in question, we could take advantage of genotypes associated with LDL cholesterol, such as *LDLR* or *PCSK9* variants. In addition, although targeting LDL was not proven to be effective in randomised trials,[85] Mendelian randomisation showed that LDL remained an adequate therapeutic target,[86] raising questions about the design of former trials to investigate the effects of LDL lowering and suggesting that the use of drugs such as PCSK9 inhibitors might remain a viable therapeutic strategy.

Despite the novel insights from omics studies, the mechanisms of VHD remain complex. In vitro, computer-based, and animal experimental studies might not accurately reflect human physiology. For example, although lipoprotein(a) has been shown to have a causal effect on Mendelian randomisation,[87] deeper investigation of an observational cohort showed that lipoprotein(a) was only associated with the initiation of aortic valve calcification, not with its progression.[88] In addition, although mouse models of aortic stenosis are used to mimic VHD, there are specific differences between mice and humans. For example, aortic stenosis rarely occurs in normocholesterolemic mice and only under conditions of very high hyperlipidaemia, a finding that is substantially different to the scenario in humans. Considering the complex mechanisms of VHD, the results of in vitro, ex vivo, or animal studies should ultimately be complemented with human studies.

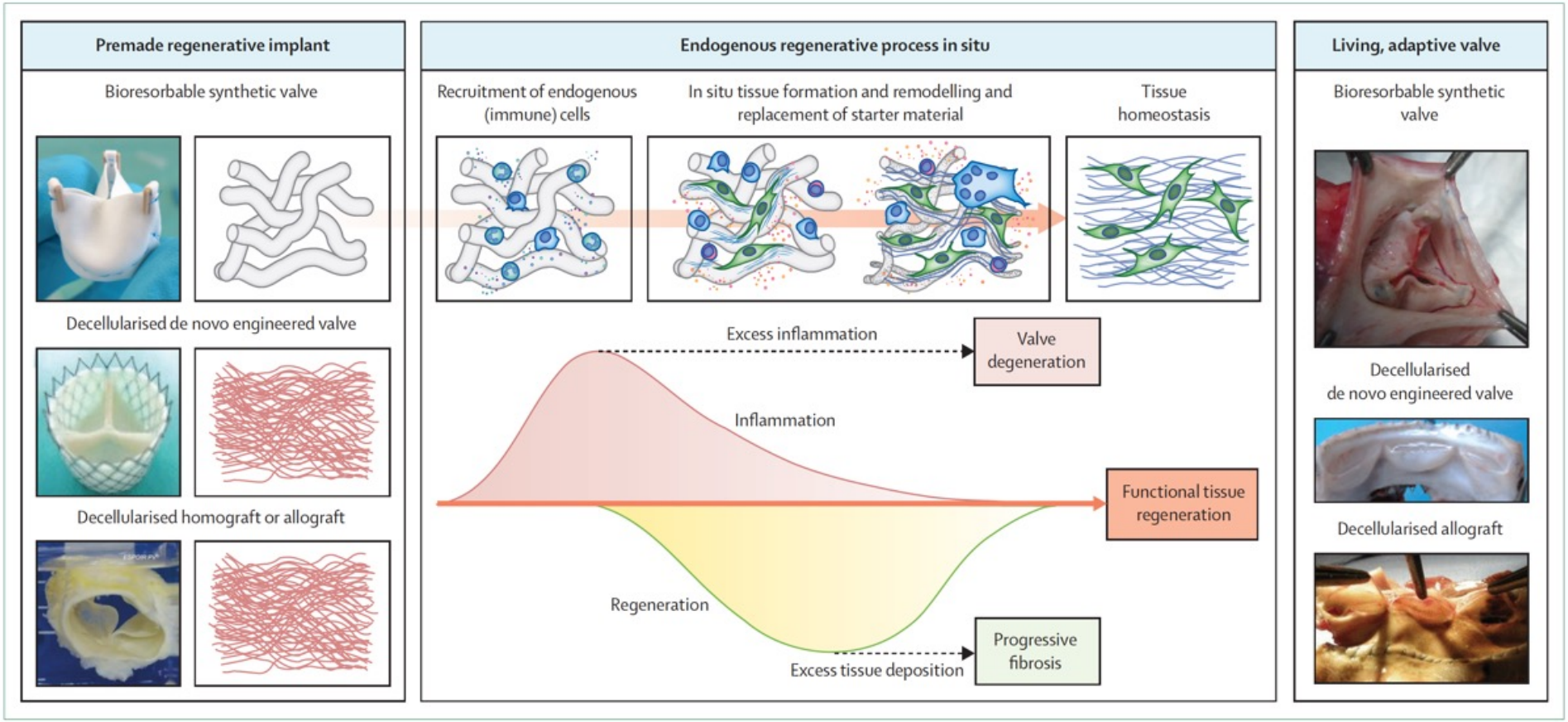

***Figure 4*: In situ heart valve tissue engineering**

Upon implantation, an acellular valvular implant induces an inflammatory response. When harnessed correctly, this inflammatory response triggers a phased tissue regenerative response initiated by the recruitment of endogenous cells, which colonise the porous valvular microstructure. In situ, the cells resorb or remodel the implanted graft material and lay down new endogenous tissue, generating an autologous living valve with the potential to grow and remodel. Schematic adapted from de Kort and colleagues[99] by permission of the authors. Valve photographs reproduced from Uiterwijk and colleagues[100] by permission of the authors; Kluin and colleagues,[101] by permission of the authors; Emmert and colleagues,[102] by permission of the American Association for the Advancement of Science; Boethig and colleagues[103] by permission of the authors, and Goecke and colleagues,[104] by permission of Elsevier.

Conclusions

In the future, the focus of VHD management will be likely to shift towards early detection and monitoring of disease progression through screening techniques. Digital medicine and artificial intelligence techniques applied to wearables, ECG, and miniaturised POCUS could enhance access to care and establish population-wide screening strategies. Artificial intelligence techniques and multiomic approaches could also help identify distinct patient phenotypes with varying severity, pathophysiological mechanisms, and therapeutic targets, thereby overcoming the challenges posed by the underlying biological heterogeneity of VHD progression. Ongoing pharmacotherapy clinical trials might lead to a new era in preventing VHD. The use of large databases and digital twin strategies for patients with established diseases could enable pre-emptive therapy planning. Furthermore, developing next-generation heart valves with repair, remodelling, and regenerative capabilities could revolutionise transcatheter and surgical strategies. Despite the barriers and challenges, these multidisciplinary approaches have the potential to substantially improve the morbidity and wellbeing of many patients worldwide and mitigate the growing burden of VHD.

BIOMEDICAL TECHNOLOGY

The DTC microbiome testing industry needs more regulation

Tests lack analytical and clinical validity, requiring more federal oversight to prevent consumer harm

"[companies] appear to engage in questionable practices that are permitted by gaps in the current regulatory framework."

"At present, there is no consensus about what constitutes a healthy human microbiome composition in any population or subpopulation."

JAMA Internal Medicine | Original Investigation

Excess Death Rates for Republican and Democratic Registered Voters in Florida and Ohio During the COVID-19 Pandemic

IMPORTANCE There is evidence that Republican-leaning counties have had higher COVID-19 death rates than Democratic-leaning counties and similar evidence of an association between political party affiliation and attitudes regarding COVID-19 vaccination; further data on these rates may be useful.

OBJECTIVE To assess political party affiliation and mortality rates for individuals during the initial 22 months of the COVID-19 pandemic.

DESIGN, SETTING, AND PARTICIPANTS A cross-sectional comparison of excess mortality between registered Republican and Democratic voters between March 2020 and December 2021 adjusted for age and state of voter registration was conducted. Voter and mortality data from Florida and Ohio in 2017 linked to mortality records for January 1, 2018, to December 31, 2021, were used in data analysis.

EXPOSURES Political party affiliation.

MAIN OUTCOMES AND MEASURES Excess weekly deaths during the COVID-19 pandemic adjusted for age, county, party affiliation, and seasonality.

RESULTS Between January 1, 2018, and December 31, 2021, there were 538 159 individuals in Ohio and Florida who died at age 25 years or older in the study sample. The median age at death was 78 years (IQR, 71-89 years). Overall, the excess death rate for Republican voters was 2.8 percentage points, or 15%, higher than the excess death rate for Democratic voters (95% prediction interval [PI], 1.6-3.7 percentage points). After May 1, 2021, when vaccines were available to all adults, the excess death rate gap between Republican and Democratic voters widened from −0.9 percentage point (95% PI, −2.5 to 0.3 percentage points) to 7.7 percentage points (95% PI, 6.0-9.3 percentage points) in the adjusted analysis; the excess death rate among Republican voters was 43% higher than the excess death rate among Democratic voters. The gap in excess death rates between Republican and Democratic voters was larger in counties with lower vaccination rates and was primarily noted in voters residing in Ohio.

CONCLUSIONS AND RELEVANCE In this cross-sectional study, an association was observed between political party affiliation and excess deaths in Ohio and Florida after COVID-19 vaccines were available to all adults. These findings suggest that differences in vaccination attitudes and reported uptake between Republican and Democratic voters may have been factors in the severity and trajectory of the pandemic in the US.

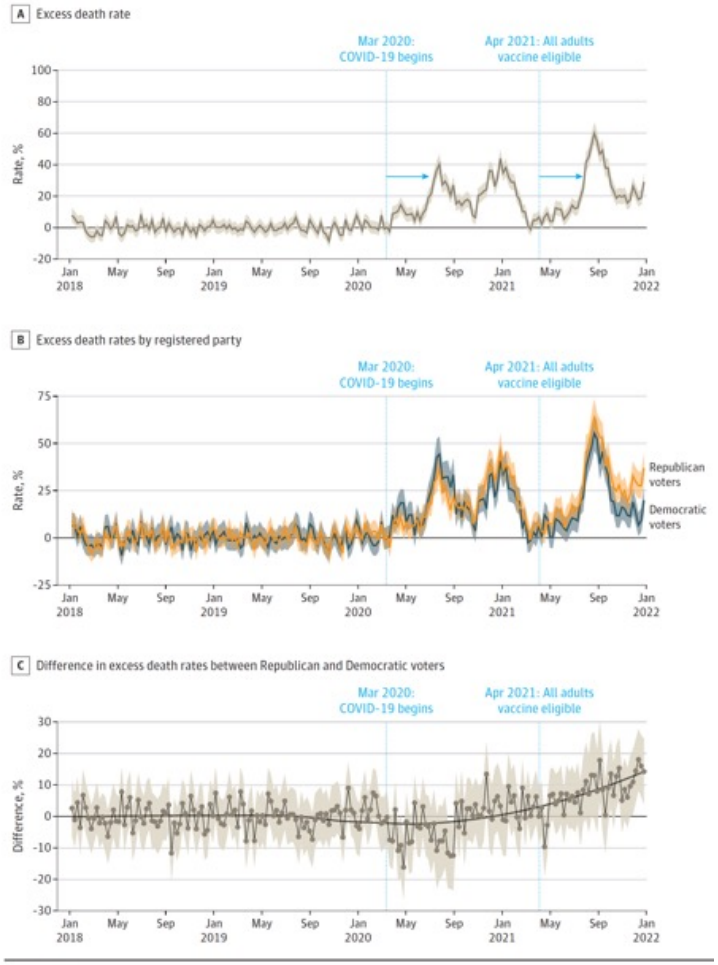

Excess Death Rates and Vaccination Rates in Florida and Ohio During the COVID-19 Pandemic

The dots are counties (Gemeinden), not people.

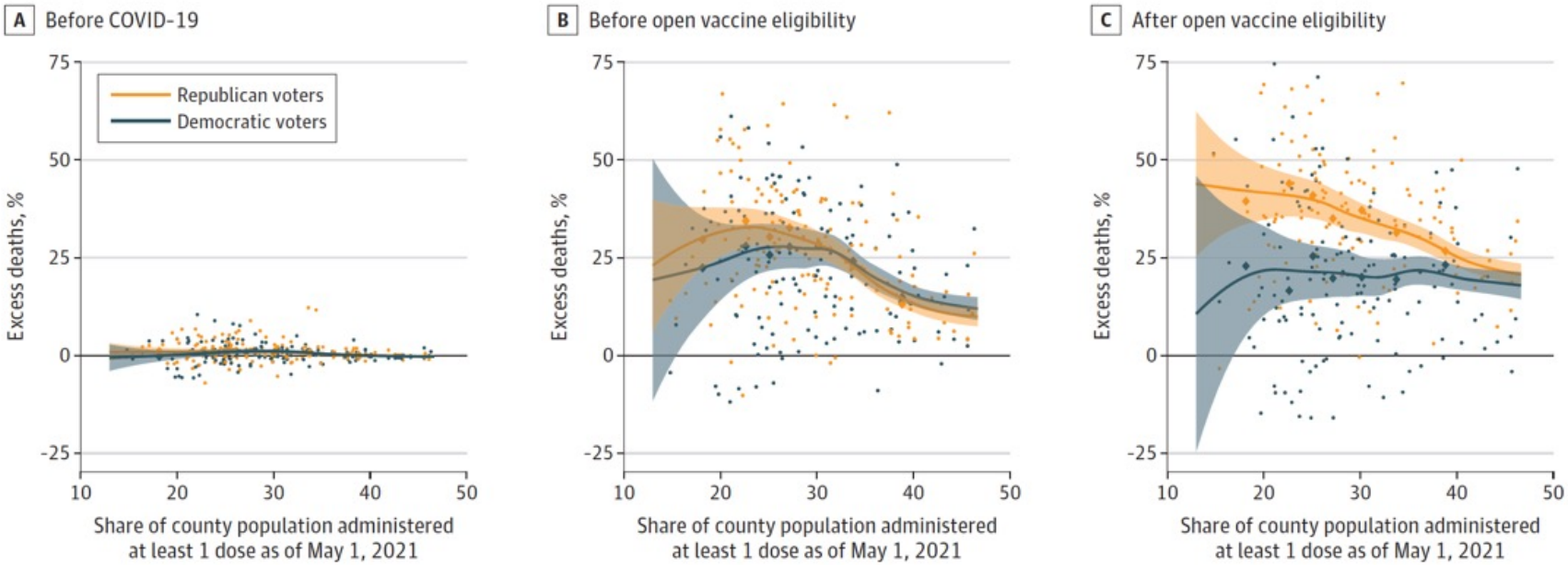

The diamonds are binned means; counties with similar vaccination rates were binned to form 8 equally sized bins. The curves were fit to the underlying data using locally estimated scatterplot smoothing. In the pre–COVID-19 period (before April 2020), excess death rates for both Republican and Democratic voters hover around 0. During the beginning pandemic but before open vaccine eligibility (April 2020 to March 2021), the association between excess death rates and county-level vaccination rates were generally negative and nearly identical for Republican and Democratic voters. However, in the period after open vaccine eligibility (April 2021 to December 2021), there was a clear difference between Republican and Democratic voters, with higher excess death rates for Republicans concentrated in counties with lower overall vaccination rates and minimal differences in counties with the highest vaccination rates.

Not just Republicans

RFK Jr: How anti-vaccine misinformation has shaped his 'truth-teller' candidacy

2 March 2024

Share

By Rachel Schraer, Health and disinformation reporter

BBC / Getty Images

America faces an election rematch in November that few voters are motivated by. As a result, independent candidates could have a bigger impact on this year's result than they have in decades, and none is making bigger waves than Robert F Kennedy Jr.

His supporters see him as a courageous truth-teller, battling nefarious corporate powers. Yet the vaccine sceptic has a history of straying from the truth and spreading health information scientists say is false. Rachel Schraer investigates these two very different images.